LBL-9017

MASTER

ELECTRONS AND KAONS IN CHARMED PARTICLE DECAYS

Joseph Michael Feller
(Ph. D. thesis)

May 1979

Prepared for the U. S. Department of Energy
under Contract W-7405-ENG-48

DISTRIBUTION OF THIS DOCUMENT IS UNLIMITED

LBL-9017

ELECTRONS AND KAONS IN CHARMED PARTICLE DECAYS*

Joseph Michael Feller
(Ph. D. Thesis)

Lawrence Berkeley Laboratory
University of California
Berk[illegible] California 94720

May 1979

NOTICE

This report was prepared as an account of work sponsored by the United States Government. Neither the United States nor the United States Department of Energy, nor any of their employees, nor any of their contractors, subcontractors, or their employees, makes any warranty, express or implied, or assumes any legal liability or responsibility for the accuracy, completeness or usefulness of any information, apparatus, product or process disclosed, or represents that its use would not infringe privately owned rights.

*This work was supported by the Physics Division of the U. S. Department of Energy under contract No. W-7405-ENG-48.

Electrons and Kaons in Charmed Particle Decays

Joseph M. Feller

ABSTRACT

Inclusive studies of the electron content, kaon content, and associated electron-kaon content of the decays of D mesons and other charmed particles produced in electron-positron annihilation are presented.

At the $\psi(3772)$ resonance the following inclusive branching ratios for D meson decays to charged kaons have been measured:

$$B(D^o \rightarrow K^{\pm} X) = .35 \pm .10$$
$$B(D^o \rightarrow K^o X) = .59 \pm .26$$
$$B(D^+ \rightarrow K^- X) = .10 \pm .07$$
$$B(D^+ \rightarrow K^+ X) = .06 \pm .06$$
$$B(D^+ \rightarrow K^o X) = .38 \pm .30$$

Also at the $\psi(3772)$ resonance the average semileptonic branching ratio for D^o and D^+ decays to electrons has been measured to be $.076 \pm .028$. The average semileptonic branching ratio of charmed particles produced in e^+e^- annihilation at center-of-mass energies from 3.9 to 7.4 GeV is found to be equal within errors to that of the D's. At all energies the electron momentum spectra are consistent with a combination of the decays $D \rightarrow Ke\nu$ and $D \rightarrow K^*(890)e\nu$.

The average kaon content of events which contain an electron from the semileptonic decay of a charmed particle has been measured to be 2.3 ± 0.4 kaons per event. The mass spectrum of opposite-charge electron-kaon pairs varies with center-of-mass energy but at all energies is consistent with some combination of the decays $D \rightarrow Ke\nu$ and $D \rightarrow K^*e\nu$.

To my brothers

Contents

Acknowledgements iv

I. Introduction 1
- A. A Brief History of Charm 1
- B. Goals of This Thesis 9

II. Apparatus 17
- A. The SPEAR Mark I Magnetic Detector 17
- B. The Lead-Glass Wall 21
  - 1. Description of the Lead-Glass Wall 21
  - 2. Gain Monitoring 23
  - 3. Energy Calibration 25
  - 4. Energy Resolution 29

III. Data Analysis 36
- A. Trigger and Track Reconstruction 36
- B. Kaon Identification 37
  - 1. Charged Kaons 37
  - 2. Neutral Kaons 44
- C. Hadronic Event Selection for Electron Studies 47
  - 1. Event Selection 47
  - 2. Acceptance 50
- D. Electron Identification 54
  - 1. Cuts 56
  - 2. Efficiency 58
  - 3. Background 63

IV. The $\psi(3772)$ Resonance 69
A. Total Cross Section around 3.772 GeV 69
B. Evidence for $\psi(3772) \rightarrow D\bar{D}$ 69
C. Identification of D Mesons at the $\psi(3772)$ 75
D. "Tagged" Events 78

V. Inclusive Branching Ratios for $D \rightarrow KX$ at the $\psi(3772)$ 80

VI. Semileptonic Decays of D Mesons at the $\psi(3772)$ 86

VII. Electron Production in Multiprong Events from 3.9 to 7.4 GeV 96
A. Inclusive Electron Cross Section 96
B. Heavy Lepton Contribution 100
C. Average Semileptonic Branching Ratio of Charmed Particles 107

VIII. Associated Production of Electrons and Kaons 112
A. Kaon Content of Electron Events 112
B. Electron-Kaon Mass Spectrum 117

IX. Conclusions 122
A. Semileptonic Decays of Charmed Particles 122
1. Semileptonic Branching Ratios 122
2. Specific Decay Modes 124
B. Kaon Content of D Meson Decays 126
C. Inclusive Kaon Production 127
1. General 127
2. Inclusive Kaon Production at the $\psi(3772)$ 128

Appendix A. Calculation of Matrix Elements for $D \rightarrow Ke\nu$ and $D \rightarrow K^*e\nu$ 131

Acknowledgements

Because the Lead-Glass Wall experiment and the preparation of this thesis have been the major activities of the last three years of my life, these acknowledgements are necessarily an account of those people who have influenced me most in those three years. I have been fortunate to be surrounded by people who have given freely of both their wisdom and their support. For this I am grateful.

My work and this thesis represent a small part of a much larger effort. The success of our experiment was the result of the dedication and hard work of many individuals. It has been a privilege to work with such a talented group of people and I am proud to have been able to make a contribution to the cooperative effort. I am especially happy to have been among people whom I truly considered to be my friends.

First and foremost, I acknowledge the guidance, encouragement, and inspiration of my thesis advisor, Dr. Angela Barbaro-Galtieri, without whom my work and this thesis would not have been possible. Lina had the awesome and unenviable task of organizing and directing the experiment. She saw it through from the first stages of planning to its fruition in exciting new discoveries. Through it all she never lost her cheerful spirit, which served as an inspiration to us all, and she never allowed the maze of details and problems to make her lose sight of the ultimate goals of the experiment.

In spite of her many responsibilities Lina always found time to discuss and plan my work with me and to share with me the insight and expertise she has gained from her extensive experience in particle physics. She also reminded me, as I occasionally needed reminding, that I did not know everything about physics and still had a lot to learn. I thank her from the bottom of my heart.

I had the particular pleasure of working very closely with a few individuals on the analyses that constitute the bulk of this thesis. On the studies of electron production I collaborated with Michael Ronan and Ronald Madaras and with Alan Litke, about whom I will say more later. The lively and frequent discussions among our "Gang of Four" were most enjoyable and productive. Mike and Ron both put a tremendous effort into the many complex steps required to extract meaningful results from an enormous amount of data. This data would not even have existed, however, if it were not for the monitoring system for which Ron took responsibility and the Large Scale Digitizer System on which Mike spent so much time.

On the studies of the kaon content of D meson decays I collaborated with Vincent Vuillemin. My work in that area was based upon what Vincent had done before and we worked together on the final results. I enjoyed immensely working with Vincent and exchanging thoughts about American and European culture and society as well as physics.

I am grateful to the members of my thesis committee, Lina Galtieri (again), Professor Ronald Ross, Professor David Jackson, and Professor Luciano Moretto for their many constructive comments and their tolerance and cooperation when I asked them to read my thesis in an unreasonably short period of time.

In the course of the data analysis I found occasional discussions with Professor Ross to be especially valuable because of his constant ability to see the larger picture and to ask questions which pointed me in the right direction. Ron homed in on key points which sometimes slipped by in the larger group dicussions and he quietly insisted on thoroughness.

I am grateful to Professor Jackson for the time he spent explaining many theoretical points to me. In spite of the many demands on his time as chairman of the Physics Department and as a much sought-after physicist and teacher he is still among the most available members of the department to students. Discussions with him on many points both inside and outside of physics were a highlight of many Friday afternoons.

I would like to thank Professor Robert Ely for his many frank comments and observations at group meetings and in smaller discussions. Bob has an uncommon degree of common sense and vast experience in experimental physics and he uses both to good effect.

Barrie Pardoe made enormous contributions to the software which was so essential to the running of the experiment and the analysis of the data. Beyond that, I thank him for our almost daily converations on far-ranging topics. Just as Lina occasionally reminded me that I don't know everything about physics, so Barrie reminded me that I don't know everything about life.

I thank Sherwood Parker for sharing with me part of his vast knowledge of physics, electronics, hardware, Berkeley, Chicago, and the world and for unconsciously teaching me to know the facts (or at least some of them) before I speak.

I thank Professor Lynn Stevenson for thoughtful discussions and advice about my future and the future of particle physics. His guidance has been invaluable.

I thank Professor Eugene Commins for teaching me most of the physics that I know in his classes.

I thank my fellow graduate students, Abe Fong and John Orthel for their companionship and encouragement.

I thank our secretaries Jo Barrera and Bev Koop for their help in many matters which were essential to the preparation of this thesis.

I thank Ray Hagstrom for his invaluable advice concerning the use of the UNIX system for preparing this thesis.

I thank Dr. William Rarita for our frequent cheerful encounters.

I reserve a special thanks for Petros Rapidis, a close friend and a fellow graduate student on the experiment. We have shared our hopes, fears, and frustrations regarding physics, graduate student life, and our futures and Petros has been a source of sympathy and encouragement.

As it turns out, Petros and I will probably be working at the same place in the immediate future. Over the last three years my friendship with Petros has been essential to the maintenance of my sanity. Over the next three years I expect it to be even more so!

I have saved for last my tribute to the person most responsible for my involvement in this experiment and in physics itself. I literally owe everything to Alan Litke. My first introduction to particle physics was in Alan's Freshman Seminar at Harvard in the spring of 1972. Alan then made it possible for me to work part-time on the pioneering e^+e^- experiment at the Cambridge Electron Accelerator. This was a unique and valuable opportunity which had a lasting effect on my life.

After Alan moved to Berkeley in the spring of 1973 he arranged for me to work at the Lawrence Berkeley Laboratory during the next two summers. This work led directly to my participation in the Lead-Glass Wall experiment as a graduate student and to the writing of this thesis.

During the experiment and the data analysis I worked closely with Alan and benefited from his constant guidance. Our frequent and lengthy discussions were my greatest source of encouragement and ideas.

In short, I am indebted to Alan Litke for all I have learned and accomplished in the last eight years. Thank you, Alan.

I. Introduction

A. A Brief History of Charm

Prior to November 1974 it was widely believed that the complex spectrum of hadrons that had been observed up until that time could be explained as composite systems of three fundamental constituents, called quarks.[1] These three quarks, up(u), down(d), and strange(s), are postulated to be fermions with fractional electric charges and baryon numbers. They form a subspace for a triplet representation of the symmetry group SU(3). The quantum numbers of the quarks are given in Table I.1. The quarks are further hypothesized to come in three "colors", color being a degree of freedom which is exactly conserved in an SU(3) symmetry and which is unobservable but necessary in order to preserve Fermi statistics.[2] Color also serves to explain the observed rate for the decay $\pi^0 \rightarrow \gamma\gamma$ by increasing by a factor of three the number of amplitudes which contribute.

The primary evidence supporting the quark model was of two types. First, the model and its underlying SU(3) symmetry were able to explain the observed spectrum of hadrons and were able to predict the existence and properties of new hadrons which had not been observed at the time the model was proposed.[3] Second, the observation of scaling behavior in deep inelastic electron scattering at the Stanford Linear Accelerator Center (SLAC) indicated that the proton and neutron were indeed comprised of point-like spin-$\frac{1}{2}$ constituents.[4]

By the 1970's, however, there were two important areas in which the experimental data disagreed with expectations of this simple three-quark model. The first problem area was in the weak interactions of strange particles; specifically, the low observed rate for the decay $K_L^0 \rightarrow \mu^+\mu^-$ and the smallness of the K_L^0/K_S^0 mass difference.

The weak interactions of the quarks and leptons are believed to arise from the coupling of the weak current to the heavy W bosons. The charged component of the current is[1,24]

$$J_\lambda = \bar{\nu}_e\gamma_\lambda(1-\gamma_5)e + \bar{\nu}_\mu\gamma_\lambda(1-\gamma_5)\mu + \bar{u}\gamma_\lambda(1-\gamma_5)(d\cos(\theta_c) + s\sin(\theta_c))$$

where θ_c is the Cabibbo angle (about 13 degrees). This current leads to the two muon decay of the K_L^0 through the diagram shown in Figure I.1a.[5] The amplitude is proportional to $\sin(\theta_c)\cos(\theta_c)$. This current also creates a mass splitting between the K_L^0 and the K_S^0 by coupling the K^0 to the $\overline{K^0}$ through the diagram in Figure I.1b. This amplitude is proportional to

Table I.1

Quark Quantum Numbers

Quark	u	d	s	c
Baryon Number	1/3	1/3	1/3	1/3
Spin	1/2	1/2	1/2	1/2
Charge	+2/3	-1/3	-1/3	+2/3
Isospin	1/2	1/2	0	0
I_3	+1/2	-1/2	0	0
Strangeness	0	0	-1	0
Charm	0	0	0	1

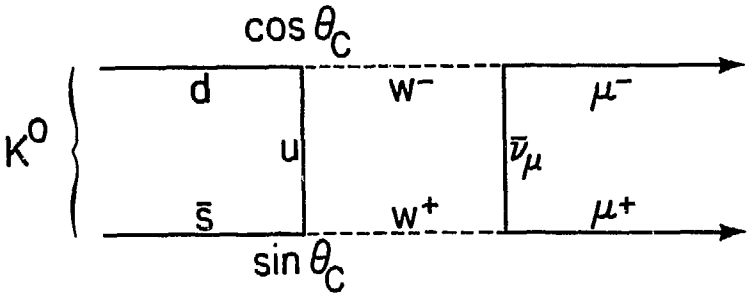

(a) $K_L^0 \rightarrow \mu^+\mu^-$ Decay

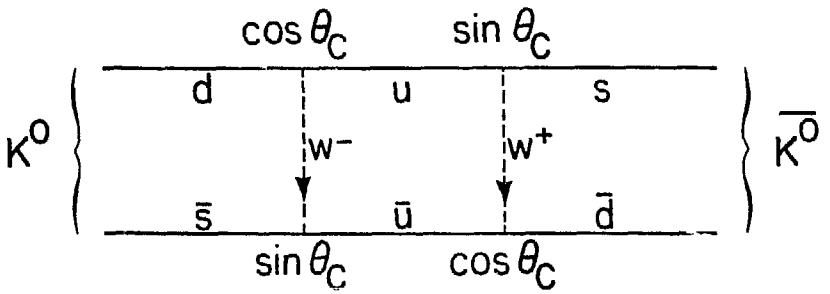

(b) K_L^0-K_S^0 Mass Splitting

XBL 791-288

FIGURE I.1

Quark diagrams for the decay $K_L^0 \rightarrow \mu^+\mu^-$ and the K_L^0/K_S^0 mass splitting.

$\sin^2(\theta_c)\cos^2(\theta_c)$. Both these effects were experimentally measured to be much smaller than predicted by this model.[6] Therefore, a mechanism was needed to suppress these diagrams. In 1970, Glashow, Iliopoulos, and Maiani[7] postulated the existence of a fourth quark which they called the charmed(c) quark. This hypothetical quark carried a new quantum number, charm, which would be conserved in all but weak interactions. The quantum numbers of this new quark are presented in Table I.1 along with the three ordinary quarks. This new quark was postulated to couple to a linear combination of the s and d quarks orthogonal to that which couples to the u quark so that the quark part of the charged weak current is given by

$$\bar{u}\gamma_\lambda(1-\gamma_5)(d\cos(\theta_c)+s\sin(\theta_c)) + \bar{c}\gamma_\lambda(1-\gamma_5)(s\cos(\theta_c)-d\sin(\theta_c))$$

This new term in the current leads to the diagrams shown in Figure I.2. These amplitudes are opposite in sign to those of Figure I.1 and are nearly equal in magnitude. Small differences arise from the difference between the u and c quark masses and lead to the non-zero rate for $K_L^o \rightarrow \mu^+\mu^-$ and the non-zero K_L^o/K_S^o mass difference. In order to explain the observed effects the mass of the c quark would have to lie roughly between I and 5 GeV.[5] (A good summary of the kaon problem and the charm solution can be found in Reference 5.)

Since the introduction of the charm hypothesis in 1970, the unified gauge theory of Weinberg and Salam[28], which includes a neutral boson Z^o in addition to the charged W's, has proven to be the most successful model of weak interactions. In this model the charmed quark is required to eliminate first-order diagrams involving the Z^o as well as to cancel the diagrams of Figure I.1.

A second puzzle which could not be explained by the simple model of three quarks was the observation, first at the Cambridge Electron Accelerator[8] and later at SLAC[9], that the ratio of the cross section for hadron production by electron-positron annihilation to the theoretical one-photon cross section for muon pair production (σ_{QED}) was rising with increasing center-of-mass energy (E_{cm}). The SLAC data on this ratio, called R, are presented in Figure I.3.[29] (This figure includes some data obtained more recently than 1974; for a historical perspective see Reference 9.)

In the quark model, hadron production in electron-positron annihilation is assumed to proceed through the production of a virtual quark-antiquark pair which then interacts to form hadrons.[10] The cross section for producing any charged point-like fermion-antifermion pair in electron-positron annihilation is given by

$$\sigma_{pair} = \frac{\pi\alpha^2}{3E^2}Q^2$$

where α is the fine structure constant (1/137.04), E is the beam energy, and Q is the absolute value of the electric charge of each member of the pair. Therefore the ratio R should just be given by

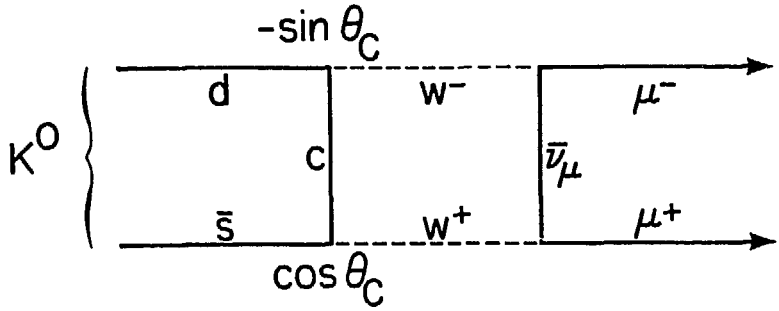

(a) $K_L^0 \rightarrow \mu^+\mu^-$ Decay

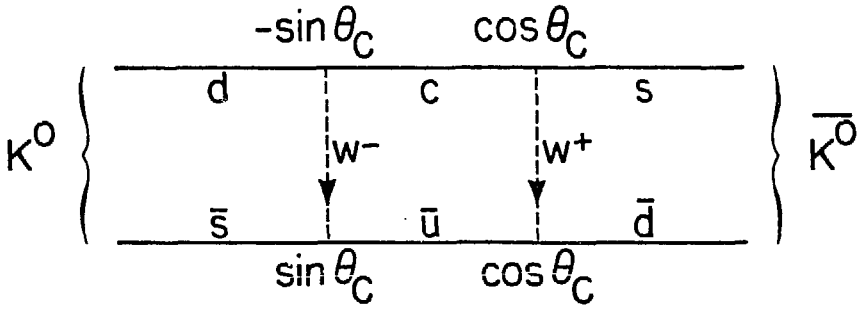

(b) K_L^0-K_S^0 Mass Splitting

XBL 791-290

FIGURE I.2

Cancelling quark diagrams for the decay $K_L^0 \rightarrow \mu^+\mu^-$ and the K_L^0/K_S^0 mass splitting in the GIM model.

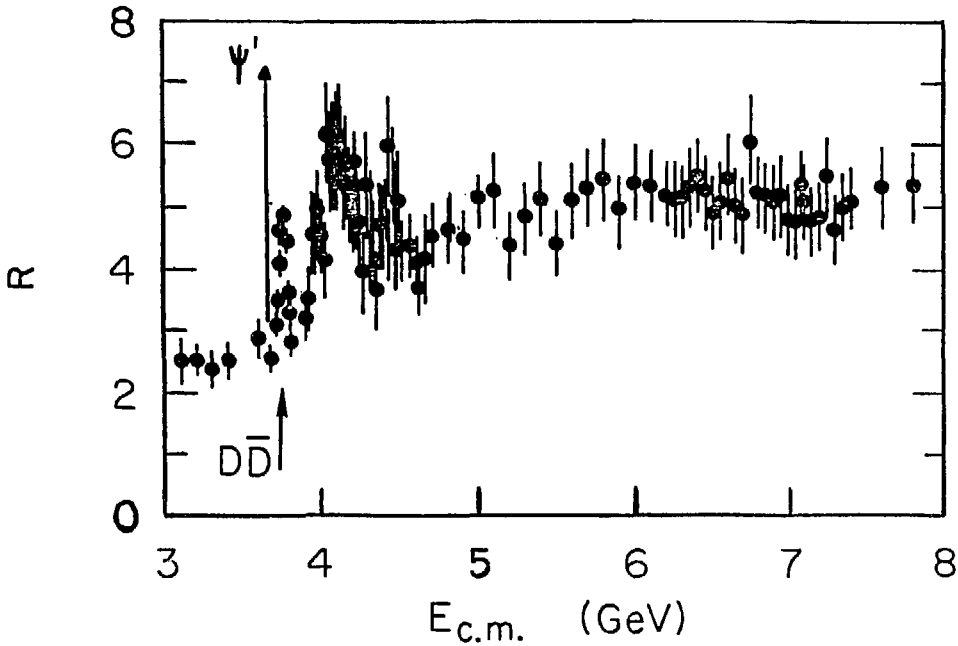

XBL 7812-13697

FIGURE I.3

R, the ratio of hadron production to muon pair production in e^+e^- annihilation, as a function of center-of-mass energy.

$$R = \frac{\sigma_{hadrons}}{\sigma_{\mu\mu}} = \sum_i Q_i^2 = 3\left[(\frac{2}{3})^2 + (\frac{1}{3})^2 + (\frac{1}{3})^2\right] = 2$$

where the sum is taken over all types of quarks: u, d, and s, each in three colors.

Looking at the data in Figure I.3 we can see that the data are roughly in agreement with this prediction in the region below about 4 GeV but R is rising in the 4 GeV region and seems to reach an asymptotic value of about five or six.

If the c quark existed it would add a term

$$R_c = 3\,(\frac{2}{3})^2 = \frac{4}{3}$$

to R. This term would only contribute if the center-of-mass energy were sufficient to produce particles containing the charmed quark and antiquark. Therefore, if the mass of the c quark were in the neighborhood of 2 GeV, it could explain part of the change in R in the 4 GeV region.

If indeed the charmed quark existed then one would expect to see charmed hadrons containing it. The lightest possible states would presumably be mesons consisting of a charmed quark plus an antiquark of the u, d, or s variety. At higher masses one would expect to see baryons containing one or more charmed quarks.[11] In the absence of observation of such states the charm hypothesis lay dormant until the fall of 1974.

At that time an astounding discovery was made simultaneously on the east and west coasts which led to an entire new field of hadron spectroscopy and eventually to a resounding confirmation of the charm hypothesis. The discovery consisted of an extremely narrow resonance with a mass of 3.1 GeV. On the west coast it was seen at the Stanford Linear Accelerator Center as a spike in the cross section for electron-positron annihilation into hadrons.[12] It was seen on the east coast at Brookhaven National Laboratory as a peak in the mass spectrum of electron-positron pairs produced in proton-beryllium collisions.[13] The surprising thing about this resonance was its combination of high mass and extremely narrow width. The width was about 70 KeV, as compared to tens or hundreds of MeV for previously discovered hadron resonances with very high masses.

This resonance, known as the $\psi(3.1)$, was interpreted as a meson consisting of a bound state of a c and a $\bar{c}$ quark.[14] (The existence of such a narrow bound state was actually predicted on the basis of this model slightly before the discovery of the ψ.[15]) It was christened "charmonium" in analogy to positronium. Presumably it could not decay into a pair of charmed particles because its mass was too low to produce the pair of "old" (u, d, or s) quarks needed to join with the charmed quarks to form charmed mesons. The ψ could then decay only by annihilation of the charmed quark and antiquark into old quarks. Such a decay is suppressed by the Okubo-Zweig-Iizuka or OZI rule which suppresses such "disconnected" diagrams[16]; thus the

narrow width.

The discovery of the ψ was followed in a few weeks by that of the ψ' at a mass of 3.684 GeV.[17] Later came the discovery of the χ states, intermediate in mass between the ψ and the ψ' [18,19]. The χ states were seen indirectly through the process

$$\psi' \rightarrow \gamma\chi,\ \chi \rightarrow \gamma\psi$$

or

$$\chi \rightarrow \text{hadrons}$$

This family of states, connected by radiative transitions, fitted nicely into the charm model which viewed them as radial and orbital excitations of the charmonium atom. The broader resonant structures in the 4 - 4.4 GeV region (see Figure I.3) were seen as higher excitations which were above threshold for decays into charmed meson pairs and thus much wider.

The ψ family of resonances possess what is referred to as "hidden charm" because the positive and negative charm of the c and $\bar{c}$ quarks cancel to give zero net charm. While the charm model's ability to explain the ψ family spectroscopy was impressive, final confirmation of the hypothesis awaited the discovery of mesons or baryons possessing "naked" charm, that is, non-zero net charm. The lowest lying state should be composed of a c quark and a $\bar{u}$ or a $\bar{d}$ quark. These states were named (in advance of their discovery) D^o and D^+.[11] Because charm is conserved in the strong and electromagnetic interactions the D mesons could only decay weakly, which would make them relatively narrow. The preferential coupling of the charmed quark to the strange quark in the weak current would make the D's decay most often into states containing one kaon.

The discovery of a pair of particles with these properties came in the spring of 1976. The D^o was seen as peaks in the mass spectra of $K^-\pi^+$ and $K^-\pi^+\pi^-\pi^+$ combinations produced in electron-positron collisions in the 4.03 GeV resonance region.[20] The D^+ was seen as a peak in the mass spectrum of $K^-\pi^+\pi^+$ combinations in the same center-of-mass energy region.[21] This so-called "exotic" combination of kaons and pions, possessing opposite charge and strangeness, was a clear indication that these particles were of a new type, since *no* quark-antiquark combination of the three old types of quarks could have these quantum numbers. The mass of both these peaks was around 1865 MeV, about 300 MeV more than half the mass of the ψ. This mass is in good agreement with what would be required to explain the rise in R and also with what was needed to resolve the problems with the neutral kaons (see above). Their narrow widths (consistent with the experimental resolution) were also in agreement with the charm hypothesis and would be unexpected if they were strongly decaying resonances composed of old quarks. Thus the charm hypothesis seemed to be fully confirmed.

Subsequent to the initial discovery of the D mesons in the $K^-\pi^+$, $K^-\pi^+\pi^-\pi^+$, and $K^-\pi^+\pi^+$ decay modes several additional decay modes were identified, some in the same experiment and some in the following experiment which formed the basis for this thesis. The additional decay modes observed were $K^o\pi^+\pi^-$ [22] and $K^-\pi^+\pi^o$ [23] for the D^o and $K^o\pi^+$ [25] for the D^+.

B. Goals of This Thesis

The measured branching ratios for the known exclusive decay modes of the D mesons are shown in Table I.2.[25] Their sum is about 20% for the D^o and about 5% for the D^+. Clearly, then, most of the decays of the D mesons have yet to be identified. The remaining decays have not been seen presumably because they are subject to high experimental backgrounds and/or low acceptances which result from high multiplicities and the presence of one or more neutral particles which are hard (π^o's, η's) or nearly impossible (neutrinos) to detect. However, there is much that can be learned by inclusive studies which do not attempt to identify every particle in a D decay but instead look at the frequency of occurence and the momentum spectrum of a particular type of particle in the decays, or correlations between two or more particles. Such an inclusive approach is common in the study of high-energy scattering where it is often virtually impossible to completely identify every final state. With the discovery of the ψ and D mesons we have entered a mass region where the number and complexity of possible final states are comparable to those of scattering experiments of a decade or so ago.

Electron-positron annihilation provides an excellent laboratory for inclusive studies of charmed particle decays. Because the probability of producing a quark-antiquark pair in electron-positron annihilation is proportional to the square of the quark charge we expect that, above the threshold for producing pairs of charmed particles, the fraction of hadronic events which originate from a $c\bar{c}$ pair would be

$$\text{charm fraction} = \frac{(\frac{2}{3})^2}{(\frac{2}{3})^2 + (\frac{2}{3})^2 + (\frac{1}{3})^2 + (\frac{1}{3})^2} = \frac{2}{5}$$

Because annihilation of the c and $\bar{c}$ quarks is suppressed by the OZI rule, almost all of the events which originate from a $c\bar{c}$ pair would be expected to contain a pair of charmed particles. This may be compared with hadron-hadron collisions in which there is a charmed particle pair produced in only about one out of every three hundred events.[26]

The center-of-mass energy determines whether or not charmed particles are produced, what types of charmed particles are produced, and the complexity of the final states which contain charmed particles. Therefore inclusive particle production rates as a function of E_{cm} are sensitive to the decay characteristics of the different species of charmed particles. At one particular

Table I.2

D Meson Decay Branching Fractions

Mode		Fraction
$D^0 \rightarrow$	$K^-\pi^+$	2.2 ± 0.6
	$\overline{K^0}\pi^+\pi^-$	4.0 ± 1.3
	$K^-\pi^+\pi^-\pi^+$	3.2 ± 1.1
	$K^-\pi^+\pi^0$	12.0 ± 6.0
$D^+ \rightarrow$	$\overline{K^0}\pi^+$	1.5 ± 0.6
	$K^-\pi^+\pi^+$	3.9 ± 1.0

center-of-mass energy, the $\psi(3772)$ resonance (see Chapter IV), a particularly clean final state is produced, consisting simply of $D\bar{D}$ pairs nearly at rest. As will be seen, this resonance makes possible the study of D meson decays to states containing kaons and electrons in uniquely unambiguous ways.

In this thesis I present inclusive studies of electrons and kaons in the decays of D mesons. I attempt to address three general areas of questions:

1. What are the inclusive branching ratios of D mesons to states containing kaons? In the GIM model the c quark, with positive charm, couples preferentially to the s quark, with negative strangeness, so we expect the states with positive charm (D^o and D^+) to decay to states with negative strangeness (K^- or $\overline{K^o}$) and vice versa (D^-, $\overline{D^o} \rightarrow$ K^+, K^o). Aside from phase space factors the fraction of decays which contain these "right-sign" kaons should be equal to $\cos^2(\text{theta}_c)$, or 95%. "Wrong-sign" kaons, that is kaons with the wrong strangeness, should be present in only about 5% of D decays. Measurements of inclusive branching ratios to right-sign and wrong-sign kaons can test these predictions of the Glashow-Iliopoulos-Maiani model. In addition, we can investigate the ratio of charged to neutral kaons, for which the GIM model makes no specific prediction.

2. What are the inclusive branching ratios of the D mesons and other charmed particles produced in electron-positron annihilation to states containing electrons? For spinless particles, such as D or F mesons, weak decays to purely leptonic states ($D^+ \rightarrow e^+\nu_e$, for example) are highly suppressed relative to semileptonic and nonleptonic decays, the suppression factor being proportional to m_l^2/m_C^2 where m_l is the lepton mass and m_C is the mass of the charmed particle. Semileptonic decays, such as $D \rightarrow Ke\nu$, do not suffer from this suppression. A very naive model would predict semileptonic branching ratios of 20% each for electrons and muons. The model is as follows: View the decay of a D as the decay of a free charmed quark, followed by a final-state interaction in which the quarks, with the possible addition of quark-antiquark pairs pulled from the "sea" of virtual pairs, recombine to form real hadrons. The c quark decays to an s quark and a virtual W^+ weak boson. The virtual W can then couple to a $u\bar{d}$ quark-antiquark pair of one of three colors, an electron and a neutrino, or a muon and a neutrino. The possible diagrams are shown in Figure I.4. Since the weak isospin of the $u\bar{d}$ pair, the $e\nu$ pair, and the $\mu\nu$ pair are all the same (1), the coupling of the W^+ to each should be the same and the branching ratios should be the same. This would imply that 60% (20% for each color) of the D decays should be purely hadronic, 20% should have an electron, and 20% should have a muon. Things may not be so simple, however. In the weak decays of K mesons there is an "enhancement" factor of about 20 for those purely hadronic decays where the change in total

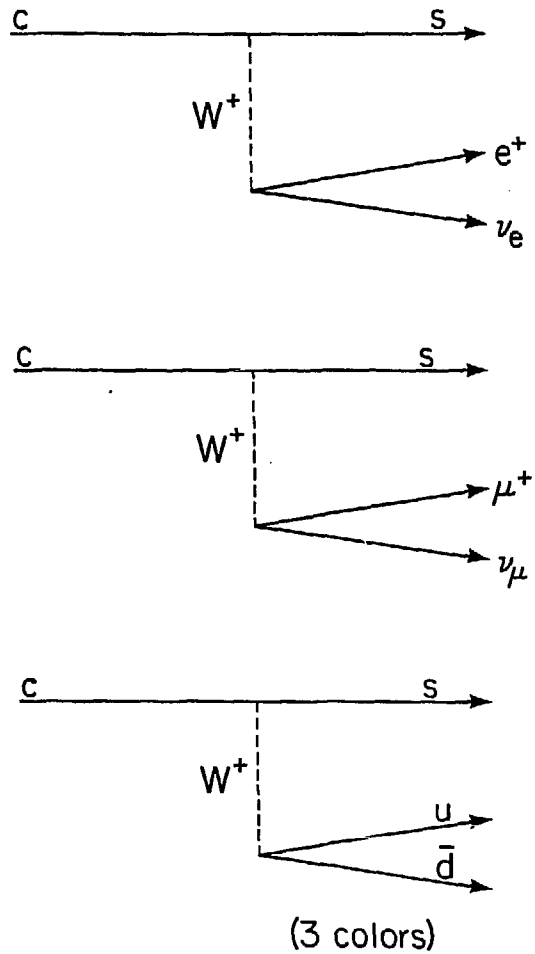

XBL 791-289

FIGURE I.4
Diagrams for the decay of a "free" charmed quark.

isospin is 1/2 (as opposed to 3/2). This effect, known as the "$\Delta I = \frac{1}{2}$ rule" is responsible for the low branching ratio for the decay $K^+ \rightarrow \pi^+\pi^0$. It has been explained in terms of "octet enhancement", that is, enhancement of the octet term in the **8** X **8** product of SU(3) hadronic currents.[27] If there is a similar enhancement in an SU(4) multiplet which contributes to the hadronic decays of the D's then the hadronic decay rates may be much greater than the semileptonic rates and the semileptonic branching ratios may be as low as one or two percent. Therefore, measurement of the semileptonic branching ratios yields indirect information about the hadronic D decays.

3. What are the properties of the multiprong electron-positron annihilation events which contain electrons? Specifically, what is the momentum spectrum of the electrons, what is the charged and neutral kaon content of the events, and what are the momentum correlations between kaons and electrons? It is necessary to ask this group of questions for two reasons. The first reason is related to an experimental problem. There is a competing source of electrons in multiprong electron-positron annihilation events, namely the τ heavy lepton. The momentum spectrum of the electrons and the kaon content of the events are used to show that most of the electrons are indeed from charmed particle decays and to set an upper limit on the contribution from heavy lepton decays. The second reason for investigating the properties of these events is to learn something about the nature of the final states in the semileptonic decays of charmed particles.

References

Chapter I

1. M. Gell-Mann, Physics Letters 8, 214 (1964)

2. M. Gell-Mann, Acta Physica Austriaca Supplement 9, 733 (1972)

3. M. Gell-Mann, Phys. Rev. 125, 1067 (1962);
M. Gell-Mann , Proc. XI Int. Conf. on High Energy Physics, CERN, 1962, p.805;
M. Gell-Mann and Y. Ne'eman, The Eightfold Way (W.A. Benjamin, New York, 1964)

4. M. Breidenbach et al., Phys. Rev. Lett. 23, 935 (1969);
J.D. Bjorken and E.A. Paschos, Phys. Rev. 185, 1975 (1969);
R.P. Feynmann, Photon-Hadron Interactions (W.A. Benjamin, New York, 1972)

5. M.K. Gaillard and B.W. Lee, Phys. Rev. D10, 897 (1974)

6. W.A. Carithers et al., Phys. Rev. Lett. 31, 1025 (1973);
S.H. Aronson et al., Phys. Rev. Lett. 25, 1057 (1970)

7. S.L. Glashow, J. Iliopoulos, and L. Maiani, Phys. Rev. D2, 1285 (1970)

8. A. Litke et al., Phys. Rev. Lett. 30, 1189 (1973);
G. Tarnopolsky et al., Phys. Rev. Lett. 32, 432 (1974)

9. B. Richter in Proc. XVII Int. Conf. on High Energy Physics, London, 1974, p. IV-37

10. N. Cabibbo, N. Parisi, and M. Testa, Lett. Nuov. Cim. 4, 35 (1970)

11. M.K. Gaillard, B.W. Lee, and J.L. Rosner, Rev. Mod. Phys. 47, 277 (1975)

12. J.E. Augustin et al., Phys. Rev. Lett. 33, 1406 (1974)

13. J.J. Aubert et al., Phys. Rev. Lett. 33, 1404 (1974)

14. A. De Rujula and S.L. Glashow, Phys. Rev. Lett. 34, 46 (1975)

15. Thomas Applequist and H. David Politzer, Phys. Rev. Lett. 34, 43 (1975)

16. S. Okubo, Phys. Lett. 5, 165 (1963);
G. Zweig, CERN Report No. 8419/TH 412 (1964), unpublished;
J. Iizuka, Supp. Progress in Theoretical Physics 37-38, 21 (1966)

17. G.S. Abrams et al., Phys. Rev. Lett. 33, 1453 (1974)

18. W. Braunschweig et al., Phys. Lett. 57B, 407 (1975)

19. G.J. Feldman et al., Phys. Rev. Lett. 35, 821 (1975);
J.S. Whitaker et al., Phys. Rev. Lett. 37, 1596 (1976)

20. G. Goldhaber et al., Phys. Rev. Lett. 37, 255 (1976)

21. I. Peruzzi et al., Phys. Rev. Lett. 37, 569 (1976)

22. M. Piccolo et al., Phys. Lett. 70B, 260 (1977)

23. D.L. Scharre et al., Phys. Rev. Lett. 40, 74 (1978)

24. N. Cabibbo, Phys. Rev. Lett. 10, 531 (1963)

25. I. Peruzzi et al., Phys. Rev. Lett. 39, 1301 (1977)

26. G. Coremans-Bertrand et al., Phys. Lett. 65B, 480 (1976);
D. Spelbring et al., Phys. Rev. Lett. 40, 605 (1978);
R. Lipton et al., Phys. Rev. Lett. 40, 608 (1978);
P. Alibran et al., Phys. Lett. 74B, 134 (1978);
T. Hansl et al., Phys. Lett. 74B, 139 (1978);
P.C. Bosetti et al., Phys. Lett. 74B, 143 (1978);
D. Drijard et al., Phys. Lett. 81B, 250 (1979)

27. B.W. Lee, Phys. Rev. Lett. 12, 83 (1964);
M. Gell-Mann, Phys. Rev. Lett. 12, 155 (1964);
S. Okubo, Phys. Lett. 8, 362 (1964)

28. S. Weinberg, Phys. Rev. Lett. 19, 1264 (1967);
A. Salam in Elementary Particle Theory, ed. by. N. Svartholm (Almquist and Wiksell, Stockholm, 1969), p.367

29. R.F. Schwitters, Proc. 1975 Int. Symp. on Lepton and Photon Interactions at High Energies, Stanford, California, p.355, (1975);
P.A. Rapidis et al., Phys. Rev. Lett. 39, 526 (1977)

II. Apparatus

The apparatus for this experiment consisted of the SLAC-LBL Magnetic Detector[1] (Mark I) with the Lead-Glass Wall[2] addition at the SPEAR electron-positron storage ring at the Stanford Linear Accelerator Center (SLAC). The Mark I detector was constructed and in operation several years before the beginning of this experiment and has been described in Ph.D. theses from previous experiments.[3] We present here only a brief description and the parameters relevant to the measurements presented in this thesis. We present a more detailed description of the design, construction, operation, and performance of the Lead-Glass Wall.

A. The Mark I Detector

The SPEAR Mark I Magnetic Detector is a solenoidal spectrometer for studying the products of high-energy electron-positron collisions. An exploded view of the detector is shown in Figure II.1. The geometry is basically cylindrical with the electron and positron beams defining the axis of the cylinder and colliding in the center.

An aluminum solenoid, 1.5 meters in radius and 3 meters long, provides a 4 kG magnetic field parallel to the cylinder axis. The beams are enclosed in a stainless steel vacuum pipe 8 cm in radius. Just outside of the beam pipe are two pairs of hemi-cylindrical scintillation counters ("pipe counters") at radii of 11 and 13 cm. Phototubes are mounted on both ends of each counter.

Following the pipe counters are two cylindrical multiwire proportional chambers and four cylindrical wire spark chambers. The proportional chambers are at radii of 17 and 24 cm and the spark chambers are at radii of 60, 91, 112, and 135 cm.

The proportional chamber wires are parallel to the beam axis and therefore provide azimuthal coordinates. The wire spacing is 2.1 mm and 2.8 mm for the inner and outer chambers respectively. The wires are read out individually. These chambers also have cathode strips for determining longitudinal coordinates by the induced pulses but this information has not been used.

Each of the four spark chambers consists of two gaps, one with wires aligned at $\pm$ 4° with respect to the beam axis and one with wires at $\pm$ 2°. Each chamber therefore provides 2 points for each track. The wire spacing on all four spark chambers is 1.1 mm. The chambers are read out through magnetostrictive wands.

This system of proportional and spark chambers measures directions and momenta of charged particles with transverse momentum greater than about 66 MeV/c in the angular region

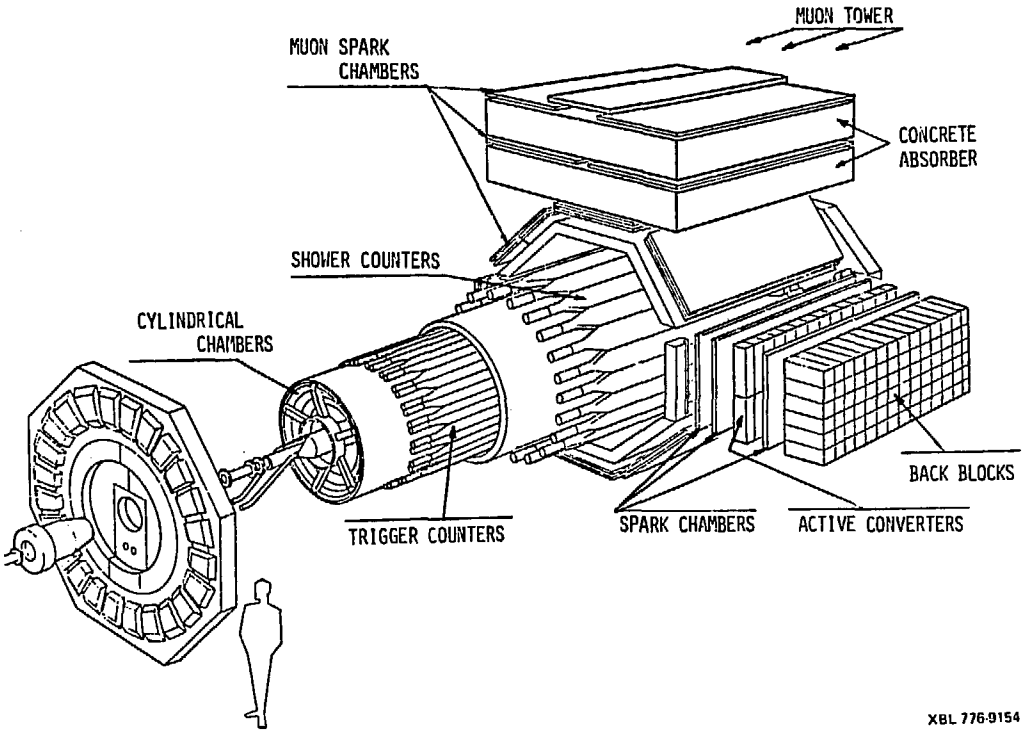

FIGURE II.1

Exploded view of the Mark I detector with the Lead-Glass Wall.

$\cos(\theta) < 0.73$, where θ is the polar angle measured with respect to the beam line. The azimuthal coverage is 100%. The momentum resolution is

$$\left(\frac{\Delta p}{p}\right)^2 = \left(.013\left(\frac{p}{1\ \mathrm{GeV}}\right)\right)^2 + \left(\frac{.006}{\beta}\right)^2$$

where β is a particle's velocity divided by the speed of light.

The first term in the resolution reflects the spatial resolution of the tracking chambers. The second term arises from multiple Coulomb scattering in the detector components.

Just inside the solenoid, at a radius of 1.5 meters, is a set of 48 1" scintillation counters. These counters, called trigger counters, are made from Pilot Y scintillator, which has an attenuation length of 3 meters. Each counter is 23 cm wide by 260 cm long and is viewed at both ends by Amperex 56DVP photomultiplier tubes.

The trigger counters cover 360° of azimuthal angle and they cover polar angles from 50° to 130° ($\cos(\theta) = 0.65$). They are used in triggering the detector and for time-of-flight measurements. Each of the 96 phototubes feeds a discriminator which provides a stop signal to a time-to-digital converter (TDC). The TDC's are started by a signal from an electrode which senses the presence of a beam in the interaction region. In addition, the pulse from each phototube is digitized by an analog-to-digital converter. The information from the ADC is used to correct the TDC outputs for pulse-height dependent effects in the TDC discriminators. After this correction is made, the times from the two phototubes on each counter are averaged to determine the time-of-flight.

Figure II.2 shows the distribution of the measured time-of-flight minus the expected time-of-flight for electrons from the Bhabha scattering reaction $e^+e^- \rightarrow e^+e^-$. The resolution is 0.4 ns.

Just outside the magnet coil is a set of 21 lead-scintillator sandwich shower counters which cover 7/8 of the azimuthal angle. These counters consist of five one-radiation length layers of lead alternating with 5 1/4" sheets of scintillator. They provide crude electron and photon identification. A simple cut on the shower pulse height associated with a track identifies electrons above 650 MeV/c with an efficiency of 89% and a probability for a hadron to be misidentified as an electron of about 20%.

The remaining 1/8 of the azimuthal angle of the detector is occupied by the Lead-Glass Wall, which is described in detail in the next section.

Directly behind the shower counters is the octagonal iron flux return of the magnet. The section of the flux return in the Lead-Glass Wall octant has been removed.

Behind the flux return are spark chambers for muon identification. Above the top octant is the "Tower of Power" consisting of two layers of concrete with spark chambers behind each layer for additional muon identification. Behind the octant opposite the Lead-Glass Wall is the

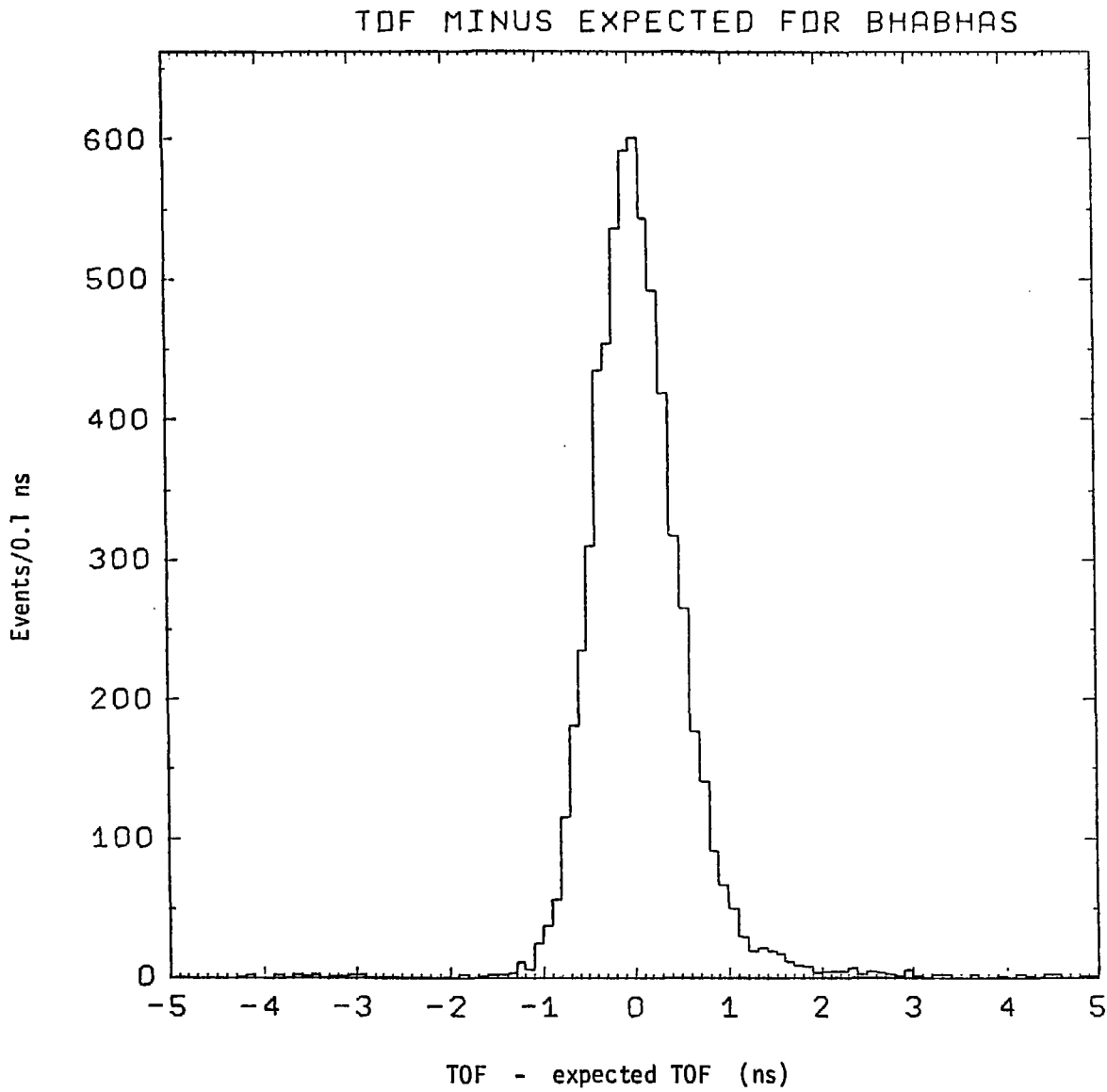

FIGURE II.2

Difference between measured and expected time-of-flight for electrons from Bhabha scattering. The resolution is σ = 0.4 ns.

"minitower" consisting of 30 cm of iron followed by spark chambers, again providing supplemental muon identification.

B. The Lead-Glass Wall

1. Description of the Lead-Glass Wall

In the west octant of the detector the iron flux return panel has been removed and the lead-scintillator shower counters have been replaced by thin scintillators which fill the role of the shower counters in the trigger logic. The Lead-Glass Wall (LGW) is immediately behind these scintillators. Note that the aluminum magnet coil, which is 1 radiation length thick, is between the interaction region of the beams and the Lead-Glass Wall. The cross section of this octant is shown in Figure II.3.

The Lead-Glass Wall is an electromagnetic shower calorimeter consisting of 318 lead-glass Cherenkov shower counters and three wire spark chambers. It covers a solid angle of 0.69 sr.

The lead-glass is in two layers, called the active converters and the back blocks. There are two planar wire spark chambers in front of the active converters and a third between the active converters and the back blocks.

The 52 active converters are each 90 cm tall, 10.8 cm wide, and 10 cm thick (3.3 radiation lengths). They are arranged in two horizontal rows of 26 counters each. The front face of the active converters is 2.23 meters from the beam line. Each active converter is viewed by an EMI 9531R 3.5" photomultiplier tube. The tubes are mounted vertically above the top row and below the bottom row.

The 266 back blocks are each 15 cm by 15 cm in cross section and 32.2 cm thick (10.5 radiation lengths). They are arranged in a matrix of 14 horizontal rows and 19 vertical columns. The front face of the blocks is 2.54 meters from the beam line. Each back block is viewed by an EMI 9618R 5" photomultiplier tube mounted horizontally on the back of the block.

The lead-glass is type F-2.[4] It has a density of 3.6 gm/cm^2, an index of refraction of 1.62, a radiation length of 3.06 cm., and a hadronic interaction length of about 35 cm. The critical energy (dE/dx times radiation length) is 18.4 MeV.

Because the counters were in the fringe fields of the magnet (about 25 gauss for the back blocks and up to 150 gauss for the active converters) it was necessary to have magnetic shields which extended beyond the tube faces. To obtain this geometry, 4"-long cylindrical lucite light pipes were used between the lead-glass and the phototubes. The light pipes had the same diameters as the phototubes. The phototubes were joined to the light pipes with a 1/32" layer of General Electric RTV 615. The light pipes for the active converters were connected to the lead-glass with a 1/16" layer of RTV 615. The light pipes for the back blocks were attached to

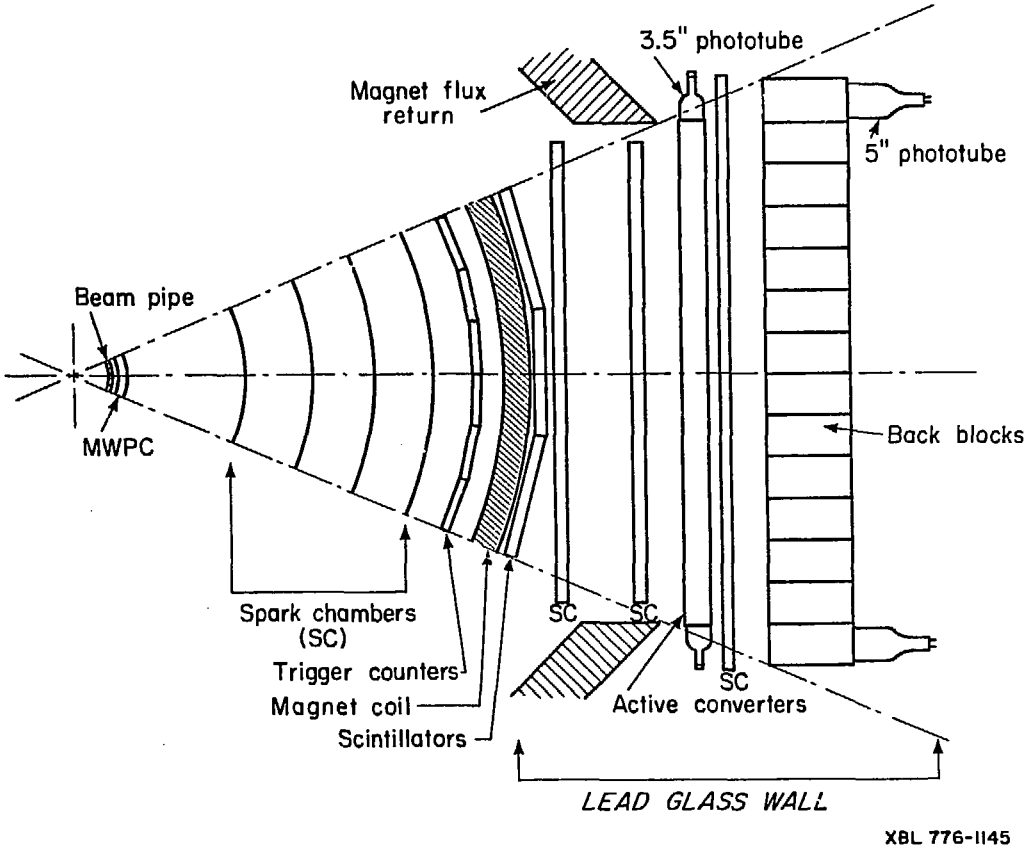

FIGURE II.3
Cross section of the Lead-Glass Wall octant of the Mark I detector.

the lead-glass with optical coupling grease surrounded by an O-ring of Dow Corning RTV 732. A set of springs was employed to press the phototube and light pipe assembly against the back blocks in order to maintain the integrity of the grease joint.

All of the counters were wrapped in aluminized vinyl to make them light-tight.

The anode signals from the phototubes, which have a full width of about 50 nanoseconds and peak currents of the order of 1 mA, are integrated and digitized by a 328-channel Large Scale Digitizer (LSD), developed and built at the Lawrence Berkeley Laboratory.[5] The LSD provides ten-bit accuracy, which we required for sufficient dynamic range, and was designed to reduce cost and complexity by sharing common timing and control signals among a large number of ADC channels. The integration gate width is 300 ns.

2. *Gain Monitoring*

In order to maintain good energy accuracy and resolution it is necessary to monitor the gain of the lead-glass - phototube - ADC system as a function of time. Changes in gain could result from discoloration of the lead-glass, lucite, RTV, or optical grease, air bubbles developing in the grease or RTV joints, change in the gain of the phototube (either cathode quantum efficiency or charge multiplication), or change in the charge conversion gain of the ADC. Changes in tube or ADC gain could result from systematic effects such as a change in the applied high voltage or replacement of a circuit board as well as from random effects.

The most direct way to monitor the gain of the entire system is to measure the response of each counter to a light source of known intensity. For a light source we used a Monsanto MV5352 high-intensity yellow light-emitting diode (LED). This LED was chosen for its brightness, stability, and long life. Although the peak output of the LED is at a lower frequency than the peak sensitivity of the phototubes, it still produces a sufficient amount of light within the sensitive range of the tubes.

Figure II.4 is a diagram of the gain-monitoring system.[7] The LED illuminates a bundle of low-attenuation plastic optical fiber cables (Dupont PFX-0716)[6] which take the light to the 318 counters. This system provides each counter with a light pulse about 300 ns wide with an integrated intensity equal to that from deposition of about 2 GeV of energy in an electromagnetic shower in the counter. The exact intensity of the light varies from counter to counter by as much as a factor of two or three. This is not a problem, however, because the purpose of this system is only to measure changes in gain with time and it is not used to measure absolute gains.

In order to monitor fluctuations in the intensity of the LED itself with time, there are three reference scintillation counters which compare the light from the LED (via fiber optics) with light from sources consisting of Americium-241 diffused in sodium iodide crystals.[8]

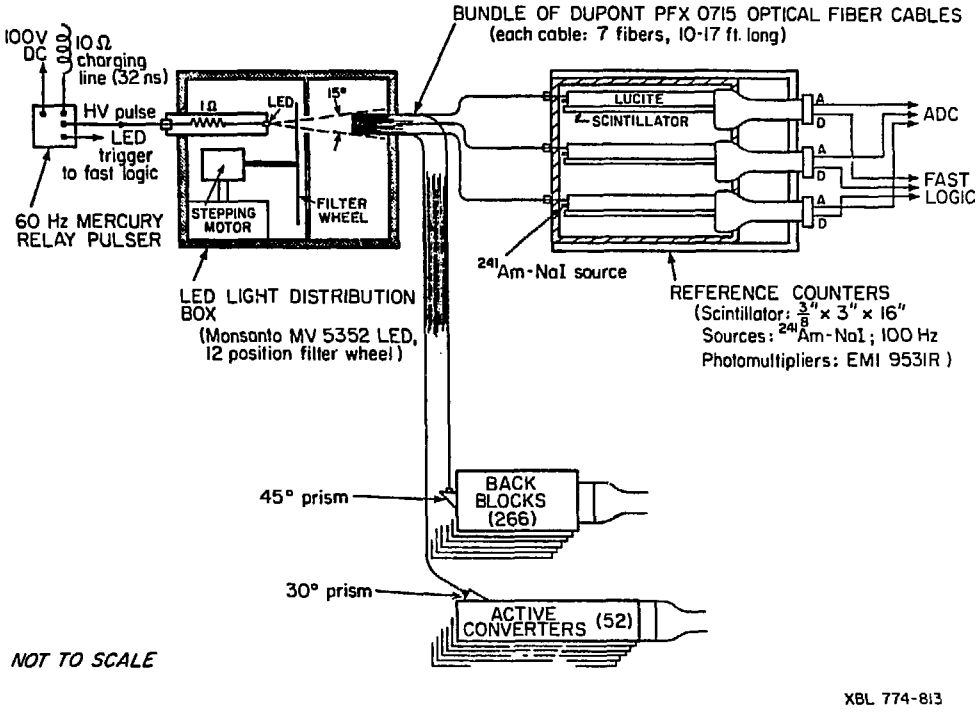

FIGURE II.4

The Lead-Glass Wall gain-monitoring system.

The gains of the counters were monitored once every 8-hour shift. The responses of each of the lead-glass counters and each of the reference counters to the LED and the response of the reference counters to the NaI-Americium sources were recorded. A gain constant was calculated for each counter and recorded. The gain constants were normalized so that they were all equal to 1.0 at the beginning of the experiment. Typical gain variations were a few percent over the lifetime of the experiment and the variations were sufficiently slow so as not to require gain monitoring more than thrice daily. In all of the data analysis all ADC readings from the Lead-Glass Wall were corrected by dividing them by the appropriate gain constants.

In addition to measuring changes in counter gains, the LED system served to bring faulty counters to the attention of the experimenters. This feature was very useful during the first month of the experiment when several counters suffered from loose phototube bases but was not needed after that.

3. Energy Calibration

After correcting for changes in counter gain with time, it is still necessary to determine for each counter the absolute calibration constant which relates the ADC reading to the amount of energy deposited. Americium-NaI sources, like those used on the reference counters, were used to adjust the high voltage on the counters so that the calibration constants would be approximately 5.4 MeV/ADC channel for the back blocks and 3.4 MeV/channel for the active converters.

The final calibration constants were determined by using electron-positron elastic scattering (Bhabha scattering) events. Because the scattering is elastic and the laboratory frame is the center-of-mass frame, these events provide electrons with energy equal to the beam energy, which is known to an accuracy of 1 MeV.

The following criteria were used to select Bhabha scattering events:

1. There are two and only two tracks forming a vertex at the intersection region (see Chapter III).
2. The measured momentum of each of the two tracks is greater than half of the beam energy.
3. The two tracks are collinear within ten degrees.
4. One of the tracks points toward the LGW and the intersection of that track with the front face of the back blocks is at least 10.5 cm (0.7 blocks) from any edge of the wall.
5. The shower pulse height in the Mark I shower counters for the track opposite the Lead-Glass Wall is consistent with that expected for an electron and inconsistent with that expected for a muon.

6. The energy deposited in the Lead-Glass Wall, as measured using the approximate calibration constants of 5.4 Mev/channel for the back blocks and 3.4 MeV/channel for the active converters was greater than 0.8 GeV and less than 5.0 GeV.

Data from the Fall, 1976 high energy (E_{beam} = 3.2 - 3.7 GeV) running was used for the calibration. 5144 events were found that met the above criteria.

Each event provides an equation of the form:

$$\sum_j P_{ij} C_j = E_i$$

where P_{ij} is the gain corrected ADC reading from the j'th counter in the i'th event, E_i is the beam energy for that event, and the C's are the 318 unknown calibration constants.

In principle the sum extends over all of the active converters and all of the back blocks. In practice the sum is taken only over a group of active converters and back blocks centered around the projected track. The algorithm for defining this group is described in the electron identification section of Chapter III.

Since we have 5144 equations in 318 unknowns, an exact solution is not possible. Instead we seek a least squares solution to minimize the quantity

$$\chi^2 = \sum_i (E_i - \sum_j P_{ij} C_j)^2$$

Differentiating with respect to the C's and setting the derivatives to zero we find

$$\sum_{ij} P_{ki}^T P_{ij} C_j = \sum_i P_{ki}^T E_i$$

or, expressed in matrix form

$$A\,C = B$$

where A_{kj} is equal to the sum over all events of the ADC reading from counter k times the ADC reading from counter j and B_k is the sum over all events of the ADC reading from counter k times the beam energy.

This is a system of 318 linear equations in 318 unknowns. Because cut (4) above resulted in an absence of any data in the active converters at the end of each of the two rows, the calibration constants for these four counters were fixed at 3.4 MeV/channel while the calibration constants for the remaining counters were found by solution of the slightly reduced system of 314 equations in 314 unknowns. The solution took about 30 seconds using the LINSYS software package on the SLAC IBM Triplex system.

Histograms of the calibration constants for the active converters and the back blocks are shown in Figures II.5 and II.6. The averages are 3.6 MeV/channel for the active converters

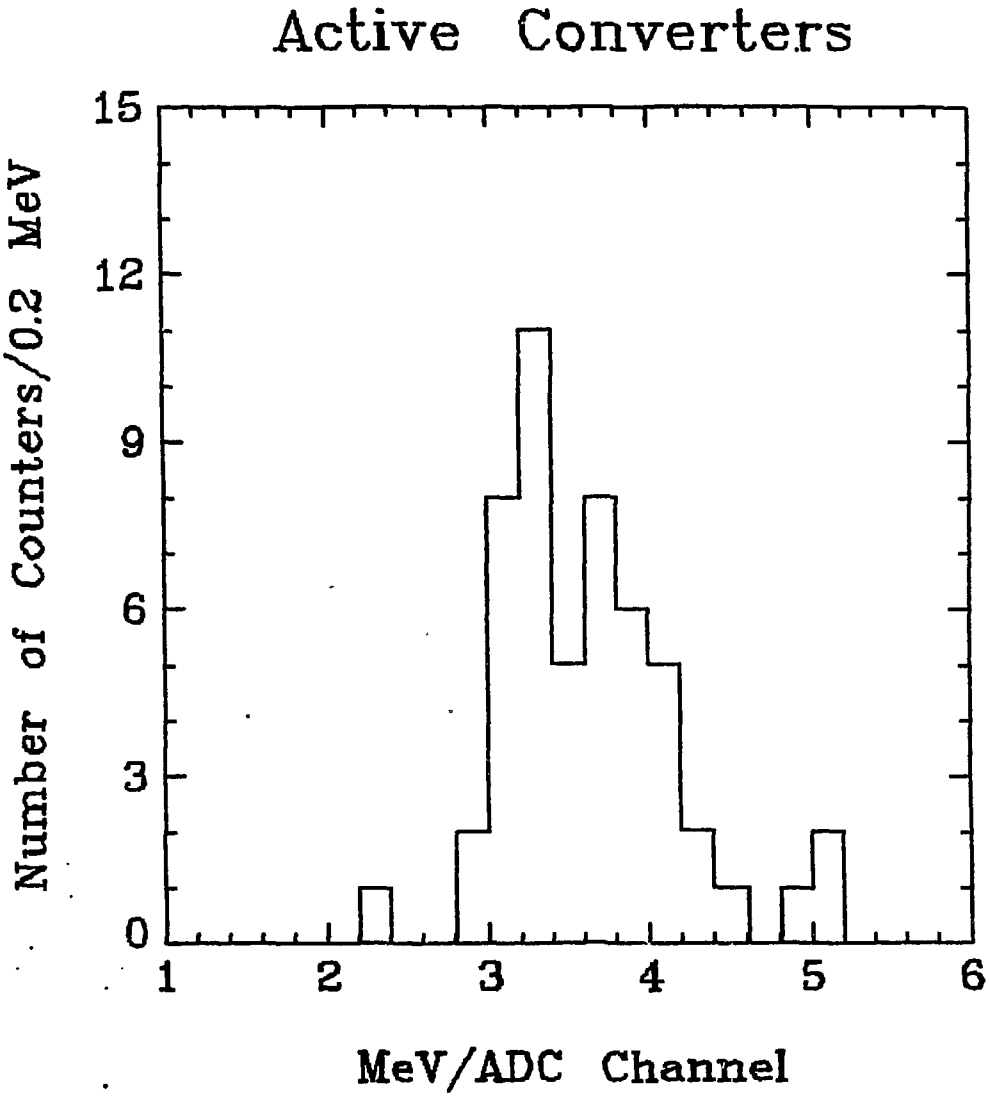

FIGURE II.5
Active converter calibration constants.

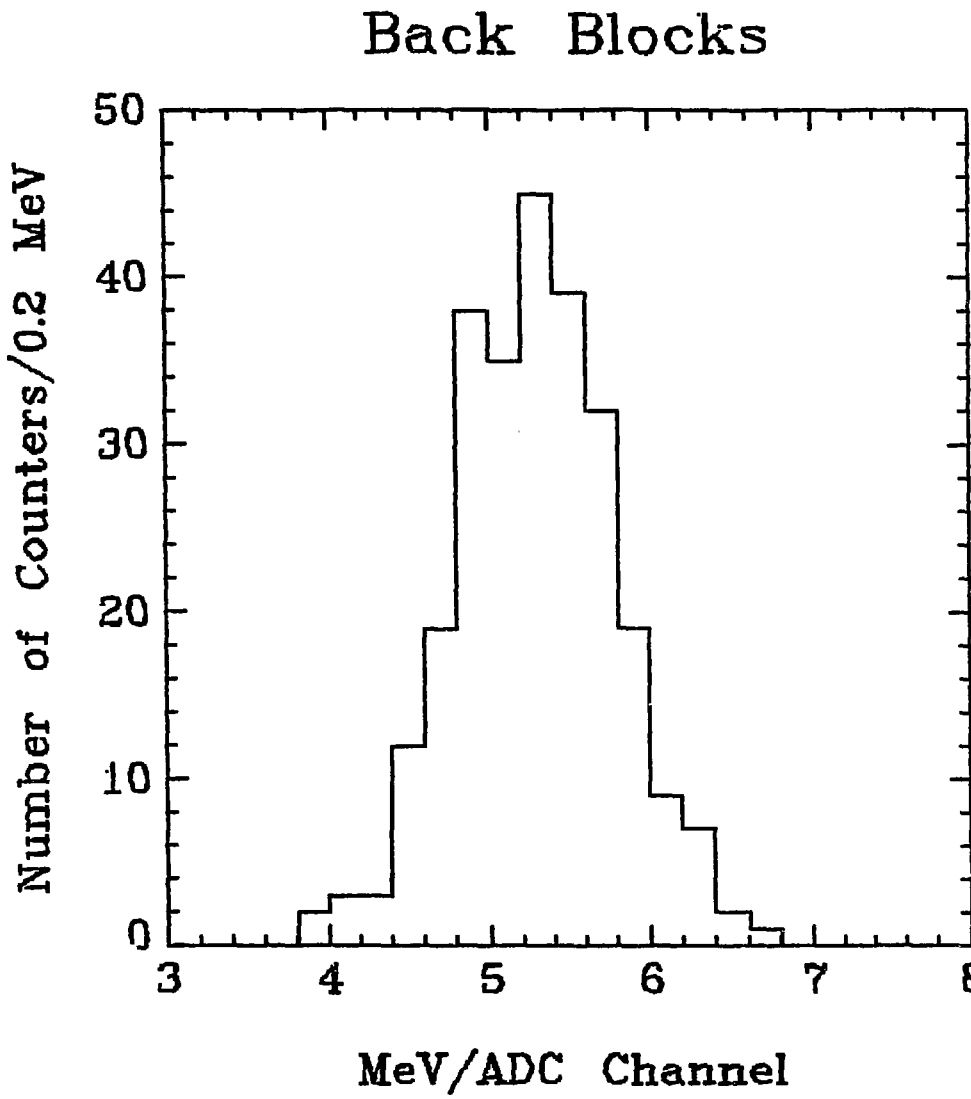

FIGURE II.6

Back block calibration constants.

and 5.3 MeV/channel for the back blocks. The FWHM is about 0.8 MeV/channel for the active converters and 1 MeV/channel for the back blocks. This indicates that our attempt to standardize the counters initially by adjusting the high voltages had an rms accuracy of about ten percent.

Figure II.7 shows the distribution of the measured energy in the LGW divided by the beam energy for the Bhabha scattering events in the high-energy data using the approximate calibration constants of 5.4 and 3.4 MeV/channel. Figure II.8 shows the same distribution using the fitted calibration constants. There is about a 30% improvement in the resolution, from a full width at half maximum (FWHM) of 17% to a FWHM of 11.5%. Events for these plots were selected using the same criteria as for the calibrattion except that cut number (6) was not applied.

In order to check the accuracy of the calibration, the procedure was repeated on two subsets of the high energy data, with each subset comprising about half of the data. Then the two sets of calibration constants were compared. The rms difference was about ten percent. This would indicate that the rms error in each of the two calibrations was $10\%/\sqrt{2}$. The actual calibration used twice as much data as these two subsets so one would expect that its error would be smaller by about another factor of $\sqrt{2}$. We therefore estimate that the calibration is accurate to about five percent.

We note that this does not imply that errors in calibration contribute five percent to the ultimate energy resolution of the LGW since in general an electron or a photon will deposit energy in more than one counter and random calibration errors will tend to be reduced by a factor of one over the square root of the number of counters sharing the energy.

4. Energy Resolution

The energy resolution of the Lead-Glass Wall is limited by the presence of the 1 radiation length aluminum magnet coil in front of it. Energy losses in the coil degrade the resolution. In tests with a subset of the LGW in an electron beam, we found that the resolution could be approximately described by the function $\sigma_E/E = 5\%/\sqrt{E}$ [9], E in GeV, without the presence of the aluminum and $\sigma_E/E = 9\%/\sqrt{E}$ with 1 radiation length of aluminum in front of the lead-glass. Subsequently, we found we were able to reproduce this resolution with the entire LGW under actual running conditions over a period of nine months, from October 1976 through June 1977.

The average energy for the events in Figure II.8 is about 3.45 GeV. σ_E/E is 4.9%, in agreement with $9\%/\sqrt{E}$. Figure II.9 shows the same distribution (measured energy/beam energy) for Bhabha scattering electrons with an energy of 1.89 GeV from data taken in May and June, 1977. The resolution is $\sigma_E/E = 6.7\%$, again in agreement with $9\%/\sqrt{E}$.

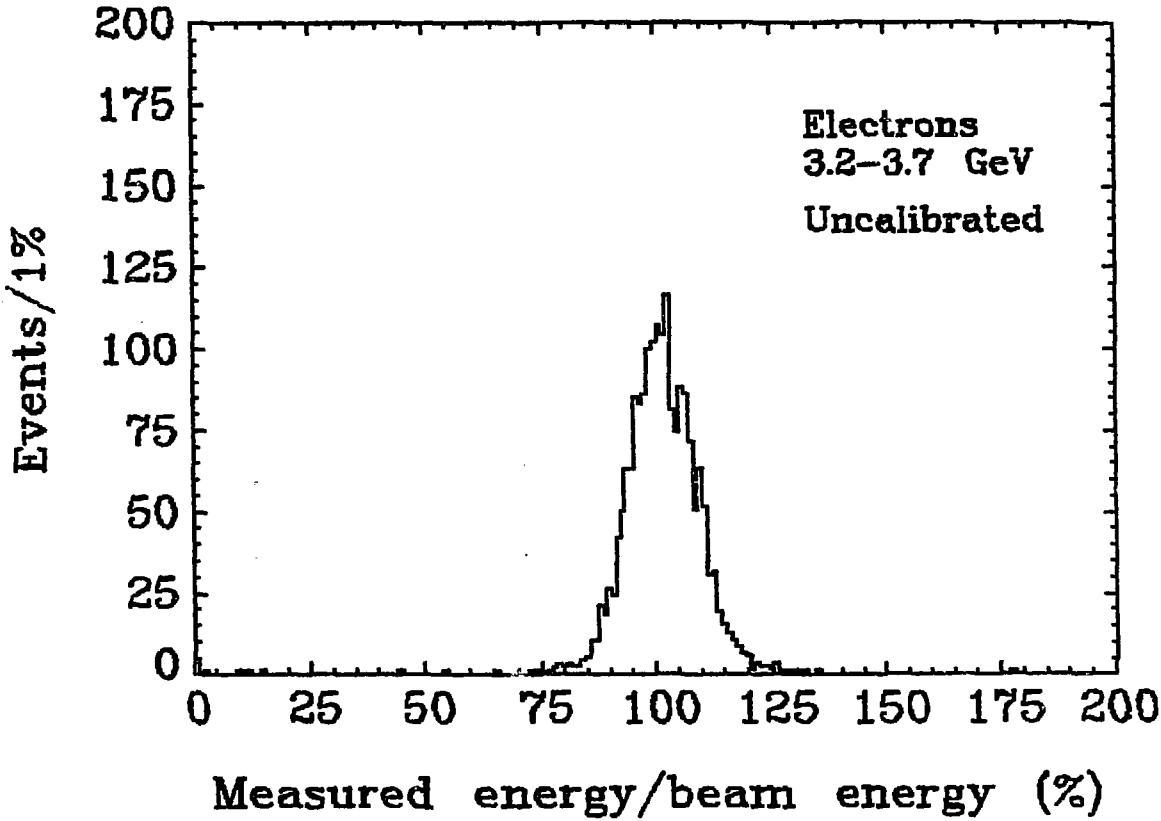

FIGURE 11.7

Measured energy divided by beam energy for 3.2-3.7 GeV electrons using fixed calibration constants.

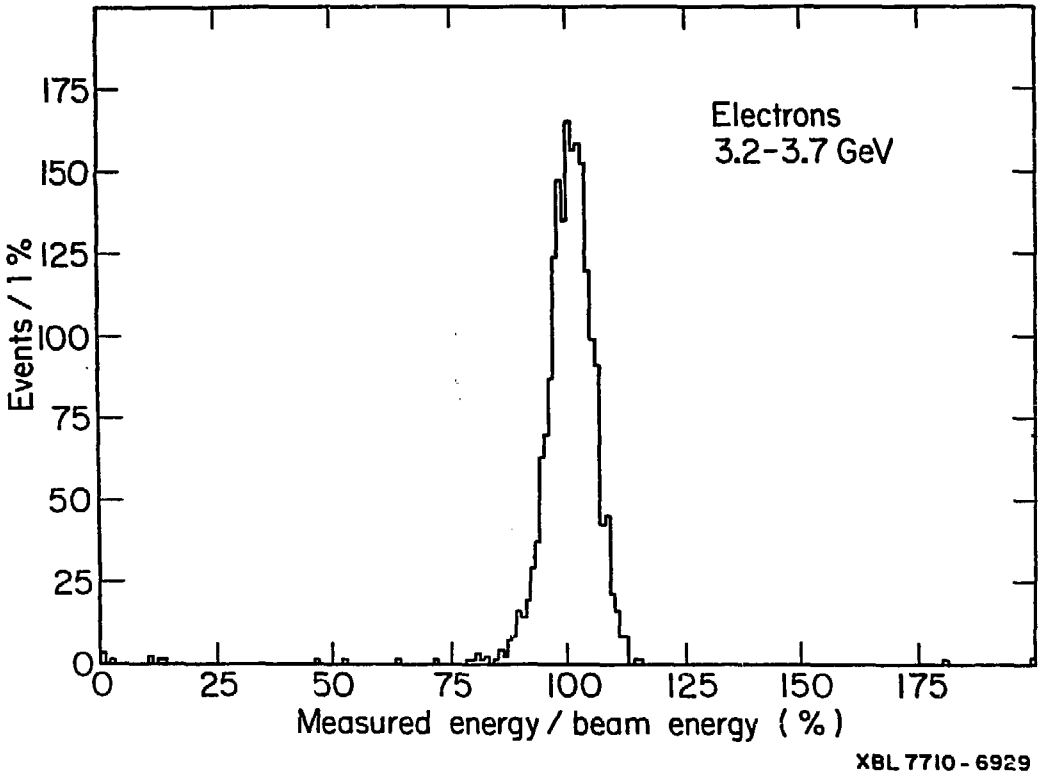

FIGURE II.8

Measured energy divided by beam energy for 3.2-3.7 GeV electrons using fitted calibration constants. The resolution is $\sigma_E/E = 4.9\%$

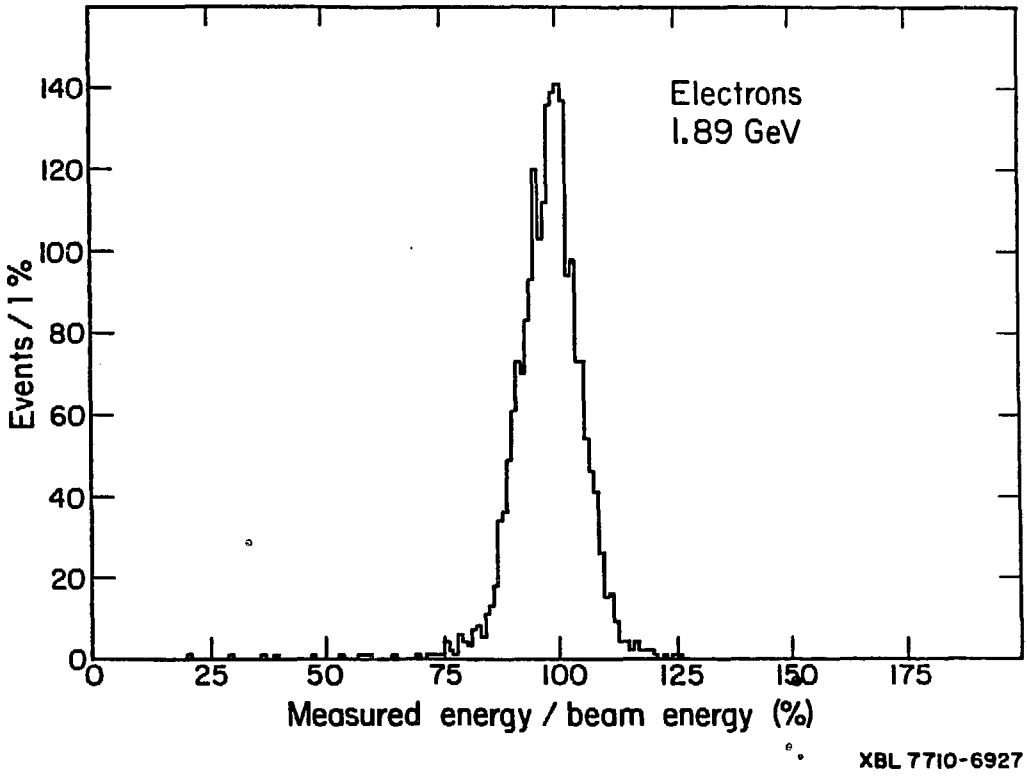

FIGURE II.9

Measured energy divided by beam energy for 1.89 GeV electrons using fitted calibration constants. The resolution is $\sigma_E/E = 6.7\%$

Figure II.10 shows the resolution as a function of energy for all of our data from 1.55 to 3.7 GeV. The fact that the resolution is no worse than the $9\%/\sqrt{E}$ found in the test beam demonstrates that errors in calibrating such a large number of counters did not contribute significantly to the resolution.

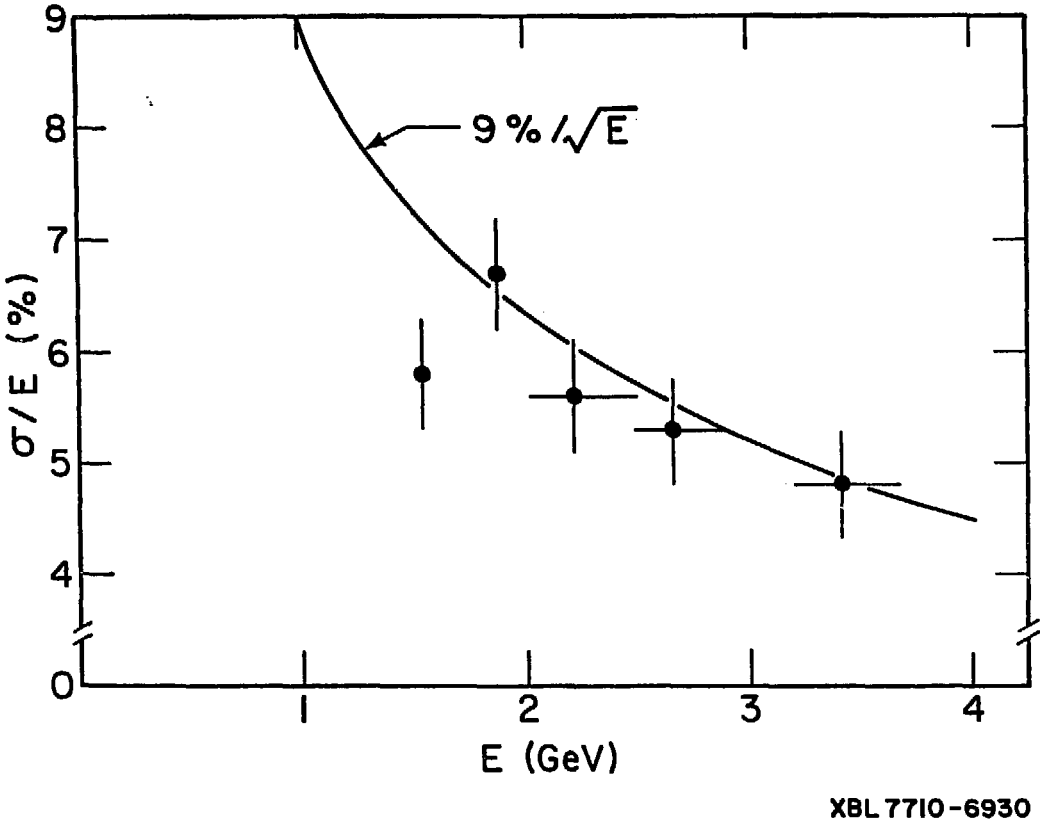

FIGURE II.10
Energy resolution of the Lead-Glass Wall as a function of electron energy.

References

Chapter II

1. F. Vannucci et al., Phys. Rev. D15, 1814 (1977)

2. J. M. Feller et al., IEEE Trans. Nucl. Sci. NS-25, 304 (1978)

3. R. Hollebeek, Ph.D. Thesis, Lawrence Berkeley Lab. Report LBL-3874 (1975);
J.E. Zipse, Ph.D. Thesis, Lawrence Berkeley Lab. Report LBL-4281 (1975);
J.S. Whitaker, Ph.D. Thesis, Lawrence Berkeley Lab. Report LBL-5518 (1976);
J.E. Wiss, Ph.D. Thesis, Lawrence Berkeley Lab. Report LBL-6725 (1977)

4. Schott Optical Glass, Inc., Duryea, Pennsylvania

5. R.F. Althaus et al., IEEE Trans. Nucl. Sci. NS-24, 408 (1977)

6. E.I. duPont de Nemours and Company, Plastics Department, Wilmington, Delaware

7. Ronald J. Madaras, Barrie Pardoe, and Ruben Pecyner, Nucl. Inst. Meth. 160, 263 (1979)

8. Harshaw Chemical Company, Solon, Ohio

9. Because the measured energy distributions have non-Gaussian tails the following two algorithms were used to measure the resolution:
   a. Take the full width at half maximum and divide by 2.355
   b. Take the width required to include 68.3% of the data.
   The resolutions quoted are the average of these two statistics.

III. Data Analysis

A. Trigger and Track Reconstruction

The two-charged particle trigger and the track reconstruction programs for the SPEAR Mark I detector have been adopted virtually unchanged for this experiment. Two new triggers, dependent upon the deposition of energy in the Lead-Glass Wall by neutral particles, were added but events from these triggers were not used in the measurements presented in this thesis. The trigger and track reconstruction algorithms are extensively discussed in four previous Ph.D. theses[1], so we give only a brief description here.

The two-charged particle trigger requires a coincidence between a signal from a pickoff electrode indicating the presence of a beam in the intersection region, signals from corresponding members of both pairs of hemi-cylindrical pipe counters, and two "TASH"'s, where TASH stands for Trigger and Associated SHower counter. A TASH consists of a signal in a trigger counter in coincidence with a signal from the shower counter behind it. In the Lead-Glass Wall octant of the detector the scintillation counters in front of the LGW replace the shower counters in the trigger logic. A typical trigger rate is about 1/second.

For each trigger the pipe, trigger, and shower counter latches, proportional chamber latches, spark chamber wand digitizers, trigger and shower counter ADC's, trigger counter TDC's, and Lead-Glass Wall ADC's are read out and recorded on magnetic tape. This constitutes the raw data of the experiment.

The track reconstruction algorithms are described in detail in the Ph.D. thesis of Dr. Robert Hollebeek.[1] Briefly, hits on at least two intersecting wires in one spark chamber are required to define a point. (This requirement was increased to three wires when the center-of-mass energy was greater than 6 GeV.) Points on three spark chambers are required to define a track. The tracks are divided into two groups, "primary" and "secondary". Primary tracks are defined as those tracks which approach within 15 cm of the beam axis and whose longitudinal (z) coordinate at the point of closest approach to the axis is less than 60 cm. Primary tracks are known as "prongs" and any reference to "prongs" in this thesis refers to primary tracks.

A primary vertex is found by fitting the primary tracks under the constraint that they come from a common origin. The vertex thus determined is required to be within 4 cm of the beam line radially and within 40 cm of the intersection point longitudinally. (For anomalous electron production measurements a more restrictive cut on the longitudinal position of the vertex was

applied. See section C below.)

B. Kaon Identification

1. Charged Kaons

Charged kaons are identified by their time-of-flight from the interaction region to the trigger counters. The path length varies from 1.5 meters for tracks at 90 degrees to about 2 meters for tracks at 50 degrees. (There is some momentum dependence in the path length. These figures are the lower limits approached by high-momentum tracks.) The average path length is 1.66 meters. The time resolution is 0.4 ns (see Chapter II).

We identify charged kaons with momentum less than 1 GeV/c. Figure III.1 shows the expected time-of-flight in a 1.66 meter flight path for pions, kaons, and protons as a function of momentum. At 1 GeV/c protons are separated from kaons by 1.4 ns, or 3.5 standard deviations, but pions are separated from kaons by only about 0.6 ns, or 1.5 standard deviations. So our primary problem is to distinguish kaons from pions.

In order to find the number of kaons we use a fitting procedure which makes optimal use of the time-of-flight information and also provides an estimate of the error arising from pion-kaon ambiguity as well as the statistical error.

We denote by T the measured time-of-flight for a charged particle. We denote by T_K and T_π the time-of-flight expected under the hypothesis that the particle is a kaon or a pion, respectively. T_K and T_π are functions of the momentum and the pathlength:

$$T_K = l\frac{\sqrt{p^2+m_K^2}}{pc}$$

$$T_\pi = l\frac{\sqrt{p^2+m_\pi^2}}{pc}$$

where p is the momentum, l is the pathlength, m_K and m_π are the kaon and pion masses, and c is the speed of light.

We define the quantity

$$d(p,l) = T_K(p,l) - T_\pi(p,l)$$

d(p,l) is the expected time of flight difference between a kaon and a pion. It depends only on the momentum and the pathlength of the particle. For any momentum and pathlength it characterizes how well kaons and pions can be separated. It is a decreasing function of the momentum and an increasing function of the pathlength. Figure III.2 is a scatter plot of d(p,l) versus momentum for a typical sample of tracks. The spread in d(p,l) for a fixed value of the

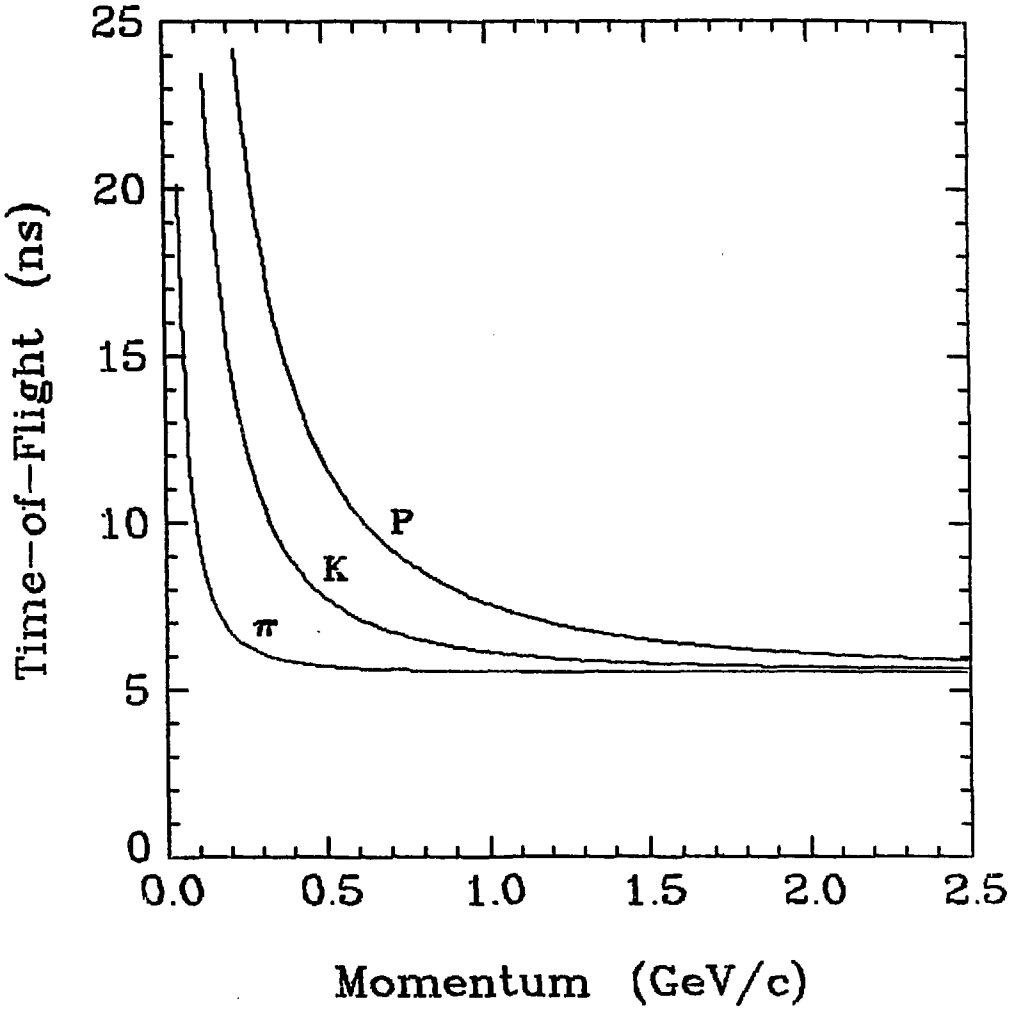

FIGURE III.1

Average expected time-of-flight for pions, kaons, and protons as a function of momentum.

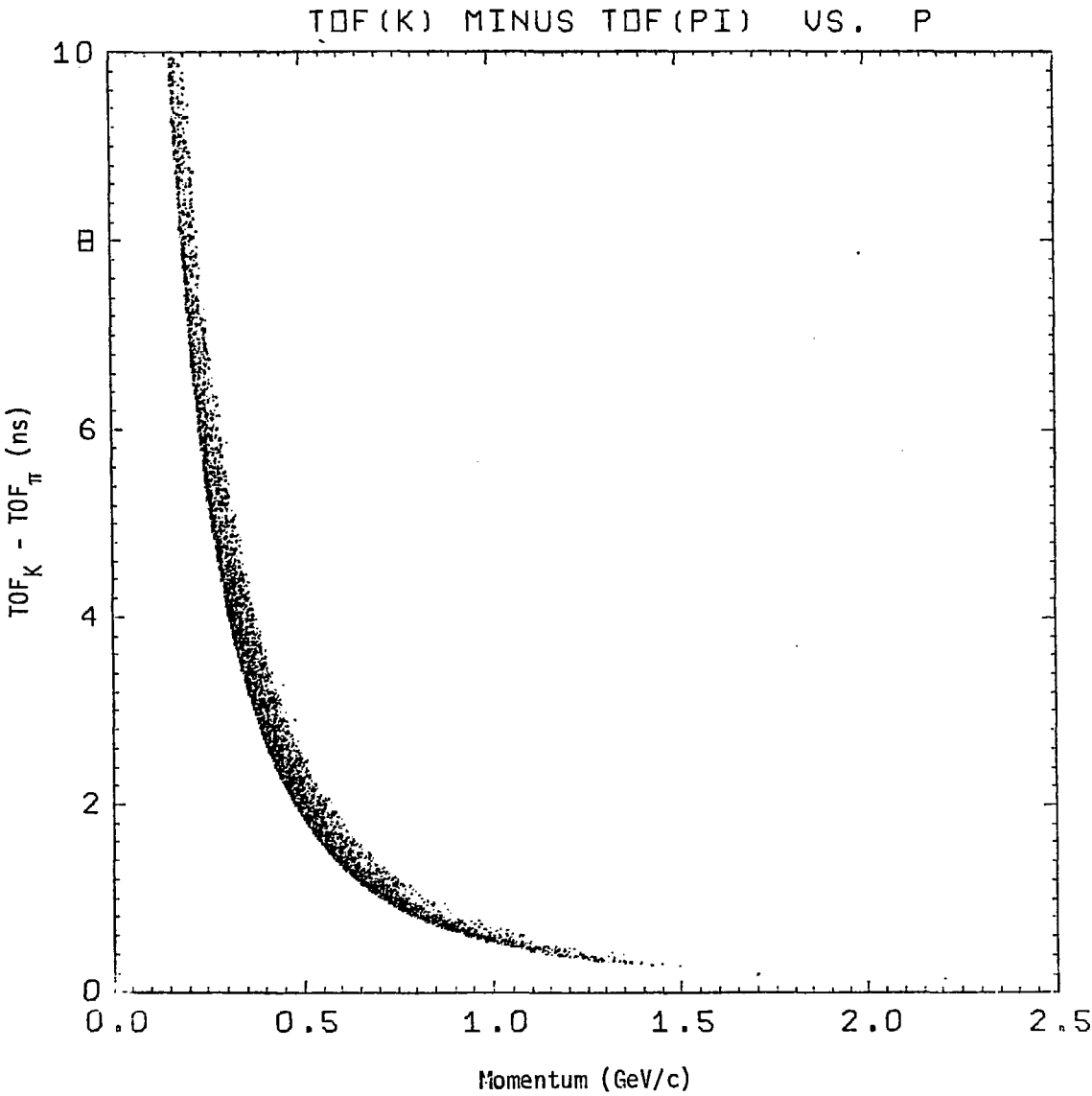

FIGURE III.2

Scatter plot of expected time-of-flight difference between kaons and pions vs. momentum.

momentum results from the spread in pathlengths.

If we make a plot of the quantity (T_K - T) for all tracks we would expect the kaons to form a Gaussian centered at zero. For a fixed momentum and pathlength the pions would form a Gaussian centered at d(p,l). However, if particles with different pathlengths and momenta were included in the same plot then the pions would occupy a broad region of the plot, their distribution being the sum of many Gaussians.

Therefore, we divide the data into 0.2 ns wide bins based on d(p,l). (Note that the bin width is half of the time-of-flight resolution.)

If we then plot the spectrum of (T_K - T) for all the tracks in one d(p,l) bin we expect the kaons to form a Gaussian centered at zero and we expect the pions to form a Gaussian centered at T_K - T = d(p,l). Both Gaussians should have an rms width of 0.4 ns; the 0.2 ns bin width in d(p,l) makes a negligible contribution.

We can then determine the numbers of kaons and pions by fitting the distribution to the sum of two gaussians. A separate fit is done for each bin in d. The means and widths of the two Gaussians are known. The only fitted parameters are the heights of the two Gaussians, i.e., the numbers of kaons and pions.

In order to eliminate background from protons we only fit that part of the spectrum for which T_K - T is > - 1.0 ns. This cut excludes less than 1% of the kaons at all momenta but it excludes 84% of the protons at 1 GeV/c and more than 99% of the protons at 800 MeV/c. Since the number of protons and antiprotons produced per event is roughly 0.1, we expect a background of less than 0.01 kaons per event from misidentified protons. This background is negligible compared to our signal.

Figure III.3 is a typical T_K - T distribution for d(p,l) = 1.8 - 2.0 ns. The fitted curve is superimposed.

The number of charged kaons determined from a fit to a T_K - T spectrum must be corrected for kaon decay in flight, the solid angle of the detector, tracking efficiency, and efficiency of the time-of-flight system, to determine the actual number of charged kaons produced. These four corrections are discussed here. (For the measurements presented in Chapter VIII there is also a trigger efficiency correction. That correction is discussed there.) Each correction is expressed as an efficiency, less than 1.0, by which the fitted numbers must be divided to obtain the produced numbers. (This is the definition of efficiency used throughout this thesis.) The total correction factor is the product of the individual corrections.

1. Decay in flight. $c\tau$ for a charged kaon is 3.71 meters, so a significant fraction of the charged kaons with momentum less than 1 GeV/c will decay in the 1.5-2.0 meter flight path from the interaction region to the trigger counters. If a kaon decays the decay can produce a kink in the track such that the tracking algorithms do not find the track or so that the

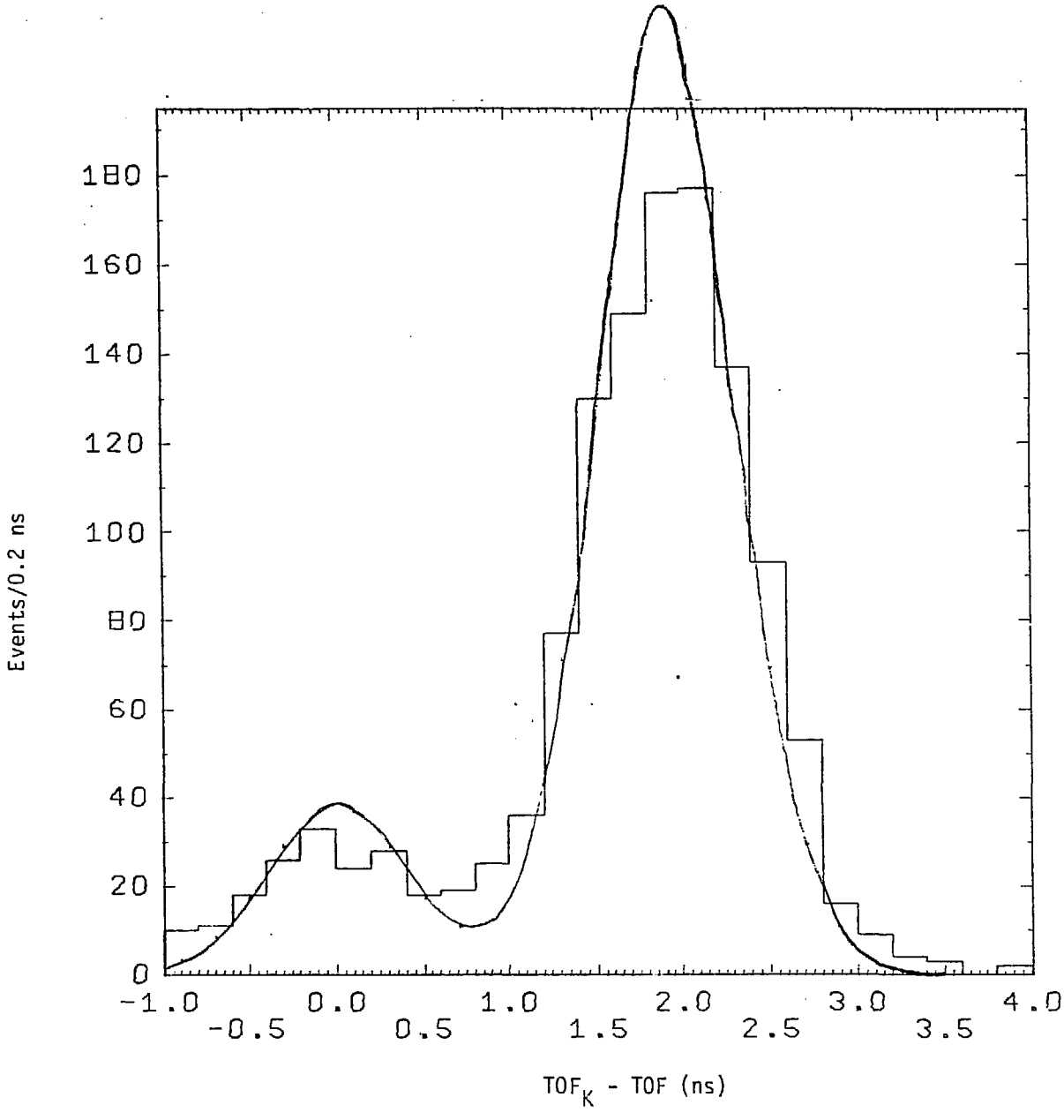

FIGURE III.3
A typical time-of-flight spectrum with fitted curve superimposed.

momentum or pathlength is mismeasured if the track is found. The charged secondary from the decay may not cross the same trigger counter as the projected track or the time-of-flight may be changed because the secondary has a different speed than the kaon. Any of these effects can cause the kaon to be missed by our kaon-counting procedure. To evaluate the loss precisely would require a Monte Carlo program which decayed kaons in the detector, propagated the charged secondaries, created sparks, attempted to fit single tracks to the sparks from the kaons and the secondaries, calculated the time from the production of the kaon to the arrival of the secondary at the trigger counter, and then fitted the resultant time-of-flight spectrum in the manner described above.

Instead, the decay correction was estimated by making a simple assumption. Clearly, any kaon which decayed after traversing the trigger counters would not be lost. A kaon which decayed before getting halfway to the trigger counters (a radius of 75 cm, between the first and second spark chambers) would have a very high probability of being lost. Even if the track were found and the momentum correctly measured and even if the secondary hit the right trigger counter, the measured time-of-flight would be closer to that expected for a pion than that expected for a kaon because the muon or charged pion from the decay would usually be very relativistic. We therefore split the difference between halfway and all the way to the trigger counters and assume that any kaon which decayed before getting 3/4 of the way to the trigger counters (a radius of 112.5 cm, just beyond the middle of the third spark chamber) would be lost and any kaon that decayed after getting 3/4 of the way to the trigger counters would be found. Figure III.4 shows the decay efficiency, that is, the fraction of kaons not lost due to decay in flight under this assumption, as a function of momentum for an average pathlength to the trigger counters of 1.66 meters. The average correction is around 0.75. (The average correction would be 0.68 if 3/4 of the way were changed to all of the way and the average correction would be 0.82 if it were changed to halfway.)

2. Solid angle. The geometrical solid angle of the Mark I detector for tracking charged particles is 0.73 x 4π sr. This is the value which was used in calculating the D to K inclusive branching ratios presented in Chapter V. In the kaon-electron correlation measurements presented in Chapter VII the solid angle correction and the event acceptance correction are correlated so the solid angle correction for those measurements is discussed separately in that chapter.

Note that the solid angle covered by the trigger counters is smaller than that covered by the spark chambers. This difference is accounted for in the correction for the efficiency of the time-of=flight system (correction 4).

3. Tracking efficiency. The tracking efficiency of the Magnetic Detector and its associated software was measured by the original SLAC/LBL collaboration by hand scanning a sample of

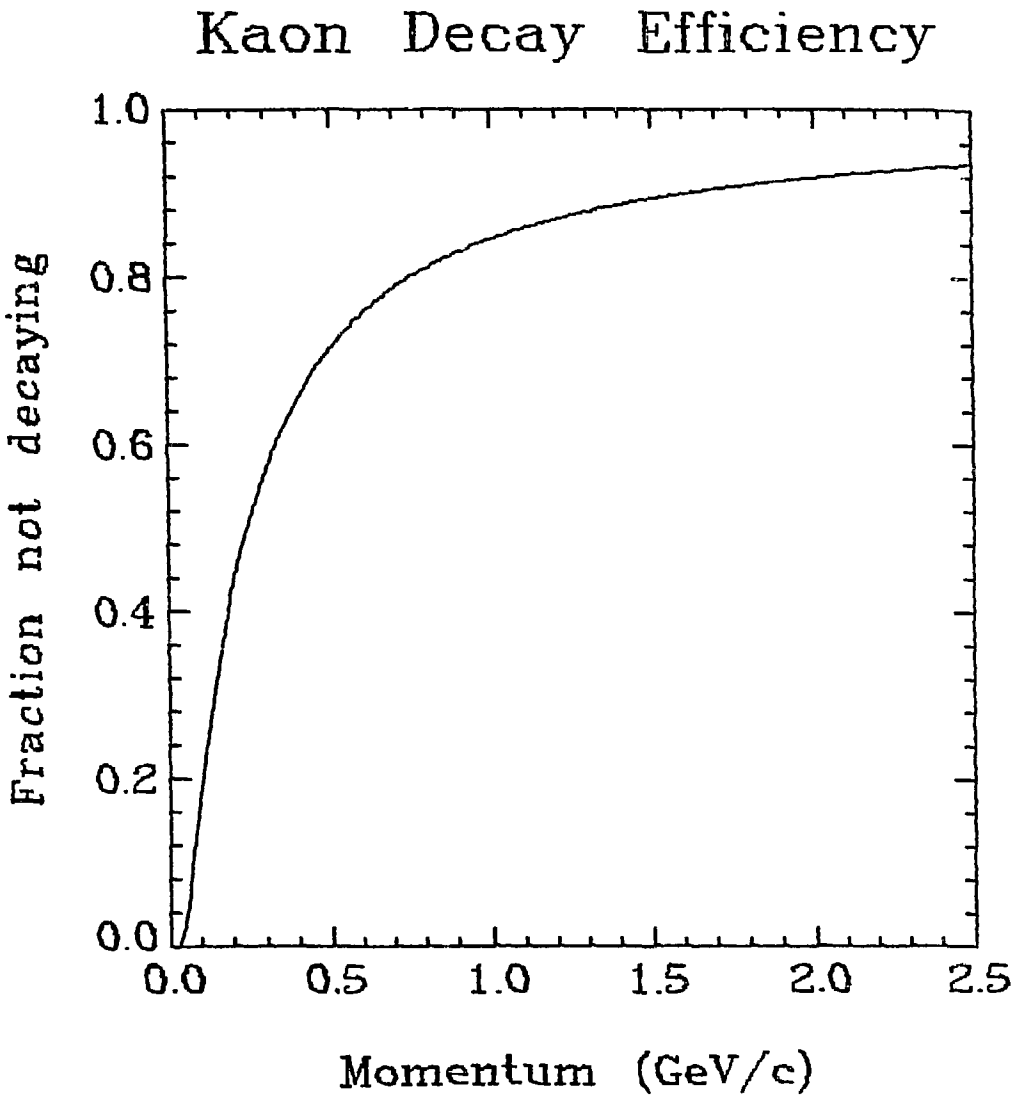

FIGURE III.4
Kaon decay efficiency as a function of momentum.

events and seeing what fraction of the tracks found in this scan were successfully identified by the computer tracking programs. The efficiency was found to be 0.98.

4. Efficiency of the time-of-flight system. If a track fails to fire a trigger counter discriminator for any reason, or if two tracks cross the same trigger counter, then there will not be a valid time-of-flight measurement. In order to eliminate tracks without good TOF measurements the longitudinal (z) coordinate of the track at the trigger counter radius was calculated by comparing the times from the two phototubes on opposite ends of the counter. If this coordinate was not within 40 cm of the projected track then the track was rejected. The efficiency of this cut was determined empirically by seeing what fraction of all tracks failed it. The efficiency was measured separately for each of the charged kaon measurements presented. The efficiency was typically 0.80 - 0.85, depending slightly on the multiplicity.

2. Neutral Kaons

Neutral kaons were identified in the decay mode $K_S^o \rightarrow \pi^+\pi^-$ by looking at the invariant mass spectra of opposite-charge pairs of particles under the assumption that they were pions. A program written by Francois Pierre was used to find the intersection in the x-y plane, or, lacking an intersection, the point of closest approach to each other, of every pair of tracks and to calculate the four-momenta of the two tracks at that point and the total four-momentum of the pair.

Pairs of oppositely charged tracks that met the following criteria were considered as candidates for K_S^o's:

1. The opening angle between the two tracks was at least 0.1 radians (5.73 degrees). This cut was used to eliminate electron-positron pairs from photon conversions.

2. The angle between the total vector momentum of the pair and a vector pointing from the origin to the intersection point was less than 0.61 radians (35 degrees).

3. The neutral track extrapolated back from the intersection point passed within 0.5 cm of the beam line.

The last two cuts insured consistency with the hypothesis that the pair of tracks came from the decay of a neutral particle produced at the origin.

For all pairs that met the above criteria the invariant mass of the pair was calculated under the assumption that both particles were pions:

$$m^2 = (E_1 + E_2)^2 - (p_1^2 + p_2^2 + 2p_1p_2\cos(\theta_{12}))$$

A typical mass distribution is shown in Figure III.5. The K^o peak is clear. In order to select K^o's we take a band between .48 and .52 GeV.

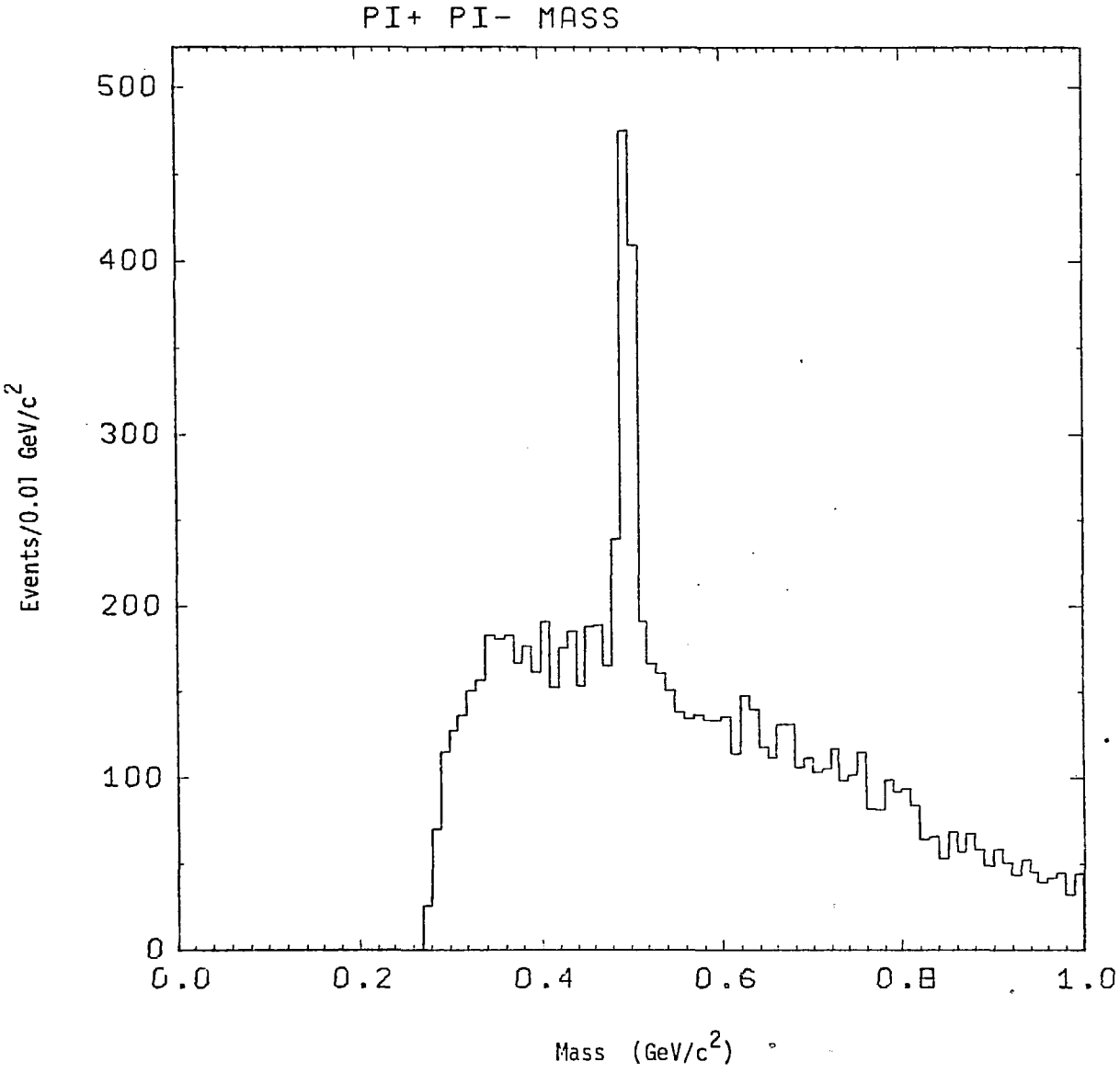

FIGURE III.5

A typical $\pi^+\pi^-$ mass distribution.

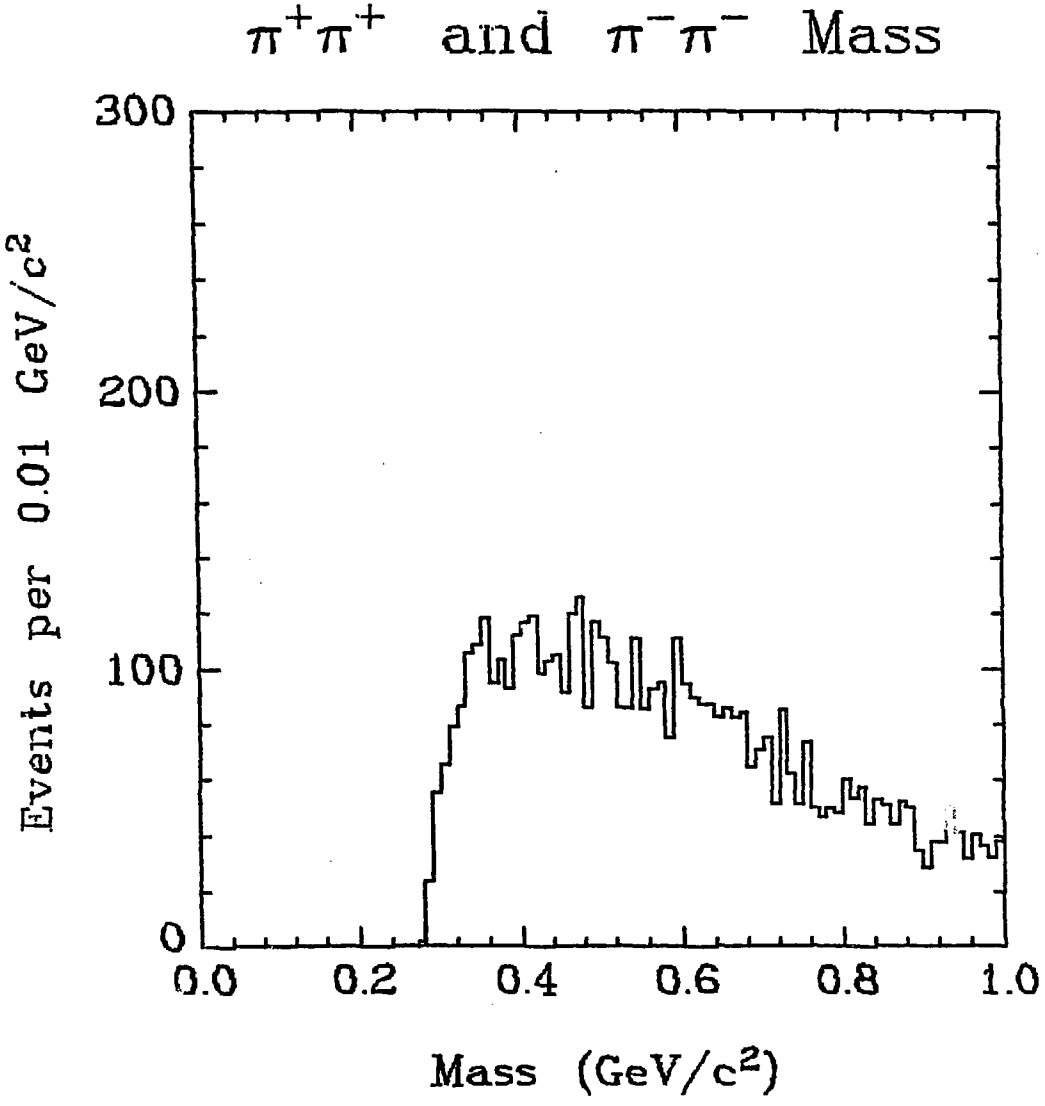

FIGURE III.6
A typical $\pi^+\pi^+$ and $\pi^-\pi^-$ mass distribution.

We determine the background from random two-pion combinations by looking at the number of combinations in the adjacent bins. The shape of the background can be estimated by looking at combinations of two pions with the same charge that meet the above four criteria. The mass distribution for same-sign pairs is shown in Figure III.6. The distribution is very nearly a straight line between 0.4 and 0.6 GeV. We therefore estimate the background under the K^o peak by taking the number of opposite-sign combinations in the .40-.48 and .52-.60 GeV mass bands and dividing by four to get the expected number of background events in the .48-.52 GeV band.

The decay mode $K_S^o \rightarrow \pi^+\pi^-$ accounts for .343 of all K^o decays. Of those, we detect only a fraction because of the limited solid angle of the detector and because of inefficiencies in the cuts described above.

Our detection efficiency as a function of K^o momentum was determined by Monte Carlo studies undertaken by Vincent Vuillemin. The Monte Carlo program simulated the production and decay of K^o's and the tracking of the decay products through the detector. The simulation data was then analyzed using the same methods (described above) that were used to analyze the real data and the fraction of K^o's that were found was determined as a function of momentum. The efficiency thus determined rises from near zero for K^o momenta below 100 Mev/c to 25% at 200 MeV/c and is roughly flat above 200 MeV/c at 25%. Because the kaon spectra we will be dealing with peak well above 200 MeV/c, our momentum averaged efficiency is essentially 25%. This, combined with the .343 probability for a K^o to decay via the mode $K_S^o \rightarrow \pi^+\pi^-$ gives us an overall efficiency of .086 for detecting K^o's.

C. Hadronic Event Selection for Electron Studies

1. Event Selection

In Chapters VI and VII we present measurements of inclusive electron production in events of the form $e^+e^- \rightarrow$ hadrons. For these measurements it is essential to have a clean sample of hadronic events, free of contamination from cosmic rays, from beam-gas scattering events, and from the electrodynamic processes $e^+e^- \rightarrow e^+e^-$, $e^+e^-e^+e^-$, $e^+e^-\gamma$, and $e^+e^-n\gamma$ where $n=2,3...$

To first order we eliminate these types of events by considering only events with three or more charged prongs ("multiprong" events) whose reconstructed vertex is within 4 cm radially and 25 cm in z of the center of the interaction region. The fraction of good hadronic events lost by these cuts on the vertex position was determined by looking at the vertex position distribution of an uncut set of high multiplicity events. Such events would be very unlikely to come from any of the above sources of contamination. It was found that 92% of these events had vertices within the cuts.

In an electrodynamic event a photon can convert to an electron-positron pair in the beam pipe, the beam pipe counters, or the cylindrical proportional chambers to create an event with three or more prongs detected. Therefore, all events were searched for opposite-charge pairs of tracks with opening angle less than 11.5 degrees ($\cos(\theta) = .98$). It was required that there be at least three charged prongs in addition to those that were in such pairs for an event to remain in the sample. (The 11.5° cut was chosen by examination of the 0° peak in the distribution of angles between pairs of oppositely charged particles.)

There still remained electrodynamic events with wide opening angle pairs or single extra electrons from pairs of which one electron went undetected because its momentum was too low or it was outside the solid angle of the detector.

In radiative electrodynamic processes the radiated photon spectrum peaks at low momenta and the photons tend to be emitted in narrow cones about the incident and outgoing electron directions. Therefore, these events should be characterized by the presence of two high-momentum electrons which are nearly back-to-back in azimuthal projection. All other particles in such an event would be electrons from photon conversions. In contrast, hadronic events with an electron produced by the weak decay of a hadron should be characterized by the presence of one, or sometimes two, electrons with the rest of the charged particles being hadrons.

Because our purpose is to use the Lead-Glass Wall to study electrons produced by the weak decays of new hadrons, it was desired to remove electrodynamic events from the data sample while removing as few events as possible which had electrons in the Lead-Glass Wall from decays of new particles. In order to accomplish this we have taken advantage of the crude electron identification capability of the lead-scintillator shower counters which cover the seven octants of the detector other than the the Lead-Glass Wall octant. By using the identification of electrons *outside* the LGW to identify electrodynamic events we avoid biases that would arise if the LGW itself were used in the identification of electrodynamic events, e.g., although some good hadronic events may be thrown out we avoid preferentially throwing out events which have an electron in the LGW.

After careful scanning of the multiprong events with an electron identified in the Lead-Glass Wall (see below) and after some experimentation it was decided to remove from the data sample all events that met one of the following two criteria:

1. There were at least two tracks with momentum greater than half of the beam energy and at least one electron outside the Lead-Glass Wall identified by the lead-scintillator shower counters.
2. There were at least two tracks which were back-to-back in azimuthal projection within 10 degrees and one track of the two had a momentum greater than half of the beam energy if it was outside the Lead-Glass Wall or greater than 4/5 of the beam energy if

it was in the Lead-Glass Wall octant. (Electrons from decays of new particles would rarely have momentum greater than 4/5 of the beam energy.) If one of the two tracks was identified as an electron by the lead-scintillator shower counters (outside the Lead-Glass Wall) then the azimuthal collinearity cut was relaxed to 20 degrees.

About 7% of all the multiprong events were removed by these cuts. A correction must be made for good hadronic events which were lost by these cuts. Clearly, the efficiency of the cuts for good events is somewhere between 0.93 and 1.00, since at least some of the events rejected by the cuts were indeed electrodynamic events. We take the efficiency to be 0.96 ± 0.04 and in so doing we cannot be off by more than 4%, which is small compared to the statistical error in our measurements. This value for the efficiency is also consistent with the results of Monte Carlo studies which have been made.

Having used the above criteria to remove electrodynamic events from our data sample and having shown that these cuts do not remove more than a few percent of the good hadronic events from the sample, it is still necessary to demonstrate that the cuts have served their purpose and that the remaining events are indeed hadronic with little or no electrodynamic contamination.

In order to do this we again utilize the crude electron identification capability of the lead-scintillator shower counters. In a sample of events with a particle in the Lead-Glass Wall which was not identified as an electron it was found that 20% of all tracks outside the LGW with momentum greater than 500 MeV/c were identified as electrons. This establishes our probability to see an electron in the shower counters in a hadronic event. Most of these are actually misidentified hadrons; we know from the measurements presented in Chapters VI and VII that about one tenth of them are real electrons. In a sample of 176 events with a particle in the LGW which was identified as an electron it was found that 23 ± 3 % of all particles outside the LGW with momentum greater than 500 MeV/c were called electrons. We assume that this sample consists of two components:

1. Good hadronic events in which most of the particles outside the LGW are hadrons but 20% are identified as electrons.

2. Electrodynamic events in which all particles are electrons and 89% (see Chapter II) are correctly identified by the shower counters.

We then take the observed fraction (.23 ± .03) and unfold to get the contributions from each category:

$$.23 = .89\,\epsilon + .20\,(1-\epsilon)$$

where ϵ is the fraction of events which are electrodynamic rather than hadronic. Solving, we find $\epsilon = .04 \pm .05$. We therefore conclude that $96^{+4}_{-5}\%$ of our events are hadronic.

Another test consists of counting the number of events with 2 or more particles outside the LGW identified as electrons. We find 17 such events in the sample of 176 events with an electron in the LGW. From the multiplicity distribution of the events and the observed misidentification rate we would expect to find 14.3 such events if all particles outside the LGW were really hadrons. We can attribute the excess of 2.7 ± 4.1 events (1.5 ± 2.3%)) to electrodynamic contamination.

A final purge of residual electrodynamic contamination was made by examining individually all events which contained any track with momentum greater than half the beam energy. A consensus of three scans (by Ronald Madaras, Michael Ronan, and myself) found 8 events out of our sample of 435 in the center-of-mass energy range from 3.9 to 7.4 GeV which were apparently electrodynamic events which had managed to pass our cuts. These 8 events were removed from the sample. Since this number is consistent with the contamination rate estimates presented above, we make no further background subtraction for electrodynamic contamination.

2. Acceptance

Of those events in which 4 or more charged particles are produced, one of which is an electron in the Lead-Glass Wall, only a fraction will trigger the detector and have at least two other charged particles detected by the proportional and spark chambers. This fraction is defined as the acceptance. The acceptance depends on the multiplicity, momentum, and angular distributions of the particles in the events. This implies a dependence in turn on the center-of-mass energy and the mechanism by which hadrons are produced .

In our center-of-mass energy region isotropic phase space models give a reasonable approximation to the observed angular and momentum distributions in electron-positron annihilation into hadrons. Detailed analysis with very high statistics reveals strong evidence of jet structure[2] but the jets are not tightly collimated and the structure is not evident on an event-by-event basis and would not be expected to affect our acceptance significantly. This is especially true in events which contain fast-decaying charmed particles because their masses are quite high (> 1.8 GeV) so their decays would yield particles with high transverse momentum with respect to the jet axis.

We therefore determine our acceptance with a Monte Carlo program which simulates the phase space production of D mesons and pions, the decays of the D mesons, and the tracking of the final-state particles through the detector. D mesons are always produced in pairs and in our simulation one of the pair decays semi-leptonically (to produce the electron for detection in the Lead-Glass Wall) and the other decays hadronically.

Two possible semi-leptonic decay modes of the D are simulated, $D \rightarrow Ke\nu$ and

$D \rightarrow K^*(890)e\nu$. The matrix elements for these decays are calculated using a simple set of assumptions suggested by Hinchliffe and Llewellyn-Smith.[3] In this model all form factors are taken to be constant and for the decay $D \rightarrow K^*e\nu$ only the term in the hadronic current proportional to the K^* polarization vector is taken to be non-zero. Barger, Gottschalk and Phillips[4] have shown that inclusion of form factors does not significantly affect the momentum spectra or correlations of the decay products. The calculation of the matrix elements using these simple assumptions is presented in Appendix A.

The hadronic decays of the other D meson are simulated by a combination of modes with branching ratios chosen to reproduce the observed charged multiplicity distributions of D^+ and D^o decays.[5] The branching ratios were also chosen to produce equal numbers of charged and neutral kaons. The latter choice was arbitrary and was made for simplicity in using the same Monte Carlo data to determine acceptances for kaons. It does not significantly affect the acceptance as long as the observed multiplicity distribution is reproduced.

In some of the simulations D^* mesons were produced instead of D's. The D^*'s were decayed into D's and photons or pions with the following branching ratios:

$$B(D^{*o} \rightarrow D^o\pi^o) = .45$$

$$B(D^{*o} \rightarrow D^o\gamma) = .55$$

$$B(D^{*+} \rightarrow D^o\pi^+) = .60$$

$$B(D^{*+} \rightarrow D^+\gamma) = .40$$

The decay $D^{*+} \rightarrow D^+\pi^o$ has not been included; as far as the acceptance is concerned this decay is equivalent to $D^{*+} \rightarrow D^+\gamma$.

The most important factor in determining the acceptance is the produced charged multiplicity distribution. We get a handle on the produced multiplicity distribution by looking at the average detected multiplicity in our actual data sample. We hypothesize that the acceptance is uniquely determined, within a reasonable error, by the average detected multiplicity. We test this hypothesis by simulating the production of many different combinations of D's, D^*'s, and pions at several different center-of-mass energies with the semileptonic decays $D \rightarrow Ke\nu$ and $D \rightarrow K^*e\nu$, making a scatter-plot of acceptance vs. average detected multiplicity for all of these simulations, and seeing whether all the points do indeed lie along a single curve.

The reactions simulated are listed in Table III.1. Each reaction was simulated with the two semileptonic decay modes of the D for a total of 26 simulations.

The scatter plot of acceptance versus average detected charged multiplicity is shown in Figure III.7. The various symbols represent differing center-of-mass energies, as shown in the caption. The error bar on one point represents a statistical error based on the number of events in the

Table III.1

Production Reactions for Monte Carlo Simulations

Center-of-Mass Energy (GeV)	Produced Particles
4.15	$D^o\overline{D^o}$
4.15	D^+D^-
4.15	$D^{*o}\overline{D^{*o}}$
4.15	$D^{*+}D^{*-}$
4.9	$D^{*o}\overline{D^{*o}}$
4.9	$D^{*+}D^{*-}$
4.9	$D^o\overline{D^{*o}}\pi^o$
4.9	$D^+D^{*-}\pi^o$
4.9	$D^+\overline{D^{*o}}\pi^-$
4.9	$D^oD^{*-}\pi^+$
4.9	$D^+D^-\pi^+\pi^-$
6.9	$D^+\overline{D^{*o}}\pi^-$
6.9	$D^{*+}D^{*-}\pi^+\pi^-$
6.9	$D^{*o}\overline{D^{*o}}\pi^+\pi^-$

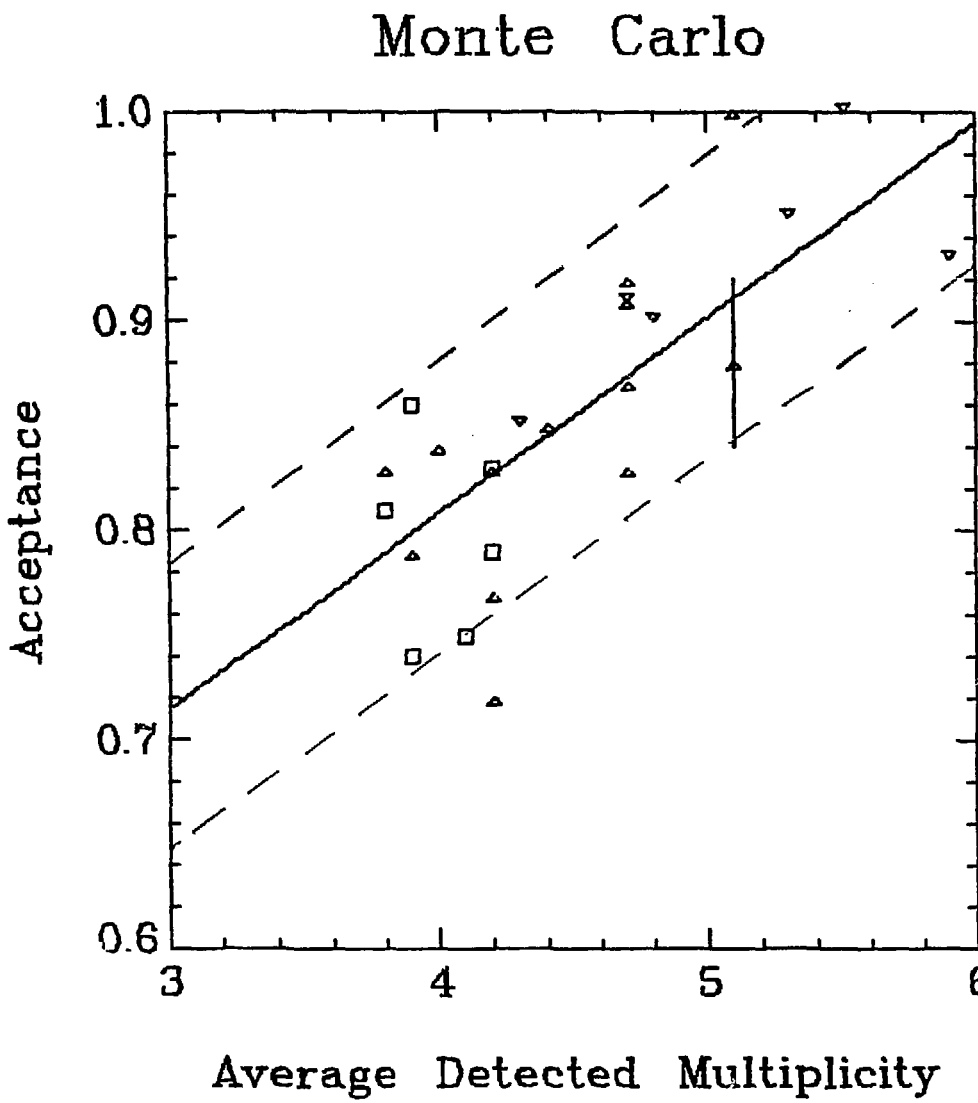

FIGURE III.7

Acceptance versus average observed multiplicity from Monte Carlo simulation.

□ E_{cm} = 4.15 GeV
Δ E_{cm} = 4.9 GeV
∇ E_{cm} = 6.9 GeV

simulation and is typical of all points.

Superimposed on the curve are a solid line and two dashed lines representing the empirical acceptance formula:

$$A = .435 + .093 \langle n \rangle \pm .07$$

We observe that 24 of the 26 points lie within the dashed lines and the remaining two points are only a fraction of the statistical error outside the lines. We therefore conclude that the acceptance can, within an error of .07, be characterized as a unique function of the average detected multiplicity, independent of center-of-mass energy and specific production mode, and we use the above formula, together with the observed average multiplicities in the data itself, to determine our acceptance at various center-of-mass energies. We note that in this manner the Monte Carlo simulation is used only to determine the relation between acceptance and detected multiplicity and not to determine the acceptance itself.

Table III.2 shows the average detected charged multiplicity, including the electron, for events with an electron identified in the Lead-Glass Wall in four different center-of-mass intervals along with the acceptance as computed from the above formula. We see that the acceptance varies from 0.81 to 0.86.

D. Electron Identification

Electrons are identified by the energy they deposit in the two layers of lead-glass blocks. When a high-energy electron enters the lead-glass it creates an electromagnetic shower. Relativistic ($\beta > 0.62$) electrons in the shower emit Cherenkov light. The total amount of light emitted is proportional to the total path length of electrons in the shower which in turn is proportional to the energy deposited. An electron of energy less than 4 GeV would be expected to deposit nearly all of its energy in the total of 13.8 radiation lengths of lead-glass in the LGW, and would be expected to deposit a significant fraction in the 3.3 radiation lengths of the active converters. Heavier particles, e.g., muons and hadrons, will not radiate significantly in the 13 radiation lengths and therefore will not create an electromagnetic shower.

When a charged particle track is observed in the proportional chambers and spark chambers of the magnetic detector we extrapolate the track to its intersection with the Lead-Glass Wall and examine the energy deposition in the lead-glass blocks near the projected track.

Inspection of the energy deposition pattern in a large number of Bhabha scattering events revealed that almost all of the electron's energy is deposited in the block through which the track from the spark chambers projects and adjacent blocks with occasional spillover into blocks removed by two from the projected track.

We therefore chose the following algorithm for finding the energy deposited by a track in the

Table III.2

Average Detected Multiplicity and Acceptance

E_{cm}	Average Detected Charged Multiplicity	Acceptance
$\psi(3772)$	4.43 ± .44	.85 ± .07
3.90 - 4.44 GeV	4.17 ± .25	.82 ± .07
4.44 - 5.71 GeV	4.04 ± .27	.81 ± .07
6.31 - 7.38 GeV	4.54 ± .25	.86 ± .07

Table III.3

Electron Identification Efficiency

Momentum (GeV/c)	Efficiency
0.3 - 0.4	.50 ± .20
0.4 - 0.5	.61 ± .20
0.5 - 0.6	.72 ± .20
0.6 - 0.7	.83 ± .20
0.7 - 2.0	.89 ± .10

Lead-Glass Wall:

1. Draw a square 30 cm on a side centered on the intersection of the projected track with the front face of the active converters. The energy deposited in all active converters whose faces are within or partly within this square is summed to find the energy deposited in the active converters (EAC). This sum will include 3, 4, 6, or 8 active converters depending on the location of the projected track within a block.

2. Draw a square 40 cm on a side centered on the intersection of the projected track with the front face of the back blocks. The energy deposited in all back blocks whose faces are within or partly within this square is summed to find the energy deposited in the back blocks (EBB). This sum will include 9, 12, or 16 blocks.

3. The total energy deposited (ETOT) is the sum of EAC and EBB.

The algorithms for choosing which blocks to include are illustrated in Figure III.8.

1. Cuts

Before attempting to separate electrons from hadrons and muons the following criteria were applied to obtain a clean sample of tracks in the LGW:

1. The intersection of the projected track with the front face of the back blocks is at least 7.5 cm (1/2 block) away from any edge of the LGW. This cut defined a fiducial solid angle of 0.0548 x 4π sr.
2. There is no other charged track whose projection into the Lead-Glass Wall is sufficiently close to that of the candidate track to have any back block or active converter included in the energy sum for both tracks. About 3% of all tracks are lost by this requirement.
3. There is less than 50 MeV of energy deposited in the back blocks above and below, but in the same vertical half of the wall as, the energy deposition square defined above for the back blocks. The purpose of this requirement was to eliminate events in which a photon was near the track of interest and the energy deposits of the two particles could be distinguished in the back blocks but would overlap in the active converters. (Recall that the active converters are 90 cm long in the vertical direction.) About 2.5% of all tracks are lost by this requirement.
4. There is no track of opposite charge the cosine of whose opening angle with the track of interest is greater than 0.98. This cut was designed to eliminate e^+e^- pairs from photon conversions. Less than 1% of all tracks are lost by this requirement.
5. The measured time-of-flight for the track does not exceed that expected for an electron by more than 1 nanosecond. By looking at a sample of electrons produced in electrodynamic processes we find that about 4% of all electrons are lost by this

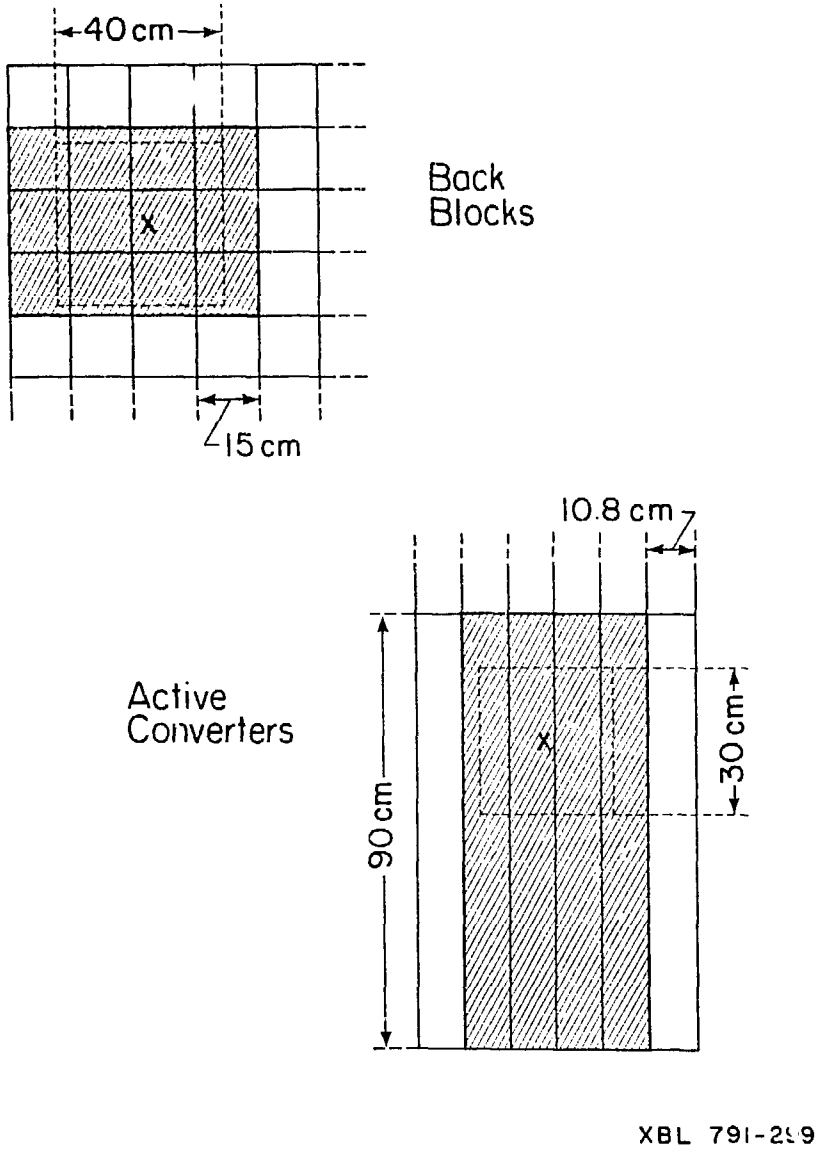

FIGURE III.8

Block selection algorithms in the Lead-Glass Wall.

requirement.

Figure III.9 is a scatter plot showing the energy deposited in the active converters (EAC) versus the total energy deposited in the LGW divided by the momentum (RTOT) for 1.55 GeV electrons from Bhabha scattering events. We see that the electrons typically deposit all of their energy in the LGW with 20-80% deposited in the active converters.

Figure III.10 is the same plot for 1.55 GeV muons from the reaction $e^+e^- \rightarrow \mu^+\mu^-$. We see that the muons typically deposit only about 500 MeV in the LGW and only about 100 MeV of that is in the active converters.

Our main problem is to separate electrons from pions in the momentum region below 1.0 GeV. Pions, unlike muons, often interact and deposit large amounts of energy in the LGW. (The lead-glass constitutes 1.3 hadronic interaction lengths. The magnet coil in front of the LGW constitutes 0.24 interaction lengths.) This, combined with the fact that the fractional energy uncertainty, σ_E/E, increases with decreasing energy, makes the separation of electrons from pions more difficult than Figures III.9 and Figure III.10 would indicate. Figure III.11 is a scatter plot of EAC versus RTOT for tracks with momentum between 500 and 750 MeV/c at the $\psi(3.1)$ resonance. These tracks are mostly hadrons (see section 2 on background below), so this plot represents the kind of background we want to reject. Figure III.12 is the same plot for 500-750 MeV/c electrons from electrodynamic processes (see section 3 on efficiency below). These are the type of tracks that we want to accept.

The following cuts are used to accept electrons and reject hadrons:

1. The total energy deposited in the LGW is greater than ECUT where

$$\mathrm{ECUT} = \mathrm{Min}\left(0.65 + 0.15\,\frac{p}{1\ \mathrm{GeV}}\,,\ 0.80\right)$$

2. The energy deposited in the active converters is greater than 150 MeV and is also greater than 1/4 of the particle's momentum.
3. The energy deposited in the back blocks is greater than 1/10 of the particle's momentum.
4. The total energy deposited in the LGW is not more than 1.5 times the particle's momentum.

These cuts are superimposed on Figures III.11 and III.12.

2. Efficiency

To measure the efficiency of our cuts for identifying electrons we use events from the electrodynamic processes $e^+e^- \rightarrow e^+e^-$ (Bhabha scattering), $e^+e^- \rightarrow e^+e^-\gamma$, and $e^+e^- \rightarrow e^+e^-e^+e^-$. These processes provide electrons over a broad range of momenta. All three processes produce two electrons in the detector which are nearly collinear in azimuthal projection with their net

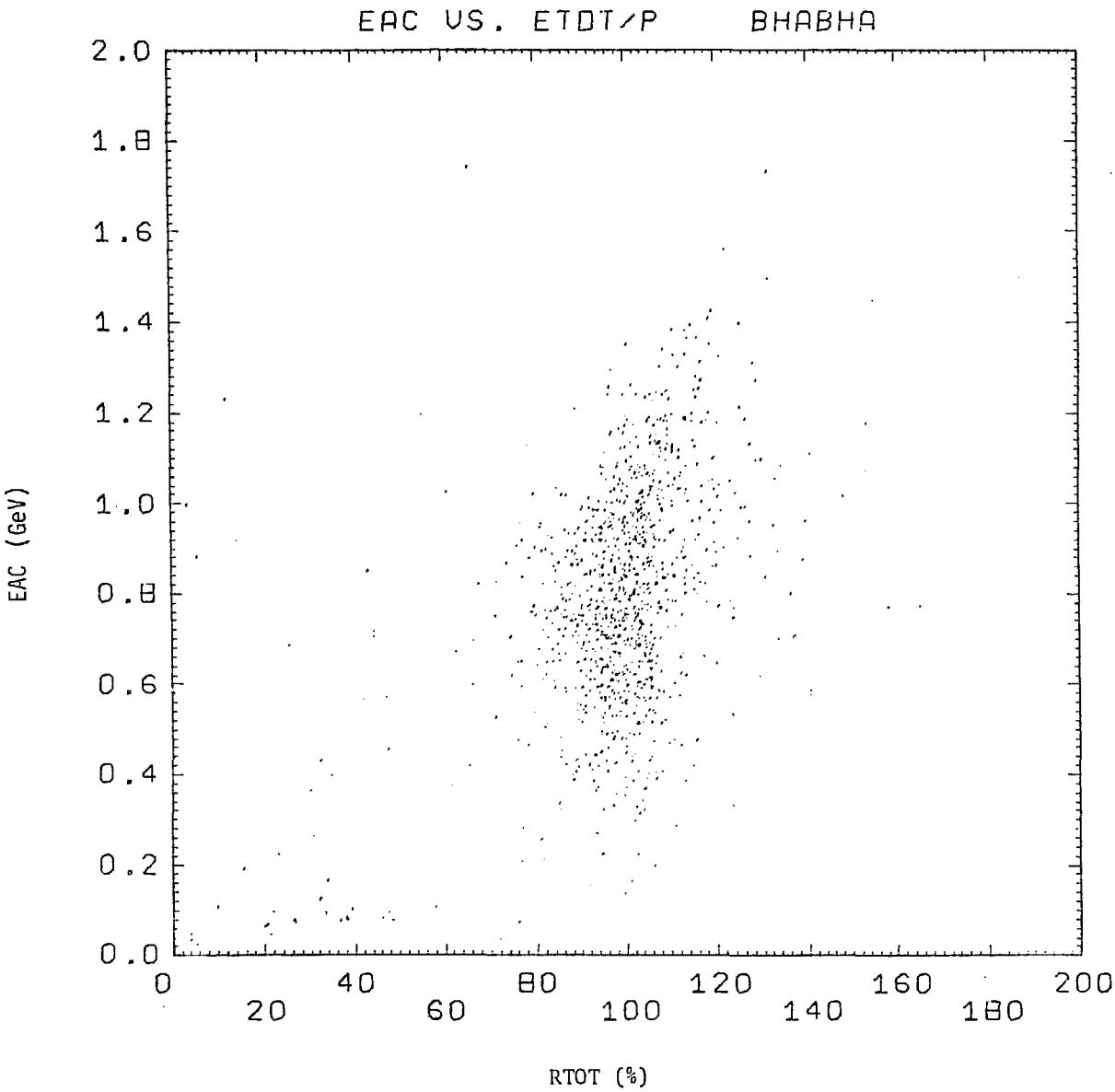

FIGURE III.9

EAC versus RTOT for 1.55 GeV/c electrons from Bhabha scattering.

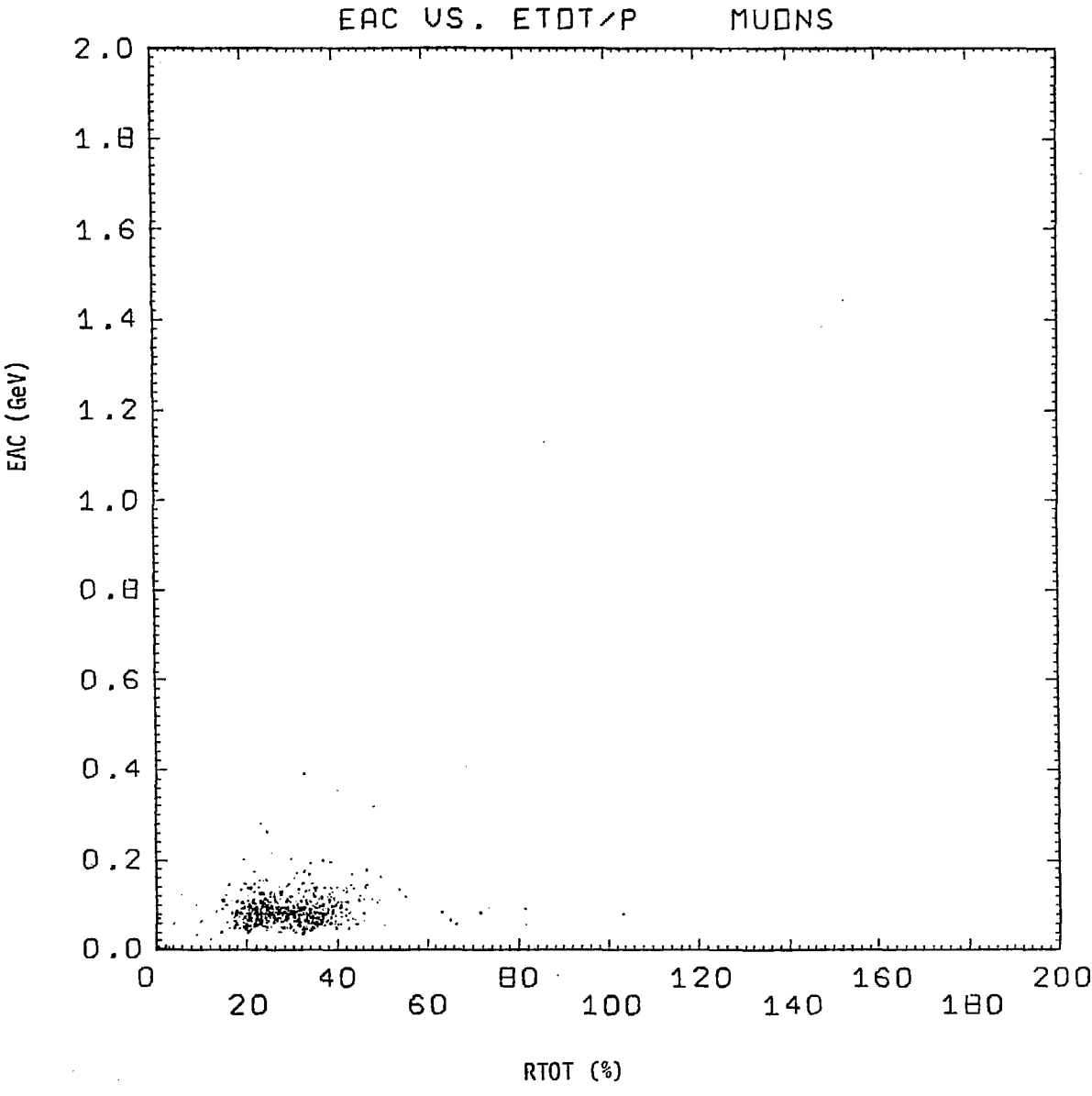

FIGURE III.10

EAC versus RTOT for 1.55 GeV/c muons.

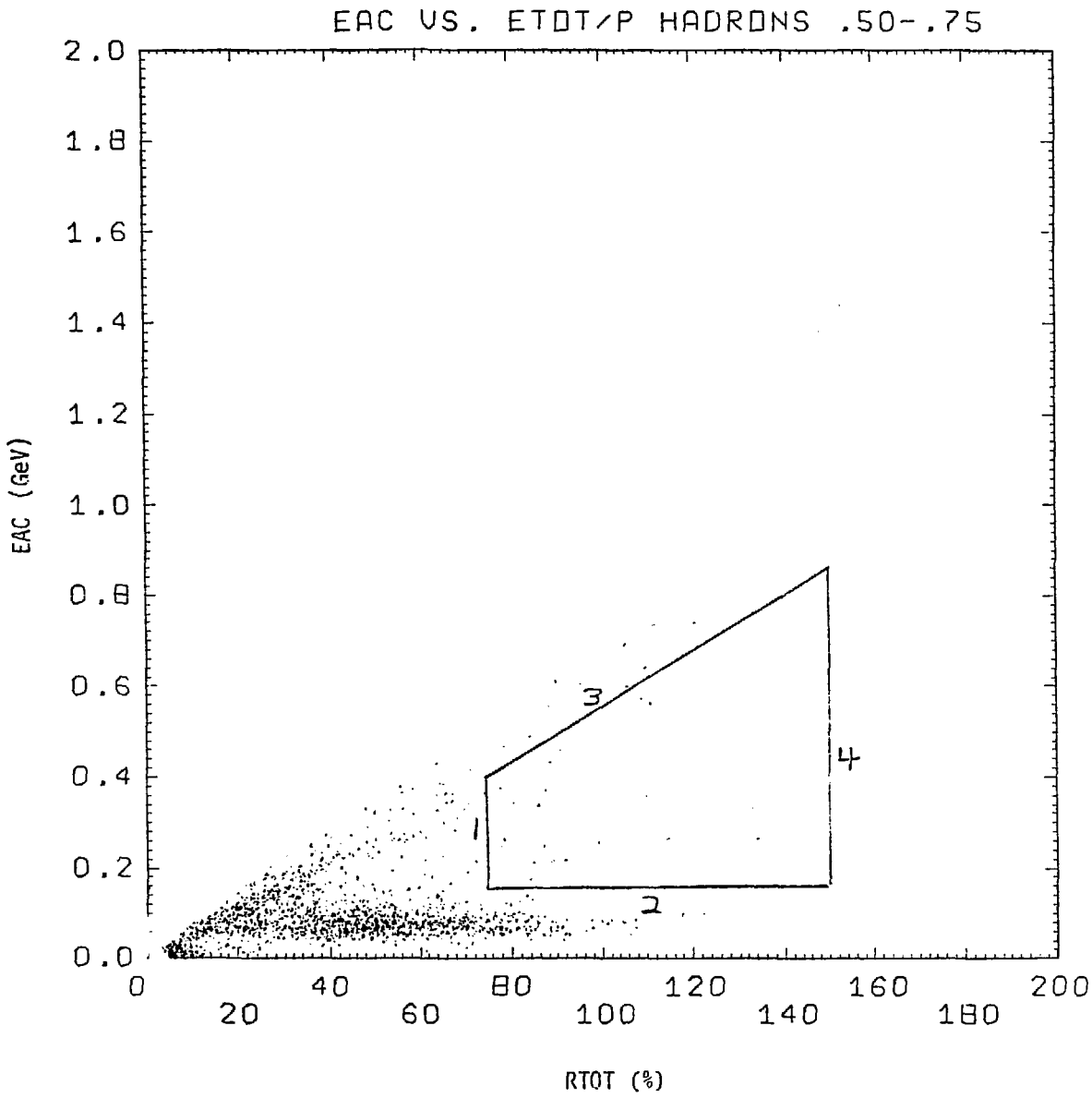

FIGURE III.11

EAC versus RTOT for 500 - 750 MeV/c hadrons at the $\psi(3.1)$. The lines represent the electron identification cuts.

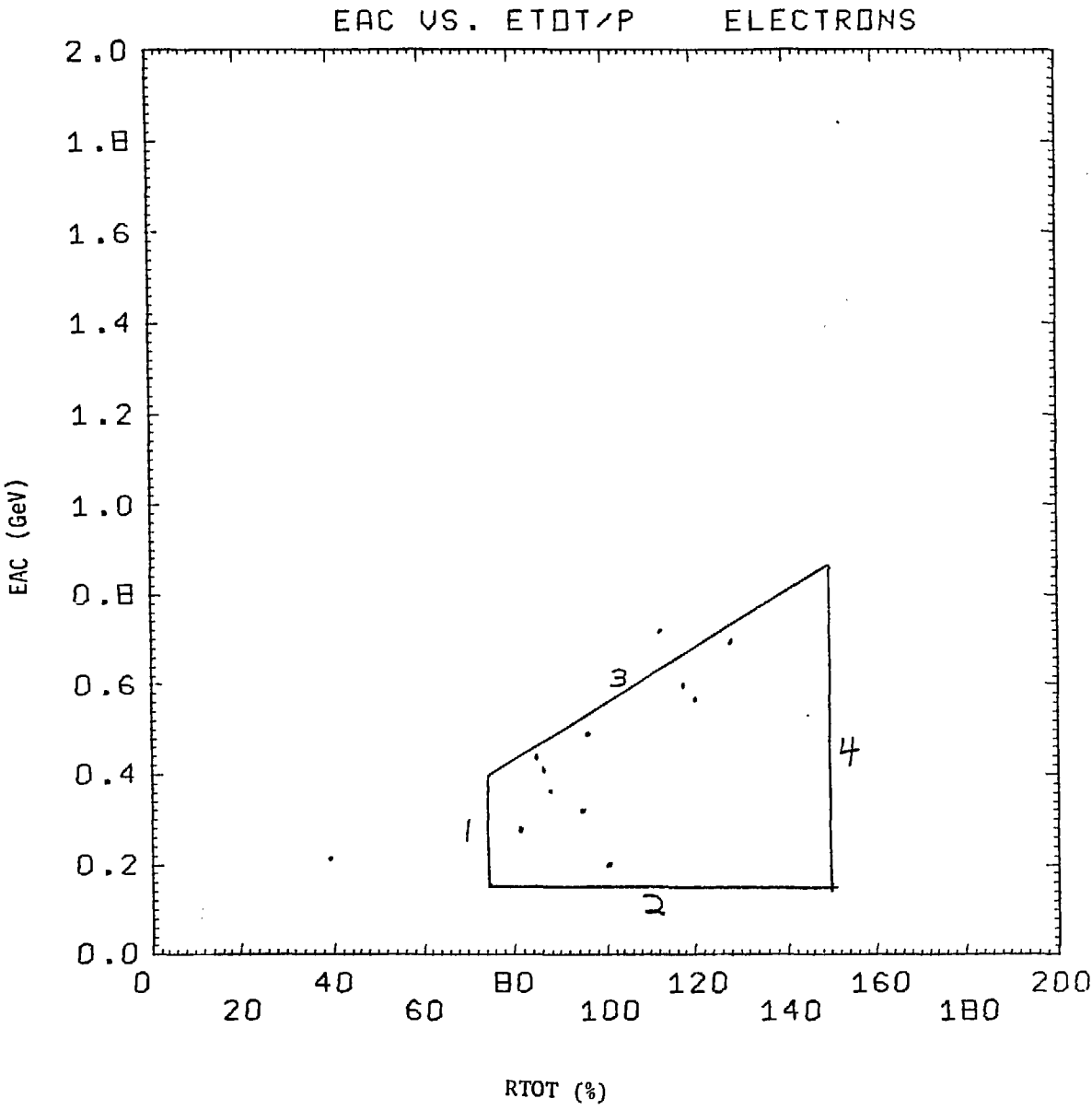

FIGURE III.12

EAC versus RTOT for electrons from high-order electrodynamic processes. The lines represent the electron identification cuts.

momentum directed along the beam line (z axis). The cuts used to select these events are similar to the cuts used to eliminate electrodynamic events from the multiprong hadronic sample. The requirements are:

1. There are two and only two tracks, with opposite charges, in the detector.
2. The two tracks are collinear in azimuthal projection within 10 degrees.
3. The cosine of the angle between the net momentum of the two tracks and the beam line is greater than 0.94.
4. One and only one of the two tracks is in the Lead-Glass Wall and the other is identified as an electron in the lead-scintillator shower counters.

Figure III.12 (see above) is the scatter-plot of EAC versus RTOT for those tracks in the LGW with momentum between 500 and 750 MeV/c from these events. There is no clustering of tracks in the region where hadrons would be expected to appear (see Figure III.11) which confirms that there is no hadron contamination in this sample.

In order to measure the efficiency of our electron cuts at all momenta we first take the electrodynamic events and apply the set of cuts described above in section 1 to get a clean sample of tracks in the LGW. We then count, for each momentum bin, what fraction of the tracks pass the electron identification cuts. This is the efficiency. The results are plotted in Figure III.13. Because the statistical error is large in the individual momentum bins, we do an eyeball fit of a smooth curve to the data, with an error also estimated by eye. The curve and the upper and lower limit error curves are superimposed on Figure III.13 and the resulting efficiencies for the various momentum bins are listed in Table III.3.

3. Background

The $\psi(3.1)$ resonance is below the threshold for production of the new particles (heavy leptons and charmed particles) which decay weakly into states containing electrons. Therefore , by counting the fraction of particles in multiprong events at the $\psi(3.1)$ which are identified as electrons by the LGW we determine the background rate for our anomalous electron production measurements at higher energies. The primary contributions to this background rate are misidentification of hadrons and photon conversion pairs of which one electron goes undetected because its momentum is too low. (If both electrons are detected one of the cuts described in Section I eliminates the pair from consideration. See al[illegible])

Figure III.14 shows the measured background rate [illegible]ction of momentum. The errors are statistical. As with the efficiency, we do an eyeball fit to smooth the data. The curve and error curves are superimposed on the data and the resultant background rates are listed in Table III.4. We note that the large uncertainty in the background rate for momenta above 1 GeV/c does not significantly affect any of our physics results because almost all of the data lies below 1

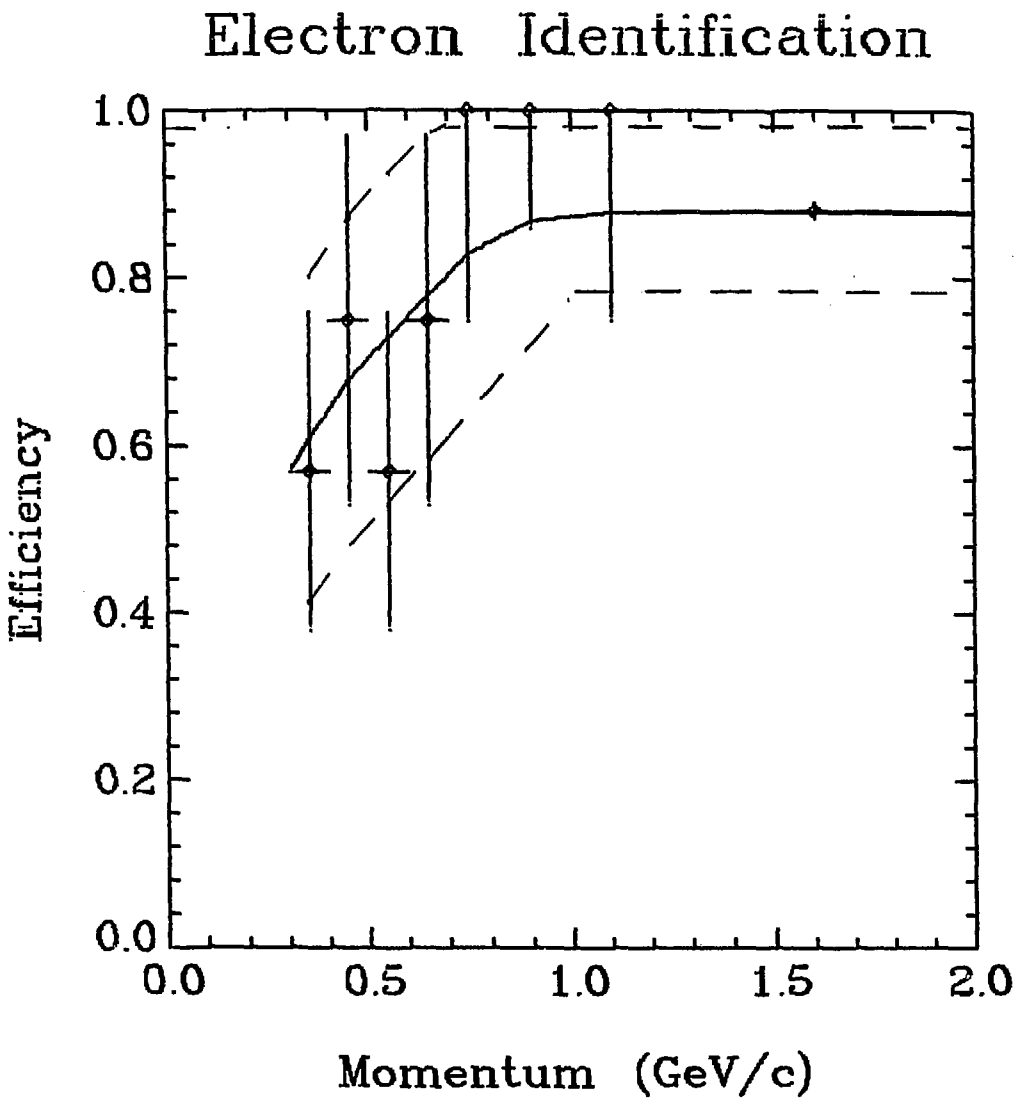

FIGURE III.13

Electron identification efficiency as a function of momentum. The solid and dashed lines show the values and errors used in the analysis.

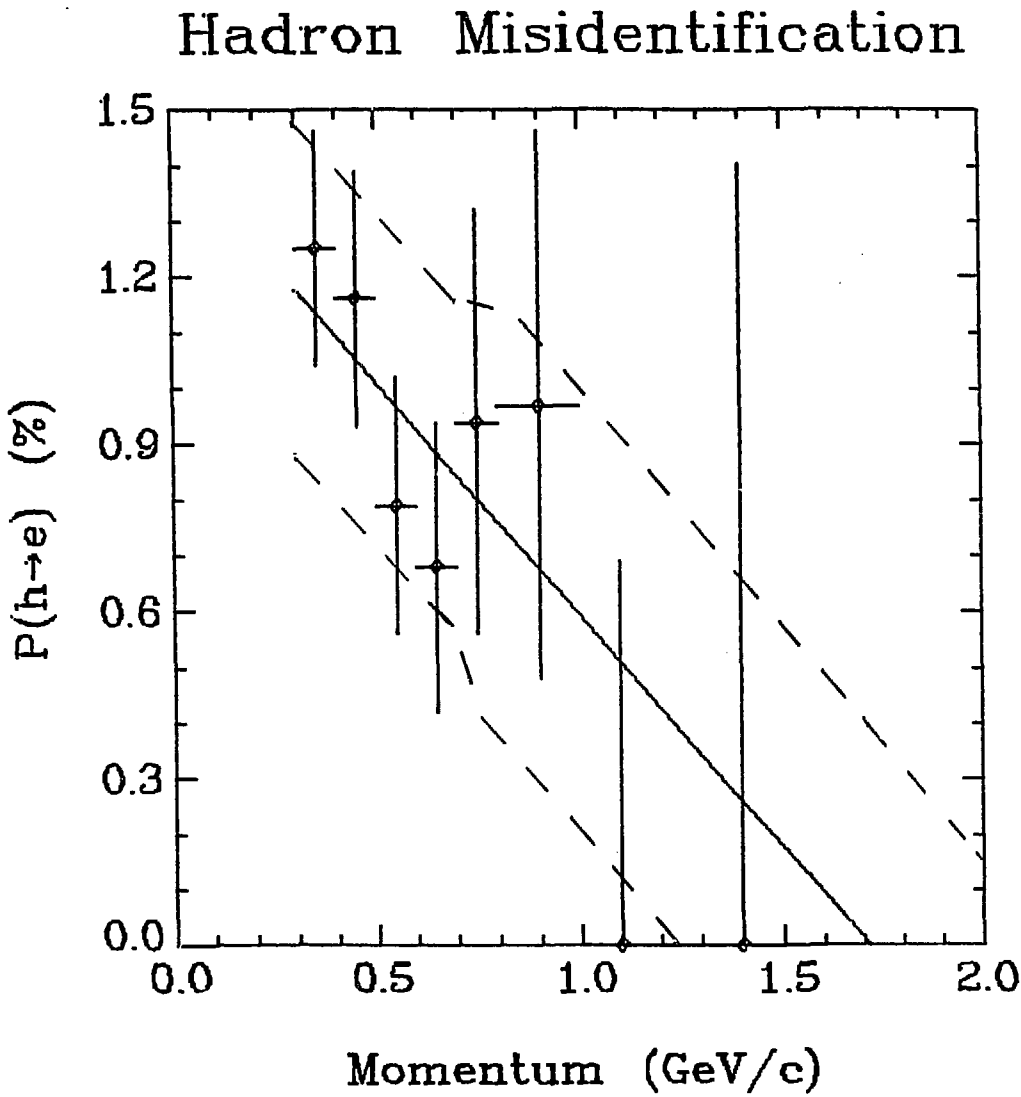

FIGURE III.14

Probability for a hadron to be misidentified as an electron as a function of momentum. The solid and dashed lines show the values and errors used in the analysis.

Table III.4

Background Electron/Hadron Ratio
for $E_{cm} < 6$ GeV

Momentum (GeV/c)	Background e/h ratio (%)
0.3 - 0.4	1.20 ± 0.30
0.4 - 0.5	1.06 ± 0.30
0.5 - 0.6	0.93 ± 0.30
0.6 - 0.7	0.80 ± 0.30
0.7 - 2.0	0.70 ± 0.40

Table III.5

Background Electron/Hadron Ratio
for $E_{cm} > 6$ GeV

Momentum (GeV/c)	Background e/h ratio (%)
0.3 - 0.4	1.50 ± 0.30
0.4 - 0.5	1.25 ± 0.30
0.5 - 0.6	1.08 ± 0.30
0.6 - 0.7	0.91 ± 0.30
0.7 - 0.8	0.81 ± 0.40
0.8 - 2.0	0.78 ± 0.40

GeV/c.

In principle the background rate could be different at higher center-of-mass energies if the flux or momentum spectrum of photons (and therefore of conversion pairs) were different. Michael Ronan has done an extensive Monte Carlo study of this problem. Briefly, he generates a photon flux and spectrum which reproduces the observed rate and spectrum of conversion pairs where both electrons are detected and then uses this rate and spectrum to predict the number of pairs in which one electron will escape detection. He finds that for center-of-mass energies below 6 GeV the ratio of such assymetric pairs to single charged hadrons is constant. For center-of-mass energies greater than 6 GeV we used a slightly modified tracking algorithm which reduced our efficiency for detecting low-momentum tracks. As a result of this change the background from assymetric conversion pairs rises somewhat. This effect was estimated by Michael Ronan's Monte Carlo studies and an appropriate increment was added to the measured background rates from the $\psi(3.1)$. The resultant increased background rates are listed in Table III.5.

References

Chapter III

1. R. Hollebeek, Ph.D. Thesis, Lawrence Berkeley Laboratory Report LBL-3874 (1975);
J.E. Zipse, Ph.D. Thesis, Lawrence Berkeley Laboratory Report LBL-4281 (1975);
J.S. Whitaker, Ph.D. Thesis, Lawrence Berkeley Labratory Report LBL-5518 (1976)
J.E. Wiss, Ph.D. Thesis, Lawrence Berkeley Laboratory Report LBL-6725 (1977);

2. G. Hanson et al., Phys. Rev. Lett. 35, 1609 (1975)

3. I. Hinchliffe and C.H. Llewellyn-Smith, Nucl. Phys. B114, 45 (1976)

4. V. Barger, T. Gottschalk, and R.J.N. Phillips, Phys. Rev. D16, 746 (1976)

5. V. Vuillemin et al., Phys. Rev. Lett. 41, 1149 (1978)

IV. The $\psi(3772)$ Resonance

In order to study the decays of charmed particles we need a source of charmed particles. The $\psi(3772)$ resonance is such a source. For reasons that will become clear in this chapter, we call it a "D Factory".

A. Total Cross-Section around 3.772 GeV

Figure IV.1 shows the total cross section for electron-positron annihilation into hadrons for center-of-mass energies from 3.6 to 4.6 GeV, normalized to the theoretical one-photon cross section for muon pair production (σ_{QED}).[1] (This is the famous ratio "R".) The open squares are data from the previous experiment using the SLAC-LBL detector and the black circles are data from this experiment. All of the data plotted includes radiative corrections.

There is a clear resonance of about 2 units in R at 3.772 GeV with a full width at half maximum of 28 MeV. This is the $\psi(3772)$. It lies on top of a non-resonant background of about 3 units of R. (Without the radiative corrections there are 1.6 units of R in the resonance and 4 units of background.)

The $\psi(3772)$ has been interpreted as a member of the charmonium family of resonances which includes the $\psi(3.1)$ and the $\psi'(3.7)$. These states are thought to consist of a bound system of a charmed quark and its antiquark ($c\bar{c}$). The $\psi(3772)$ is interpreted as a $^3d_1$ state.[2]

The lowest threshold for producing a pair of charmed particles, $D^o\overline{D^o}$, is marked on Figure IV.1. The threshold for D^+D^- is 10 MeV higher. Figure IV.1 also shows the threshold for producing the next more complicated state containing charmed particles, $D^o\overline{D^o}\pi^o$. We note that the $\psi(3772)$ is above the thresholds for $D^o\overline{D^o}$ and D^+D^- but below the threshold for $D^o\overline{D^o}\pi^o$. This means that the $\psi(3772)$ can decay into a pair of D mesons but not into any more complicated state containing charmed particles.

B. Evidence for $\psi(3772) \rightarrow D\overline{D}$

Figure IV.2 shows the cross section times branching ratio for production of the D^o meson and it's decay into $K^-\pi^+$, in the neighborhood of the $\psi(3772)$. The curve represents the resonant part of the total cross section, normalized to the point at 3.772 GeV. It is clear that production of D mesons is significantly enhanced at the resonance.

On theoretical grounds one expects the decay to two D mesons to be the dominant decay

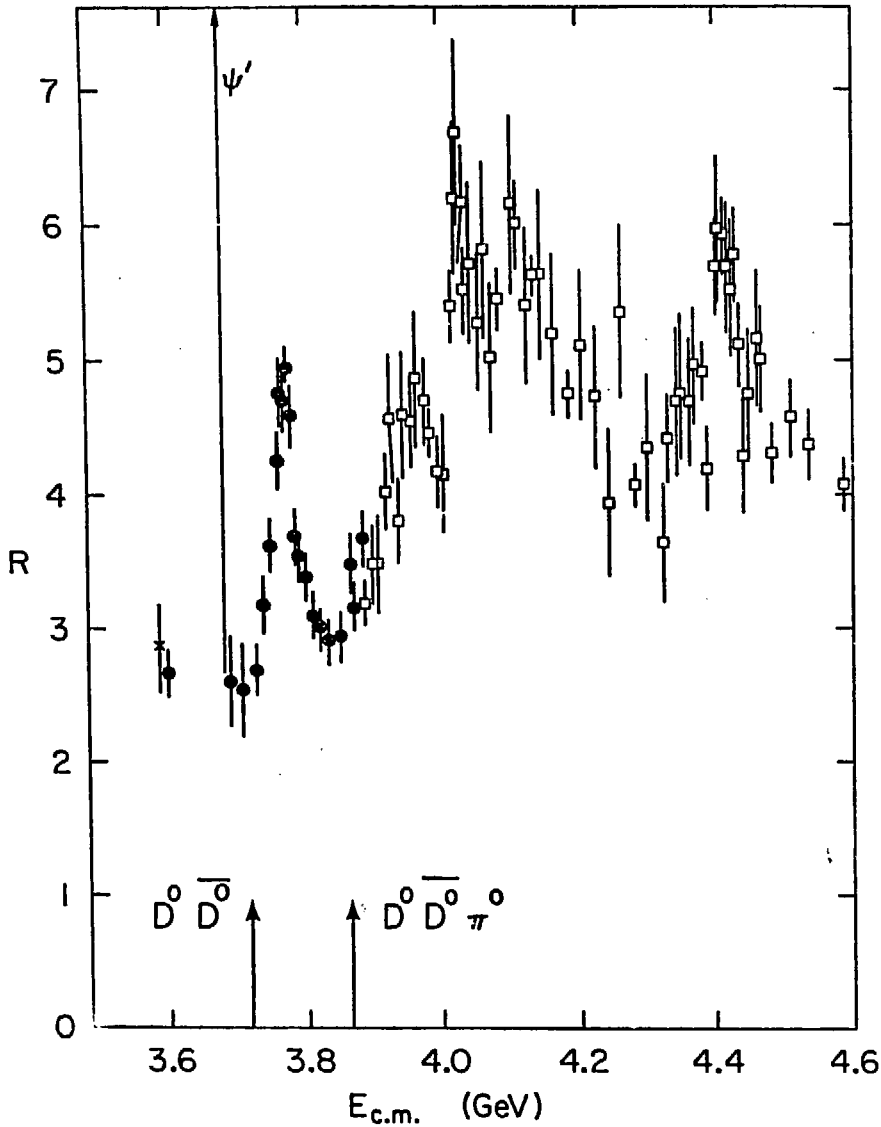

XBL 7711-10394B

FIGURE IV.1

The ratio $R = \dfrac{\sigma(e^+e^- \to \text{hadrons})}{\sigma(e^+e^- \to \mu^+\mu^-)}$ from E_{CM} = 3.6 to 4.6 GeV. The black circles are data from this experiment.

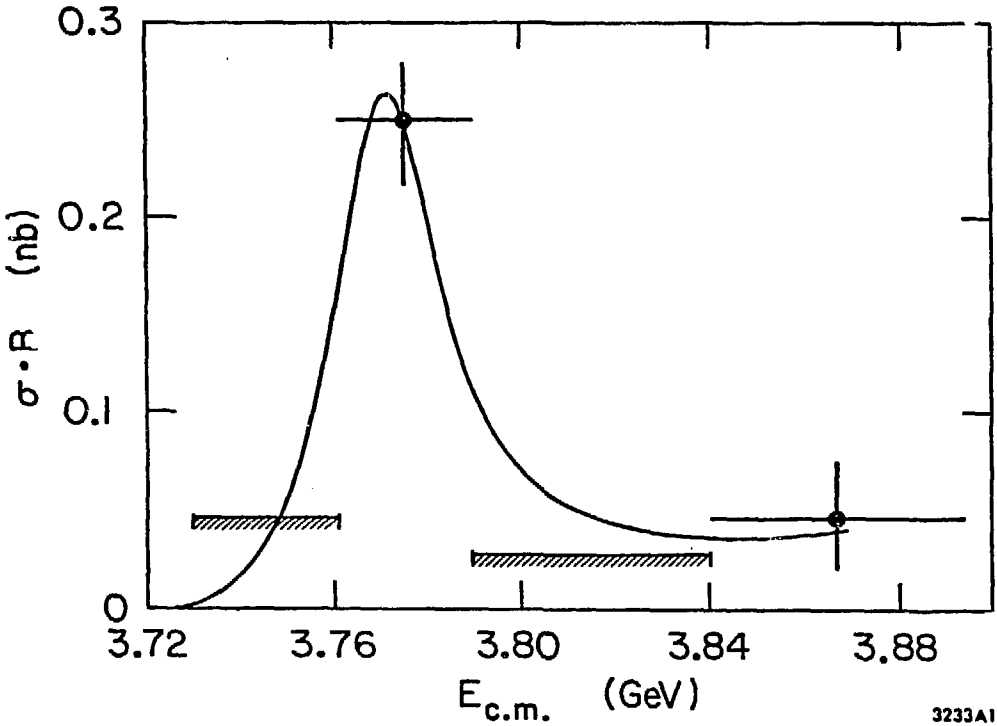

XBL 7711-10396

FIGURE IV.2

Cross section times branching ratio for $D^0 \to K^-\pi^+$ in the neighborhood of the $\psi(3772)$ resonance. The curve shows the shape of the resonance and is normalized to the point at 3.772 GeV.

mode of the $\psi(3772)$. Decays to non-charmed states require annihilation of the c and the $\bar{c}$ quarks and are therefore suppressed by the OZI rule (see Introduction). The only Zweig-allowed decays are $D^0\overline{D^0}$ and D^+D^-. Figure IV.3 shows quark diagrams for Zweig-allowed and Zweig-forbidden decays of the $\psi(3772)$.

There are three pieces of experimental evidence to support the hypothesis that the $\psi(3772)$ decays predominantly to $D\bar{D}$ ($D\bar{D}$ is used to signify $D^0\overline{D^0}$ and/or D^+D^-):

1. The width of the $\psi'(3.7)$, which lies 42 MeV below $D^0\overline{D^0}$ threshold is only 0.24 MeV.[3] The $\psi(3772)$, 46 MeV above threshold, is more than 100 times as wide (28 MeV). This dramatic increase in width for such a small change in mass suggests that the dominant decay channel of the wider resonance is a channel that is not accessible to the narrower one (namely, $D\bar{D}$).

2. In the decay $\psi(3772) \rightarrow D\bar{D}$ the D mesons are produced nearly at rest in the center-of-mass ($\beta = 0.15$). This would imply that the maximum momentum of any decay product of the D mesons would be slightly more than half of the D mass or slightly more than 1/4 of the center-of-mass energy. One would expect therefore that if the $\psi(3772)$ decays 100% of the time into $D\bar{D}$ then there should be no tracks with momentum greater than 1 GeV in the resonant part of the cross section. In contrast, if the $\psi(3772)$ decays directly into light particles such as pions then there could be tracks with momentum up to 1/2 of the center-of-mass energy. Figure IV.4a shows the number of multiprong events divided by the luminosity as a function of center-of-mass energy in the $\psi(3772)$ region. (This is not the true cross section because no detector acceptance corrections have been made.) The data have been binned so that most of the resonance appears in one bin. Figure IV.4b is the same graph for only those events which contain one or more tracks with momentum greater than 1 GeV. There is no peak, consistent with the hypothesis that all of the resonant part of the cross section is going into $D\bar{D}$ and thus contains no particles above 1 GeV/c. If we assume that that part of the resonant cross section which does not go into $D\bar{D}$ would have the same fraction of tracks above 1 GeV/c as the non-resonant cross section then we can use this measurement to calculate what fraction of the resonant cross section is not going into $D\bar{D}$. The result is $-.09 \pm .23$ of all $\psi(3772)$ decays are not going into $D\bar{D}$. (The result is negative because there is actually a statistically insignificant dip in the cross section for events with a fast track.) This implies that the branching ratio of the $\psi(3772)$ into $D\bar{D}$ is $1.09 \pm .23$.

3. Using branching ratios for D decays determined from the "tagged" events (see section D below) it is possible, within limited statistics, to make a direct measurement of the cross section for D^0 and D^+ production at the $\psi(3772)$. Dividing this cross section by the resonance cross section then yields the branching ratios for $\psi(3772)$ decays to $D^0\overline{D^0}$ and D^+D^-. The results are[4]

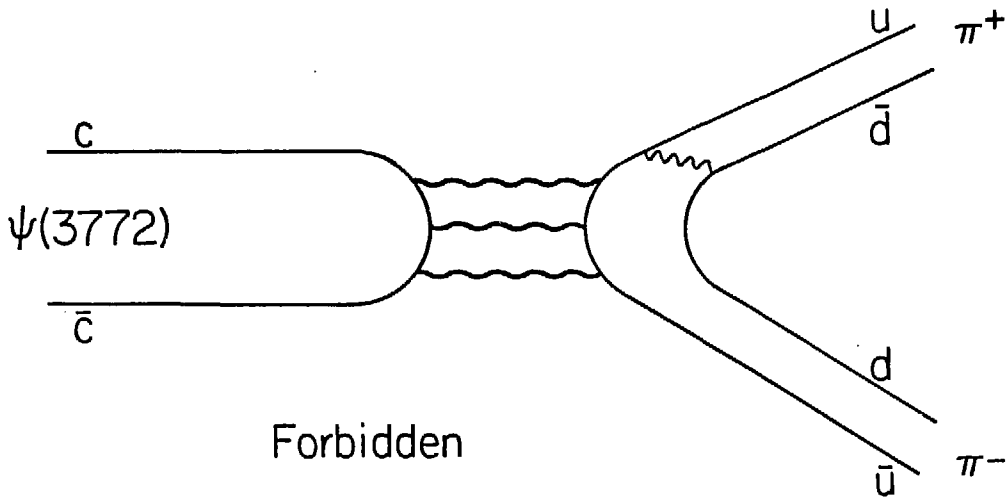

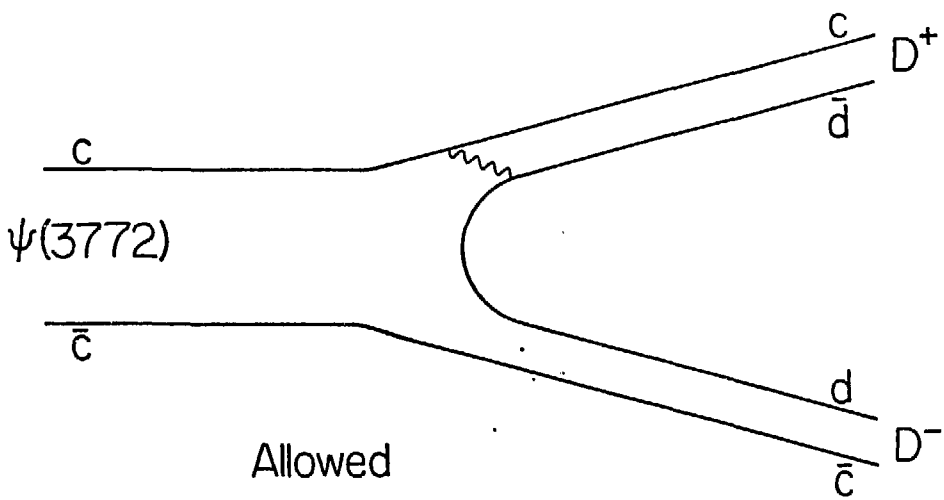

XBL 791-285

FIGURE IV.3

Diagrams for Zweig-allowed and Zweig-forbidden decays of the ψ(3772).

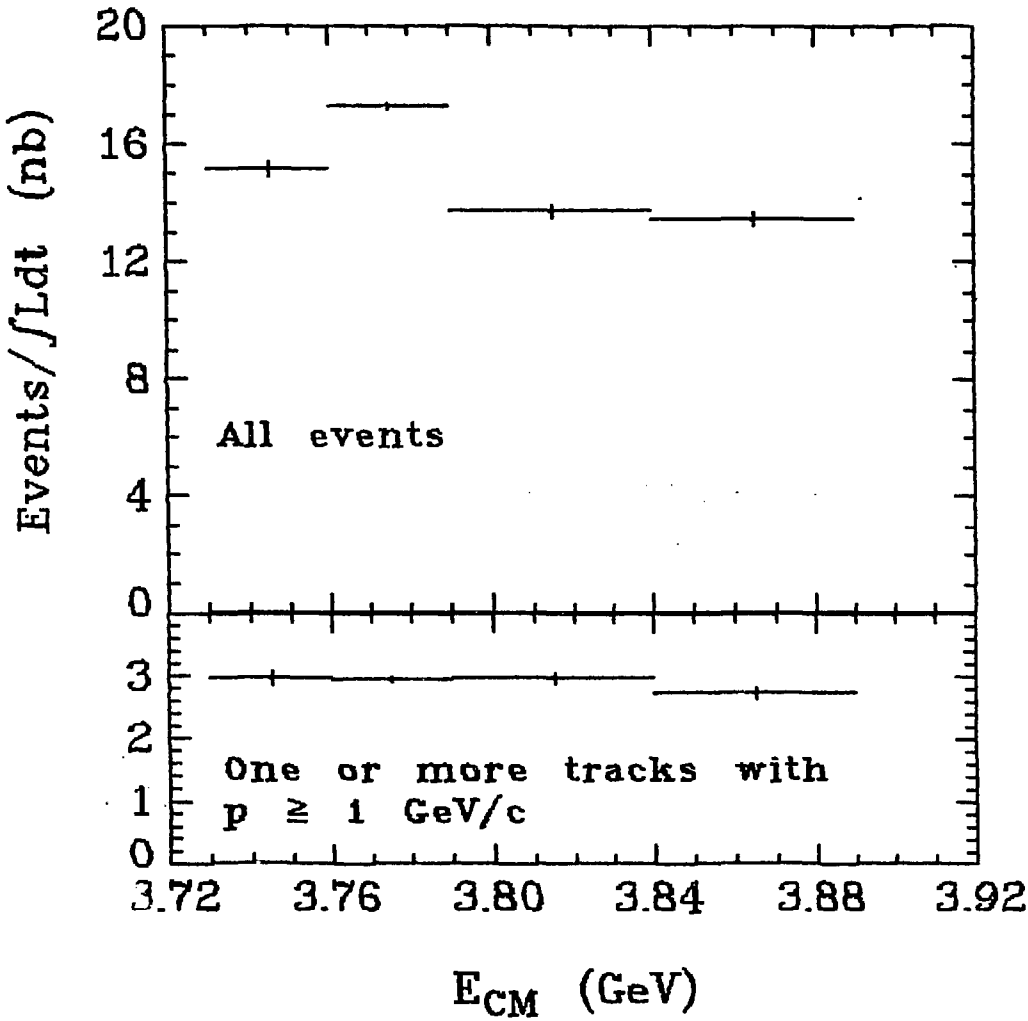

FIGURE IV.4

Number of hadronic events divided by integrated luminosity in the neighborhood of the $\psi(3772)$.

a) All hadronic events.

b) Only events with one or more tracks with $p \geqslant 1$ GeV/c.

$$B(\psi(3772) \rightarrow D^o\overline{D^o} = 0.34 \pm 0.18$$

$$B(\psi(3772) \rightarrow D^+D^- = 0.36 \pm 0.16$$

or

$$B(\psi(3772) \rightarrow D\overline{D} = 0.70 \pm 0.24$$

We remind the reader that a 100% branching ratio for the decay of the $\psi(3772)$ into $D\overline{D}$ would not imply that all of the hadronic events produced at that energy are $D\overline{D}$ events because there are 4 units of R in the background under the 1.6-unit resonance.

C. Identification of D-Mesons at the $\psi(3772)$

When pairs of D mesons are produced at the $\psi(3772)$ resonance the energy of each D meson is equal to the beam energy (1886 MeV), which is known to an accuracy of 1 MeV. This fact allows the identification of D mesons with an unprecedented signal-to-noise ratio.

In order to find D's, combinations of kaons and pions, such as $K^-\pi^+$ for the D^o and $K^-\pi^+\pi^+$ for the D^+, are selected. The combinations are required to have a total measured energy within 50 MeV of the beam energy. This cut on the measured energy greatly reduces the background. Then the mass of the system is calculated using the relation

$$m^2 = E_b^2 - p^2$$

where E_b is the beam energy.

Using the beam energy instead of the measured energy greatly reduces the error. The error is given by

$$(dm)^2 = \left(\frac{p}{m}dp\right)^2 + \left(\frac{E_b}{m}dE_b\right)^2$$

The dominant contribution is from the first term. The D masses are about 1865 MeV and at the $\psi(3772)$ their momentum is only about 280 MeV/c so p/m = .15 and the mass resolution is about 7 times better than the momentum resolution. Without the constraint that the D energy is equal to the beam energy the mass resolution would be of the order of the momentum resolution or worse.

Figures IV.5 and IV.6 show the mass spectra for $K^-\pi^+$ (D^o) and $K^-\pi^+\pi^+$ (D^+) combinations using the above technique. The D peaks are unmistakeable, to say the least.

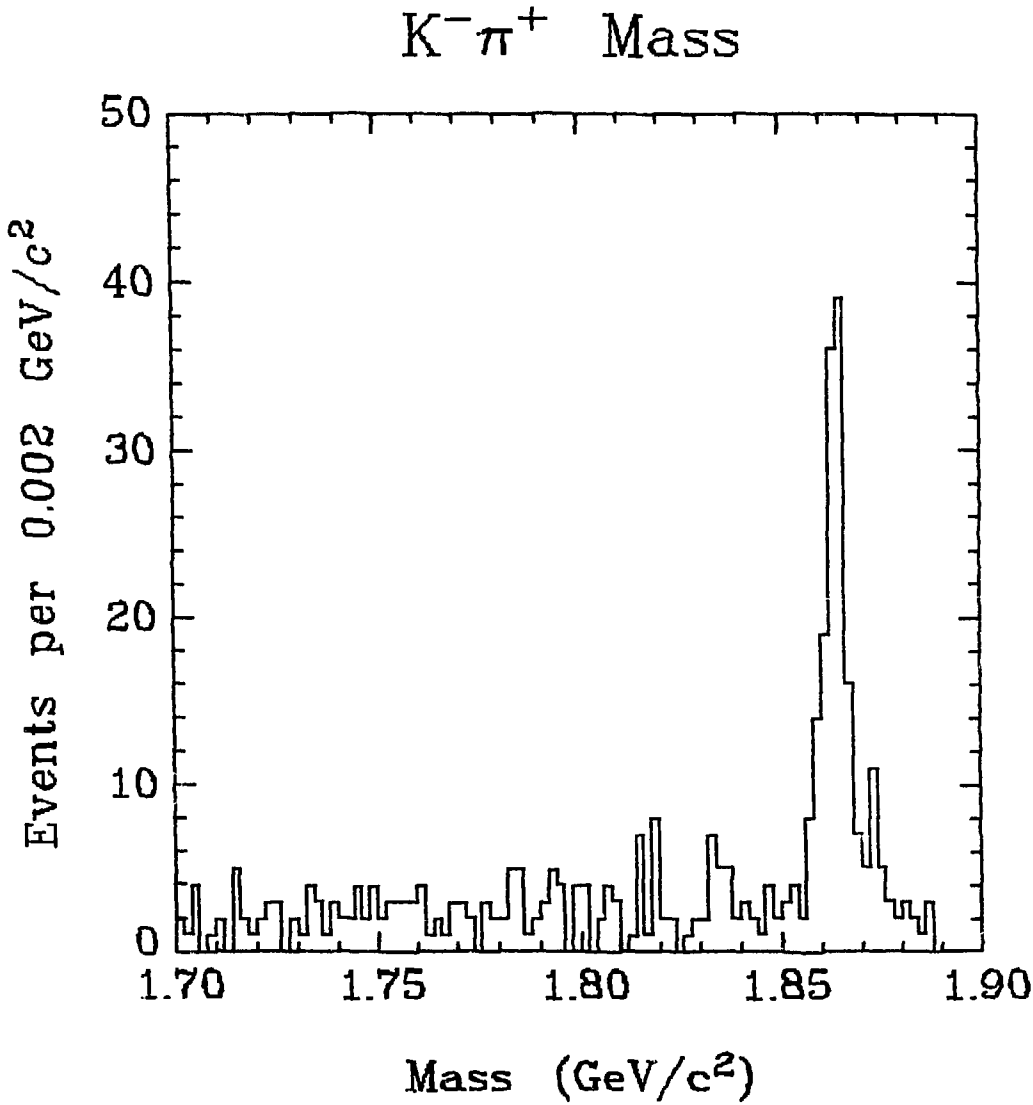

FIGURE IV.5

$K^{\mp}\pi^{\pm}(D^{o})$ mass spectrum at the $\psi(3772)$.

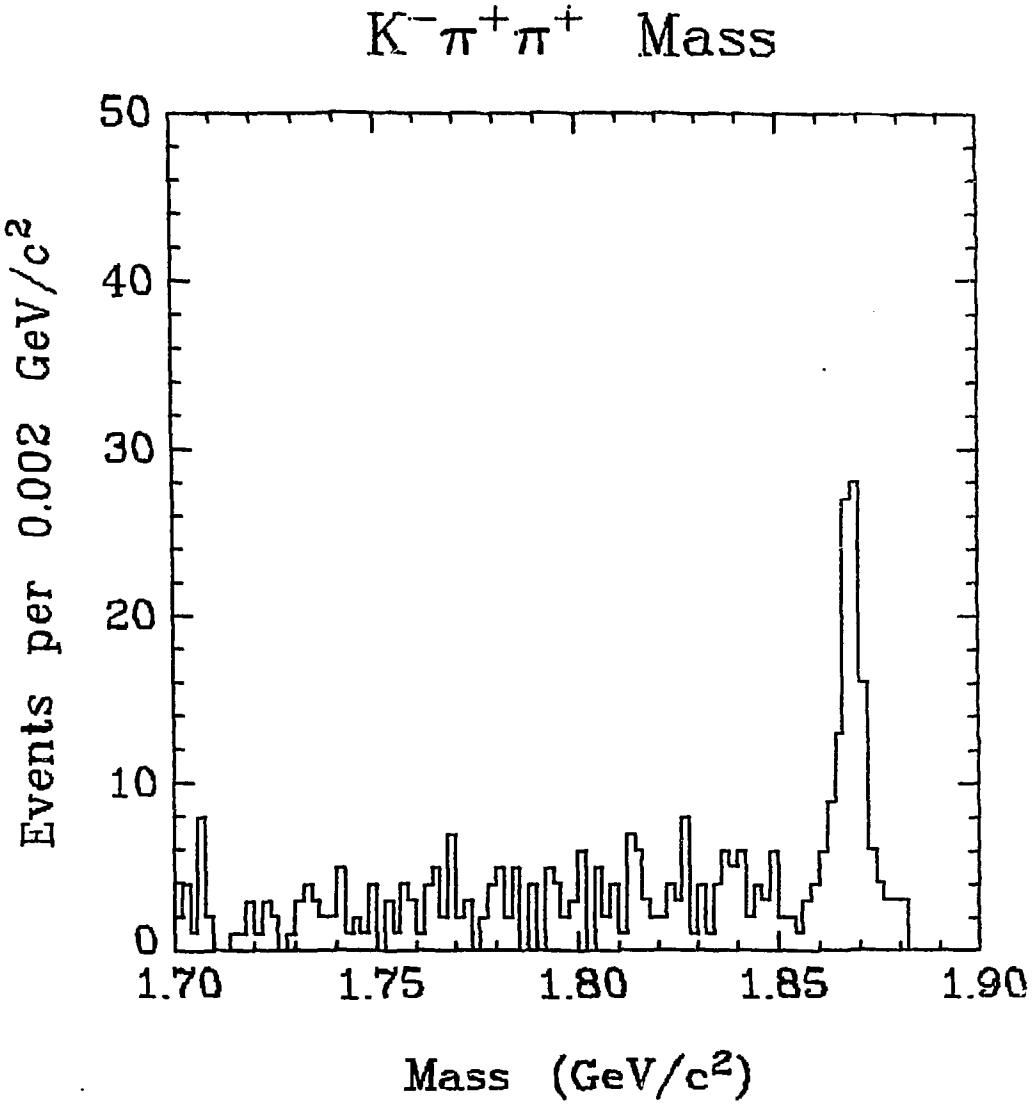

FIGURE IV.6
$K^{\mp}\pi^{\pm}\pi^{\pm}(D^+)$ mass spectrum at the $\psi(3772)$.

D. "Tagged" Events

The particularly simple nature of the final state ($D\bar{D}$) in $\psi(3772)$ decays affords a unique opportunity to make inclusive studies of D decays. Since only a D and a $\bar{D}$ are produced, if a $D(\bar{D})$ is identified by the procedure described in Section C above, then all other tracks observed in the event must be decay products of the $\bar{D}(D)$. Therefore, by studying the recoil system in such "tagged" events we can learn a lot about D decays even without completely reconstructing the recoil D. In essence, we have a D nearly at rest in the center of our detector and we watch it decay. We know it is there because we have seen its charge conjugate partner. This type of inclusive study is particularly valuable since most of the exclusive decay modes of the D's have not yet been observed due to low acceptances and/or high backgrounds.

(These same tagged events can also be used to study exclusive decay channels of the D mesons. By measuring the frequency of occurence of specific decay channels in the recoil system one measures branching ratios in a manner independent of any assumptions about the D production cross sections. These measurements yield results which are consistent with those presented in Table I.2 but with larger statistical errors.)

Although nature has been kind in providing such a clean laboratory for studying D decays, it has been rather stingy with regard to the numbers of these tagged events. The only decay modes which give a sufficiently clean sample of tagged events are $K^-\pi^+$ for the D^o and $K^-\pi^+\pi^+$ for the D^+. (All references to a specific charge state also refer to the charge conjugate state, such as $K^+\pi^-\pi^-$ for the D^-.) The combination of small branching ratios for these modes and the acceptance of the detector leaves us with 139 D^o events and 105 D^+ events in $\pm$ 8 MeV bands about their respective masses, 1863 and 1868 MeV.

We estimate the background from the number of events in the 1750-1850 mass region, with the assumption of a flat background. This assumption is consistent with the observed background distribution. (See Figures IV.5 and IV.6.) We find 154 $K^-\pi^+$ events and 136 $K^-\pi^+\pi^+$ events in this region. Scaling by the relative bin widths (16/100) we find estimated backgrounds of 22 $\pm$ 2 D^o events and 25 $\pm$ 2 D^+ events for a net signal of 117 D^o events and 80 D^+ events.

In the next chapter we use these events to measure the inclusive branching ratios of D mesons to states containing kaons.

References

Chapter IV

1. P.A. Rapidis et al., Phys. Rev. Lett. 39, 526 (1977)

2. K. Lane and E. Eichten, Phys. Rev. Lett. 37, 477 (1976)

3. V. Luth et al., Phys. Rev. Lett. 35, 1124 (1975)

4. V. Vuillemin, private communication

V. Inclusive Branching Ratios for $D \to KX$ at the $\psi(3772)$

According to the model which predicted the existence of charmed particles, that of Glashow, Iliopoulos, and Maiani[1] (GIM), the charmed quark couples preferentially to the strange quark in the weak interactions. This would imply that hadrons with positive charm should decay into states with negative strangeness. Conservation of energy and baryon number forbid the presence of strange baryons in D meson decays so we would expect the strangeness to appear in the form of kaons. Figure V.1 is a quark diagram illustrating a typical decay, $D^o \to K^-\pi^+$.

If the GIM model is correct then roughly 95% ($\cos^2(\theta_C)$) of D decays should contain kaons of the "Cabibbo-preferred" strangeness, that is, negative strangeness from positive charm and vice versa. In addition, about 5% ($\sin^2(\theta_C)$) of the decays would be expected to include a kaon of the opposite or "Cabibbo-suppressed" strangeness which can be produced if the "other end" of the W propagator couples to a u-$\bar{s}$ quark pair instead of a u-$\bar{d}$ quark pair (see Figure V.1). These percentages may be modified by phase space or dynamical effects.

In this chapter we use the tagged D events at the $\psi(3772)$ to measure the kaon content of D meson decays by counting kaons in the recoil system.

In principle there are a total of 16 single kaon branching ratios to be measured. CPT symmetry requires the equality of branching ratios for charge conjugate modes (For example, $B(D^+ \to K^-X) = B(D^- \to K^+X)$) reducing the number to 8, namely

1) $D^o \to K^-X$
2) $D^o \to \bar{K}^oX$ Cabibbo-favored
3) $D^+ \to K^-X$
4) $D^+ \to \bar{K}^oX$

5) $D^o \to K^+X$
6) $D^o \to K^oX$ Cabibbo-suppressed
7) $D^+ \to K^+X$
8) $D^+ \to K^oX$

In practice, we cannot distinguish a K^o from a $\bar{K}^o$, reducing the number of measurements to six. In addition, the fact that the kaon and the pion in the tagging decay $D^o \to K^-\pi^+$ have very high momentum (typically 800 MeV) makes them hard to distinguish on an event-by-event

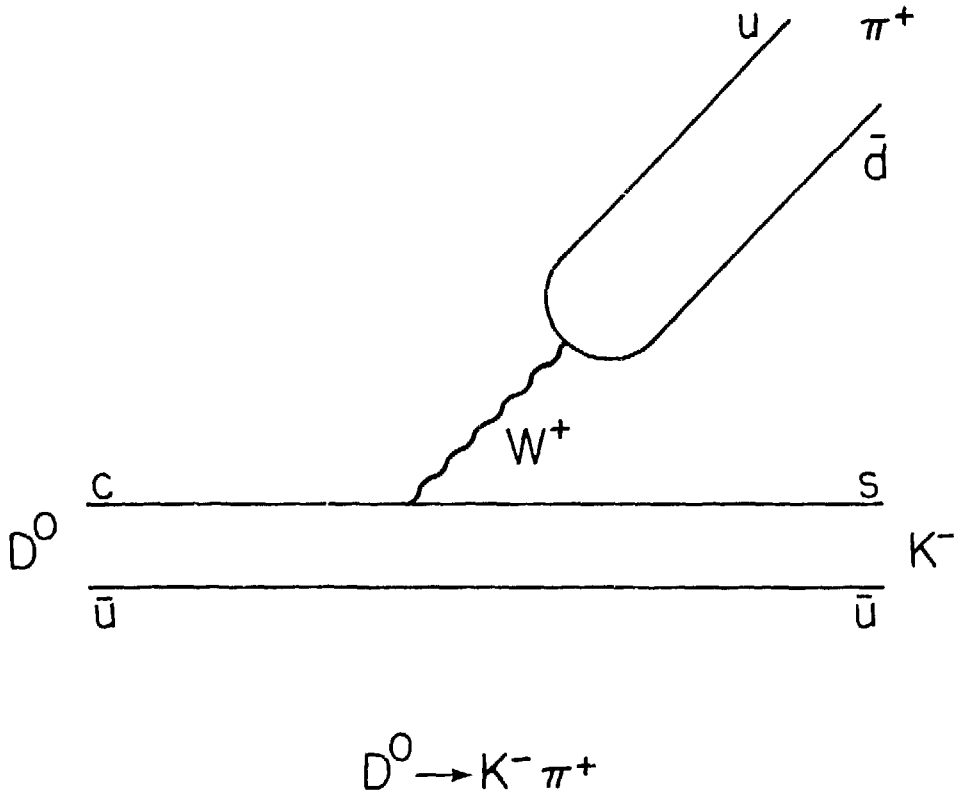

XBL 791-286

FIGURE V.1
Quark diagram for the decay $D^0 \to K^-\pi^+$.

basis, leading to an ambiguity between D^0 and $\overline{D^0}$. Because we utilize CPT symmetry, this is equivalent to an ambiguity between K^+ and K^- in the decay of the D^0. We therefore do not measure the branching ratios for decays 1) and 5) separately but instead measure the combined branching ratio for $D^0 \rightarrow K^+X$. We note that there is no such sign ambiguity in the charged D decays. We therefore measure a total of 5 inclusive branching ratios.

Henceforth in this chapter we use the symbol K^0 to refer to both K^0 and $\overline{K^0}$, since they are not separated experimentally, and all references to a specific charge state also refer to the charge conjugate state. (For example, our measurement of K^+ content in D^+ decays also includes the K^-'s found in D^- decays.)

The measurements of the five inclusive branching ratios are presented in Table V.1.[2] For each of the five modes, the first column shows the number of tagged events remaining after background subtraction (see Chapter IV). The second column shows the number of kaons found in the recoil systems of these events using the kaon identification techniques described in Chapter III. For neutral kaons, the third column gives the number of background kaons expected from random two-pion combinations (see Chapter III).

The numbers of kaons from background events, that is, events in which the tagging $K\pi$ or $K\pi\pi$ combination is not really a D, are determined by counting the numbers of kaons in the recoil systems of events with a $K\pi$ or $K\pi\pi$ combination in the 1.75-1.85 GeV mass region (below the mass of the D), and then scaling these numbers by the ratio of the mass bin widths (16/100) in the same way that the numbers of background events were measured in Chapter IV. The resulting backgrounds are shown in the fourth column of Table V.1.

The fifth column of Table V.1 gives the efficiency for kaon detection in each of the five modes. For neutral kaons this is the 0.086 determined from the Monte Carlo simulation discussed in Chapter III. For charged kaons the efficiency is the product of the solid angle and the decay, tracking, and time-of-flight measurement efficiencies:

$$\epsilon_{K^\pm} = \frac{\Delta\Omega}{4\pi}\,\epsilon_{decay}\,\epsilon_{track}\,\epsilon_{TOF}$$

All of these efficiencies are discussed in Chapter III. The solid angle factor is simply the 0.73 physical solid angle of the detector; because the D's are nearly at rest ($\beta = 0.15$) there are no significant effects of angular correlation between the "tagged" D and the recoiling D. The efficiency is not the same for all three of the charged kaon branching ratios measured because the decay efficiency is an average which depends on the observed momentum spectrum of the kaons and because the time-of-flight measurement efficiency is determined separately for the D^0 and D^+ samples.

The backgrounds in columns 3 and 4 are subtracted from the numbers of kaons in column 2 and the differences are divided by the efficiencies in column 5 to arrive at the corrected

Table V.1

Measurement of Kaon Content of D Decays

Mode	# Events	# Kaons	Background from Random Combinations	Background from Background Events	Efficiency	Corrected # Kaons	Branching Ratio
$D^0 \rightarrow K^0X$	117 ± 2	7.0 ± 2.6	0.8 ± 0.4	0.3 ± 0.3	.086	68.6 ± 30.8	.59 ± .26
$D^0 \rightarrow K^+X$	117 ± 2	21.2 ± 5.1		2.4 ± 0.6	.46	41.4 ± 11.4	.35 ± .10
$D^+ \rightarrow K^0X$	80 ± 2	4.0 ± 2.0	0.8 ± 0.4	0.6 ± 0.4	.086	30.2 ± 24.2	.38 ± .30
$D^+ \rightarrow K^-X$	80 ± 2	4.8 ± 2.2		1.4 ± 0.5	.42	8.1 ± 5.4	.10 ± .07
$D^+ \rightarrow K^+X$	80 ± 2	2.8 ± 1.7		1.1 ± 0.4	.39	4.5 ± 4.6	.06 ± .06

numbers of kaons shown in column 6. These numbers are then finally divided by the numbers of events (column 1) to obtain the inclusive branching ratios which are shown in the last column of Table V.1:

$$B(D \to KX) = \frac{N_K - N_{bkgd}}{\epsilon\, N_D}$$

Summing the charged and neutral kaon branching ratios we get the following total branching ratios for D decays into kaons

$$B(D^0 \to KX) = .92 \pm .14$$

$$B(D^+ \to KX) = .54 \pm .31$$

In Table V.2 we compare the measured branching ratios with those expected from the statistical model of Quigg and Rosner.[3] This model assumes equal reduced matrix elements for all isospin channels in the decay and therefore the branching ratios are determined simply by phase space and isospin Clebsch-Gordan coefficients. The model assumes that all decays include one kaon of the Cabibbo-preferred strangeness. It makes separate predictions for semileptonic and nonleptonic decays; these have been combined using the average semileptonic branching ratio whose measurement is presented in the next chapter.

We see that the charged kaon content observed in D^0 decays (.35 ± .10) is somewhat less than that predicted by the statistical model while the charged kaon content in D^+ decays (.10 ± .07) is much less than predicted. The latter observation implies that if most of the D^+ decays contain a kaon then neutral kaons must dominate by a large factor. Unfortunately, the large error on the neutral kaon content in D^+ decays (.38 ±.30) does not permit a meaningful test of this hypothesis.

The significance of these results is discussed further in the Conclusions (Chapte

Table V 2

Comparison of $D \rightarrow KX$ Data with Statistical Model

Mode	Statistical Model	Measured
$D^0 \rightarrow K^0X$	.52	.59 ± .26
$D^0 \rightarrow K^+X$	.48	.35 ± .10
$D^+ \rightarrow K^0X$	.67	.38 ± .30
$D^+ \rightarrow K^-X$	.33	.10 ± .07
$D^+ \rightarrow K^+X$	.0	.06 ± .06

References

Chapter V

1. S.L. Glashow, J. Iliopoulos and L. Maiani, Phys. Rev. D2, 1285 (1970)

2. V. Vuillemin et al., Phys. Rev. Lett. 41, 1149 (1978)

3. C. Quigg and Jonathan L. Rosner, Phys. Rev. D17, 239 (1978);
Jonathan L. Rosner in Deeper Pathways in High-Energy Physics, Proceedings of Orbis Scientiae, Coral Gables, 1977, p.489

VI. Semileptonic Decays of D Mesons at the $\psi(3772)$

Since the D mesons decay weakly one expects that sometimes the decay products would include leptons. The vector nature of the weak current suppresses purely leptonic decays, such as $D^+ \rightarrow \mu^+\nu_\mu$, by a factor of m_l^2/m_D^2 relative to semileptonic and nonleptonic decays. Semileptonic decays do not have this suppression and they may be significant. Figure VI.1 is a quark diagram for a possible semileptonic decay, $D^o \rightarrow K^-e^+\nu_e$.

Unfortunately, the small solid angle of the Lead-Glass Wall (.0548 x 4π sr) and the small number of tagged events (139 D^o and 105 D^+) render impossible the use of the tagged events to study the semileptonic decays of D mesons. Even if there were no enhancement of the hadronic decays and the semileptonic branching ratios to electrons were 20% (see Chapter I), we would still expect only about one event each from the D^o and the D^+.

Instead, we measure the inclusive cross section for electron production at the $\psi(3772)$ and assume that the background from processes other than D decays is equal to that at the $\psi(3.1)$ when expressed as a ratio of electrons to hadrons. The total cross section for production of D mesons is obtained by assuming that the resonant part of the cross section goes 100% into $D\overline{D}$ (See Chapter IV for evidence supporting this assumption.) and the ratio $\sigma_e/\sigma_{resonant}$ is taken as an average branching ratio. Unfortunately, this technique does not allow us to distinguish those electrons which come from neutral D's from those which come from charged D's nor to determine whether the electrons have the expected sign (e^+ for D^o and D^+ and e^- for $\overline{D^o}$ and D^-).

At the $\psi(3772)$ our total data sample represents an integrated luminosity of 1326 inverse nanobarns. In this sample there were 2380 events which met the hadronic event selection criteria described in Chapter III and had a track in the Lead-Glass Wall which met the criteria (also described in Chapter III) for a clean track in the LGW.

The number of electrons in this sample of 2380 tracks is determined by taking the number of tracks which pass the electron identification cuts (Chapter III), subtracting the background determined using the background rates from Table III.3, and then dividing by the electron identification efficiency from Table III.2 :

$$N_{corr} = \frac{N_{obs} - N_{backgr}}{\epsilon_{electron\ ID}}$$

where N_{corr} is the corrected number of electrons, N_{obs} is the number of identified electrons, N_{backgr} is the estimated background, and $\epsilon_{electron\ ID}$ is the electron identification efficiency.

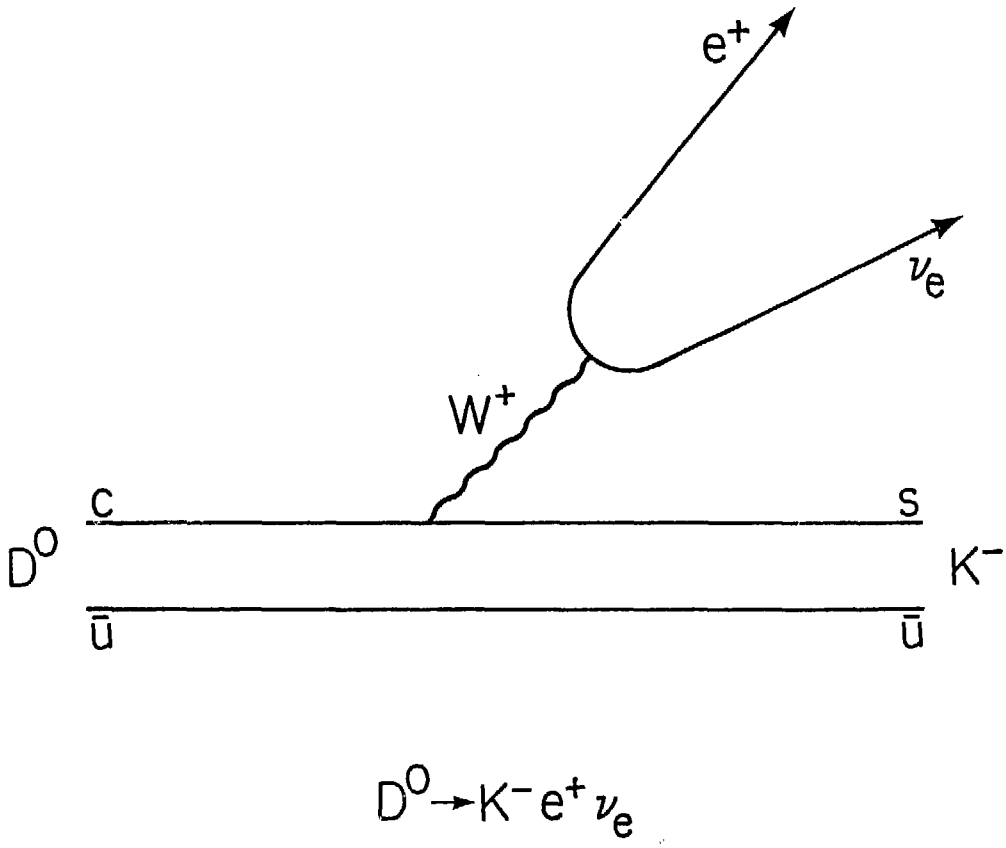

XBL 791-287

FIGURE VI.1

Quark diagram for the decay $D^0 \rightarrow K^- e^+ \nu_e$

Table VI.1 shows, in 100 MeV/c momentum bins, the number of clean tracks, the number of identified electrons, the expected background, the electron identification efficiency, and, in the last column, the corrected number of electrons. The bottom row of the table gives the total for each column.

In order to calculate differential and total cross sections from the corrected numbers of electrons it is necessary to correct for the solid angle of the Lead-Glass Wall, the tracking efficiency of the detector, the acceptance of the detector, and the efficiency of the cuts designed to select clean hadronic events and the cuts used to obtain a clean sample of tracks in the Lead-Glass Wall:

$$\sigma_e = \frac{N_{corr}}{\int Ldt} \frac{1}{(\frac{\Delta\Omega}{4\pi})_{LGW} \epsilon_{track} A \epsilon_{event\ cuts} \epsilon_{clean\ track\ cuts}}$$

The determinations of all of these correction factors are presented in Chapter III. They are summarized in Table VI.2. The total correction factor, which we call the overall efficiency, is 0.037 ± .003. It is independent of electron momentum and it includes all efficiency factors except for the efficiency of the electron identification cuts on the energy deposited in the Lead-Glass Wall, which is momentum-dependent (see above). Note that the overall efficiency is dominated by the solid angle of the Lead-Glass Wall, 0.0548.

Dividing by this correction factor and by the integrated luminosity we find a total cross section of 1.12 ± 0.33 nb for producing an anomalous electron with momentum greater than 300 MeV/c in a hadronic event in which four or more charged particles are produced at the $\psi(3772)$ resonance. Here "anomalous" electrons are electrons which are produced by processes which are not present at the $\psi(3.1)$ resonance, where the background rate was measured.

An identical procedure has been employed to measure the cross section for anomalous electron production at center-of-mass energies immediately above and below the $\psi(3772)$. Figure VI.2 shows the cross section as a function of center-of-mass energy from 3.73 GeV to 3.89 GeV. The superimposed curve is the shape of the resonant part of the total cross section, normalized to the point at 3.772 GeV. We see that the anomalous electron cross section is consistent with zero on either side of the resonance and has a peak which is associated with the resonance.

Since there is evidence that the $\psi(3772)$ decays predominantly into $D\bar{D}$, it is natural to assume that these electrons come from semileptonic decays of D mesons. (There is a smaller contribution from the τ heavy lepton; see Chapter VII, section B.)

Figure VI.3 shows the differential cross section with respect to electron momentum at the $\psi(3772)$. Superimposed on the figure are momentum spectra expected for three possible semileptonic D decay modes, $D \rightarrow Ke\nu$, $K^*e\nu$, (both Cabibbo favored) and $\pi e\nu$ (Cabibbo

Table VI.1

Electron Analysis at the $\Psi(3772)$

Momentum Range	Clean Tracks	Identified Electrons	Background Electrons	Electron ID Efficiency	Corrected Electrons
0.3 - 0.4	657	15	7.9 ± 2.0	.50 ± .20	14.2 ± 10.4
0.4 - 0.5	506	17	5.4 ± 1.5	.61 ± .20	19.1 ± 9.5
0.5 - 0.6	406	14	3.8 ± 1.2	.72 ± .20	14.2 ± 6.7
0.6 - 0.7	271	5	2.2 ± 0.8	.83 ± .20	3.4 ± 3.0
0.7 - 0.8	205	5	1.4 ± 0.8	.89 ± .10	4.0 ± 2.7
0.8 - 0.9	125	0	0.9 ± 0.5	.89 ± .10	-1.0 ± 0.6
0.9 - 1.0	79	0	0.6 ± 0.3	.89 ± .10	-0.6 ± 0.4
1.0 - 1.1	52	1	0.4 ± 0.2	.89 ± .10	0.7 ± 1.2
1.1 - 1.2	20	1	0.1 ± 0.1	.89 ± .10	1.0 ± 1.1
1.2 - 1.3	21	0	0.1 ± 0.1	.89 ± .10	-0.2 ± 0.1
1.3 - 1.4	15	0	0.1 ± 0.1	.89 ± .10	-0.1 ± 0.1
1.4 - 1.5	14	1	0.1 ± 0.1	.89 ± .10	1.0 ± 1.1
1.5 - 1.6	2	0	0.0 ± 0.0	.89 ± .10	0.0 ± 0.0
1.6 - 1.7	3	0	0.0 ± 0.0	.89 ± .10	0.0 ± 0.0
Totals	2376	59	22.9 ± 3.1	<.65>	55.7 ± 16.3

Table VI.2

Summary of Efficiency Factors
for Electron Analysis at the $\Psi(3772)$

	Source	Factor
	LGW Solid Angle	.0548 ± .00
	Detector Acceptance and Trigger Efficienc,	.85 ± .07
	Tracking Efficiency	.98 ± .01
Cuts to select clean hadronic events	Vertex Cut	.92 ± .01
	Electrodynamic Event Cuts	.96 ± .04
Cuts to select clean tracks	Time-of-Flight Cut	.96 ± .01
	γ Nearby Cut	.98 ± .01
	Track Nearby Cut	.97 ± .01
	Pair Cut	.99 ± .01
	Product (Overall Efficiency)	.037 ± .003

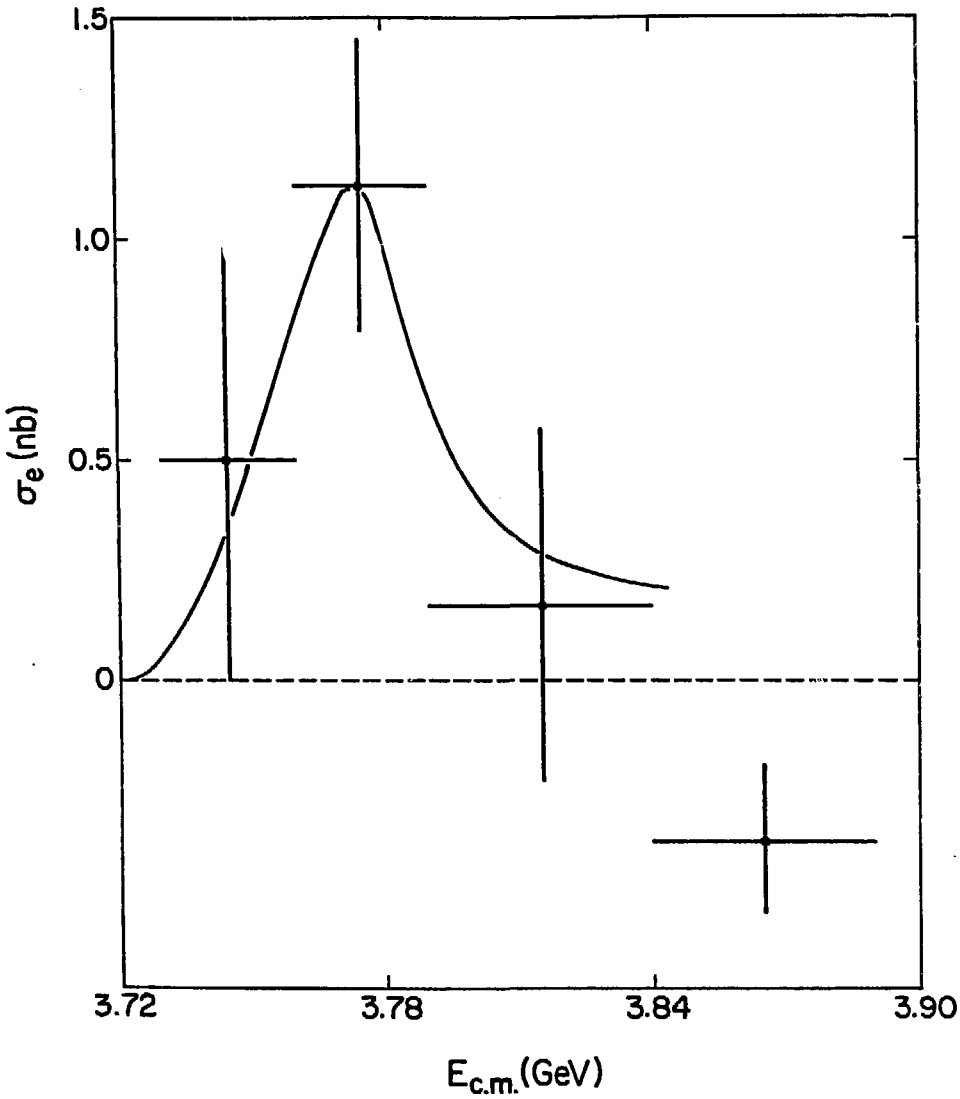

XBL 791-291

FIGURE VI.2

The ratio $R_e = \dfrac{\sigma(e^+e^- \to e^\pm + \text{hadrons})}{\sigma(e^+e^- \to \mu^+\mu^-)}$ in the neighborhood of the $\psi(3772)$. The curve shows the shape of the resonance and is normalized to the point at 3772 GeV.

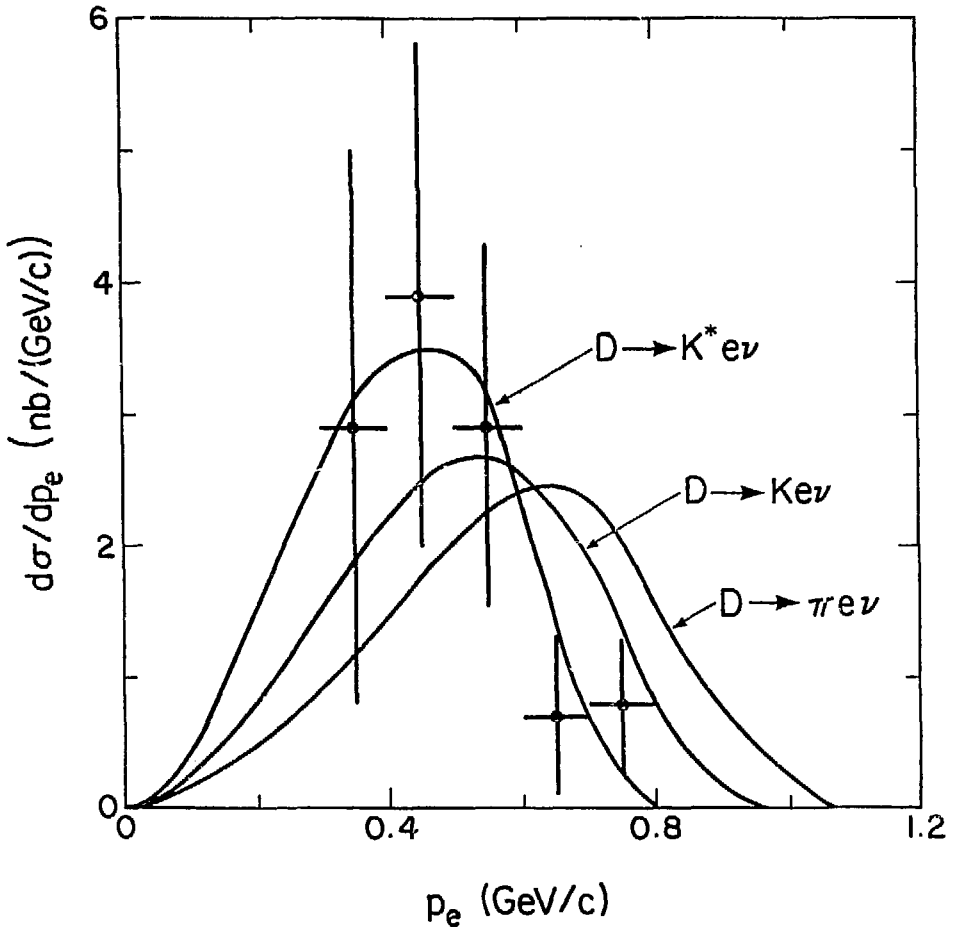

XBL 791-292

Figure VI.3
Electron momentum spectrum at the $\psi(3772)$.

suppressed). The curves are calculated according to the same simple model of Hinchliffe and Llwellyn-Smith used in the acceptance Monte Carlo simulations (see Chapter III). The shapes are very similar to those obtained by Ali and Yang[1] in a more sophisticated calculation in which they used the full V - A form of the hadronic current and included hadronic form factors.

We see that the spectrum is consistent with dominance of either of the Cabibbo-favored decay modes but is less consistent with the Cabibbo-suppressed mode $\pi e\nu$. The spectrum is inconsistent with the helicity-suppressed decay $D^+ \rightarrow e^+\nu_c$, which would produce a flat spectrum from about 800 MeV/c to about 1100 MeV/c.

Assuming, consistent with the momentum spectrum and the energy-dependence of the cross section, that these electrons do indeed come from semileptonic decays of D mesons and further assuming, as indicated by the evidence presented in Chapter IV, that the $\psi(3772)$ decays into $D\bar{D}$ 100% of the time, we can calculate an average semileptonic branching ratio for the D mesons.

First, however, we must correct for two categories of events that lie outside the physical region to which our measurements are sensitive, namely, events in which the electron has a momentum of less than 300 MeV/c and events in which a total of only two charged particles are produced. (The acceptance calculation (Table III.2) accounts for events in which four or more charged particles are produced but less than three are detected.) The estimation of the fraction of events falling into these two categories is purely dependent on physical assumptions and is independent of the apparatus.

Using the decay model of Hinchliffe and Llewellyn-Smith we find that in the decay mode $D \rightarrow Ke\nu$ 86% of the electrons will have greater than 300 MeV/c of momentum and in the mode $D \rightarrow K^*e\nu$ 78% of the electrons will be above 300 MeV/c. The spectra of Ali and Yang give virtually the same answer. These fractions change by less than 2% with increasing D momentum for D momenta up to 3 GeV/c.

Using the expected charged multiplicity distributions (including charged pions from K_S^0 decays) for the $Ke\nu$ and $K^*e\nu$ decays and the measured multiplicity distributions for all D decays from the tagged events[2] we find that 83% of all $D\bar{D}$ events in which one D decays semileptonically in the $Ke\nu$ mode will have a total of at least four charged particles produced (including the electron) and 93% will have at least four charged particles produced when the semileptonic decay mode is $K^*e\nu$. (We have averaged D^o and D^+.)

We note that the product of the two correction factors is 71% for $Ke\nu$ and 73% for $K^*e\nu$, so our final answer is virtually independent of whether we assume that $Ke\nu$ or $K^*e\nu$ is the dominant decay mode.

Using an average correction of 72% we arrive at a total cross section for anomalous electron production at the $\psi(3772)$ of 1.56 ± 0.46 nanobarns.

The height of the $\psi(3772)$ resonance is 10.3 ± 2.2 nanobarns.[3] If it decays 100% of the time into $D\bar{D}$ then the total cross section for D and $\bar{D}$ production is 20.6 ± 4.4 nanobarns. Taking the ratio of the anomalous electron production cross section to the D production cross section we find

$$B(D \rightarrow eX) = .076 \pm .028$$

where $B(D \rightarrow eX)$ is the inclusive semileptonic branching ratio for a D to decay into an electron plus anything.

Because this measurement does not distinguish betweeen charged and neutral D decays it actually represents a weighted average of the D^o and the D^+ semileptonic branching ratios, weighted by the relative production cross sections for $D^o\overline{D^o}$ and D^+D^- at the $\psi(3772)$.

If the $\psi(3772)$ is a state of unique isospin, either 0 or 1, then the absolute values of the Clebsch-Gordan coefficients for $D^o\overline{D^o}$ and D^+D^- production are equal. (If the charmonium model is correct then the $\psi(3772)$ has isospin 0.) In that case the only difference between the two branching ratios is that which results from the D^o-D^+ mass difference which gives the $D^o\overline{D^o}$ mode a higher momentum. The momentum dependence of the partial decay width of a vector particle to a pair of equal-mass pseudoscalars is given by

$$\Gamma \approx \frac{p^3}{1 + rp^2}$$

where p is the momentum of each of the decay products and r is an interaction radius. In the decay of the $\psi(3772)$ to $D^o\overline{D^o}$ the momentum is 288 MeV and the momentum for the D^+D^- decay is 253 MeV. This gives us a $D^o\overline{D^o}$ to D^+D^- ratio of 59:41 for r = 0 and 53:47 for r = ∞.[4] We therefore take the branching ratio for $\psi(3772) \rightarrow D^o\overline{D^o}$ to be 0.56 ± 0.03 and the D^+D^- branching ratio to be 0.44 ± 0.03.

A precise statement of our result is then

$$0.56\, B(D^o \rightarrow eX) + 0.44\, B(D^+ \rightarrow eX) = 0.076 \pm 0.028$$

In this analysis we have only considered the decay modes $D \rightarrow Ke\nu$ and $D \rightarrow K^*e\nu$ in making the corrections for two-prong events and for electrons with momentum less than 300 MeV/c and we have shown that the result is virtually the same if either of these two modes is assumed to be dominant. If instead the mode $K\pi e\nu$ were dominant our result would be higher by about one half of the quoted error. Modes containing two or more pions are not consistent with our observed electron momentum spectrum.

References

Chapter VI

1. A. Ali, T.C. Yang, Phys. Lett. 65B, 275 (1976)

2. V. Vuillemin et al., Phys. Rev. Lett. 41, 1149 (1978)

3. I. Peruzzi et al., Phys. Rev. Lett. 39, 1301 (1977)

4. P.A. Rapidis et al., Phys. Rev. Lett. 39, 526 (1977)

VII. Electron Production in Multiprong Events from 3.9 to 7.4 GeV

Figure VII.1 shows the ratio R of the hadron production cross section in e^+e^- annihilation to the theoretical one-photon cross section for muon pair production (σ_{QED}) as a function of center-of-mass energy from 3 to 8 GeV.[1] Below 3.5 GeV R is constant at about 2.6. Above 3.5 GeV there is a complex region of several resonances followed by another plateau at about 5.5. About one unit of the 5.5 is attributed to production and decay of the τ heavy lepton (see section B below). Charmed particle production is the most plausible explanation for the rest of the increase above the low-energy plateau and for the series of broad resonances starting with the $\psi(3772)$.

If this is indeed the case then we would expect significant electron production from weak decays of charmed particles at all center-of-mass energies above the $\psi(3772)$ and we would expect the shape of the inclusive electron cross section as a function of center-of-mass energy to have structure similar to that of the total cross section. At these higher center-of-mass energies new thresholds for charmed particle production open up and there may be electrons from semileptonic decays of F mesons and charmed baryons as well as from D mesons.

In this chapter we present measurements of the cross section and momentum spectra for electron production in multiprong events from 3.9 to 7.4 GeV, we use the electron momentum spectrum to set an upper limit on the contribution of the τ heavy lepton, and we calculate an average semileptonic branching ratio of the charmed particles produced in this center-of-mass energy range.

A. Inclusive Electron Cross Section

The data has been divided into ten center-of-mass energy bins. The binning was chosen on the basis of our distribution of integrated luminosity and the physical regions defined by the shape of the total hadronic cross section. (The binning was chosen before examination of the data itself.) Table VII.1 lists, for each bin, the energy range, the average energy (weighted by the integrated luminosity), and the number of events with a track in the Lead-Glass Wall which met the event and clean track selection criteria described in Chapter III.

Table VII.2 lists, for each bin, the number of electron candidates, the expected background, the average electron identification efficiency, the corrected number of events after background subtraction and division by the average electron identification efficiency, and the inclusive cross

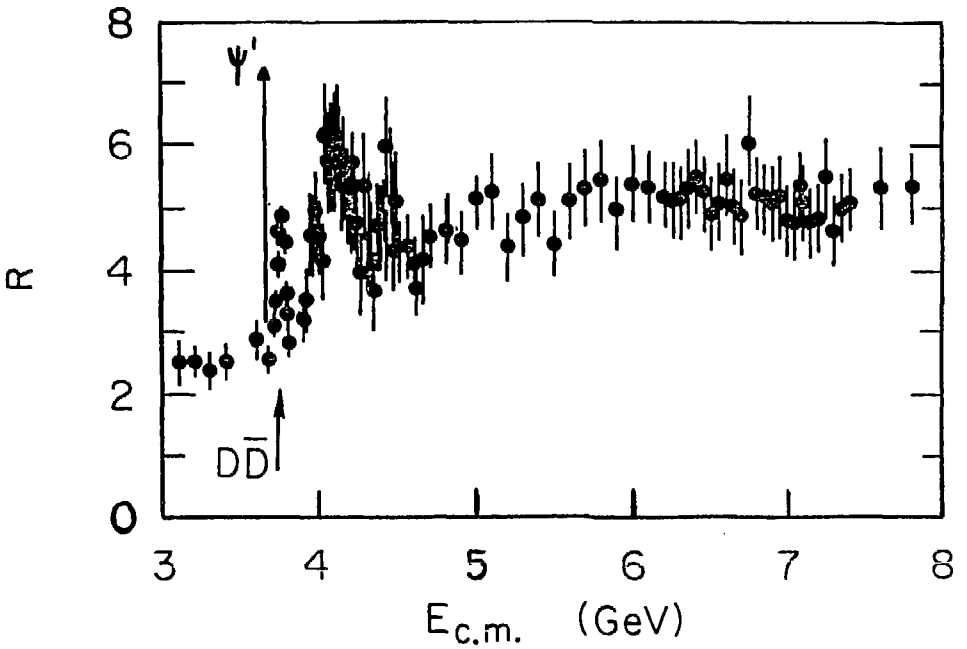

XBL 7812-13697

FIGURE VII.1

The ratio $R = \frac{\sigma(e^+e^- \to \text{hadrons})}{\sigma(e^+e^- \to \mu^+\mu^-)}$ from $E_{cm} = 3$ to 8 GeV.

Table VII.1

Data Sample from 3.9 to 7.4 GeV

Bin	E_{cm} Range (GeV)	$<E_{cm}>$	$\int Ldt$ (nb^{-1})	Clean Tracks
1	3.90 - 4.00	3.954	183	296
2	4.00 - 4.15	4.070	644	1229
3	4.15 - 4.17	4.164	872	1551
4	4.17 - 4.37	4.274	893	1362
5	4.39 - 4.44	4.416	204	334
6	4.44 - 4.90	4.694	2020	3134
7	4.90 - 5.71	5.312	1273	1703
8	6.31 - 6.78	6.534	2516	2717
9	6.96 - 6.98	6.970	1138	1120
10	7.16 - 7.38	7.322	2148	1943
	Total		11891	15389

Table VII.2

Electron Analysis from 3.9 to 7.4 GeV

$<E_{cm}>$	N_{cand}	N_{backgr}	ϵ_{ID}	N_{corr}	σ_e	R_e
3.954	7	2.9 ± 0.4	0.69	5.9 ± 4.3	0.92 ± 0.68	.17 ± .12
4.070	42	11.8 ± 1.6	0.68	44.4 ± 12.3	1.97 ± 0.57	.38 ± .11
4.162	53	14.8 ± 2.0	0.67	57.3 ± 14.9	1.88 ± 0.51	.38 ± .10
4.274	35	13.0 ± 1.7	0.64	34.5 ± 11.6	1.10 ± 0.38	.23 ± .08
4.416	7	3.2 ± 0.4	0.58	6.5 ± 4.8	0.91 ± 0.68	.20 ± .15
4.694	87	29.5 ± 3.8	0.73	79.1 ± 17.9	1.12 ± 0.27	.28 ± .07
5.312	48	15.8 ± 2.0	0.69	47.0 ± 12.9	1.05 ± 0.30	.34 ± .10
6.534	73	28.9 ± 3.0	0.74	59.9 ± 14.8	0.64 ± 0.17	.32 ± .08
6.970	37	11.8 ± 1.2	0.75	33.4 ± 9.5	0.79 ± 0.23	.44 ± .13
7.332	64	20.5 ± 2.1	0.75	57.8 ± 13.2	0.73 ± 0.18	.45 ± .11
Total	453	152.2 ± 6.6	0.71	425.8 ± 39.0		

section for producing electrons with momentum greater than 300 MeV/c in multiprong events. The cross section is obtained by dividing the corrected number of events by the overall efficiency and by the integrated luminosity (see Chapter VI). The background electron/hadron ratio, the electron identification efficiency, and the acceptance factor which enters into the overall efficiency are taken from Tables III.3, III.2, and III.1 respectively. The average electron identification efficiency quoted in Table VII.2 represents the average of the momentum-dependent efficiency listed in Table III.2, weighted by the observed momentum spectrum in each center-of-mass energy bin.

R_e, the inclusive electron cross section divided by the QED muon pair cross section, is shown in the last column of Table VII.2 and is displayed as a function of center-of-mass energy in Figure VII.2. Also included are the points from the $\psi(3772)$ region (see Chapter VI). One can see that the electron cross section, within errors, follows the structure in the total cross section. It drops to near zero just above the $\psi(3772)$, rises again around 4 GeV, and then levels out to a plateau where the value of R_e is about 0.33. (The error on the point at E_{cm} = 4.4 GeV is too large to see any resonant structure there.) The fact that the electron production cross section drops to near zero at the dips in the total cross section tends to confirm the hypothesis that the electron production is associated with the decays of new particles.

In order to examine the electron momentum spectra we divide the data into three coarse energy bins so as to obtain reasonable statistical precision. The three bins cover center-of-mass energy ranges 3.9-4.44, 4.44-5.71, and 6.31-7.38 GeV. The momentum spectra are shown in Figures VII.3-VII.5. The curves superimposed on the spectra are discussed in the next section.

B. The Heavy Lepton Contribution

A source of electron production in multiprong electron-positron annihilation events which has not been discussed up until now is the production and decay of the τ heavy lepton. The existence of the τ was first inferred from the observation of anomalous events at SPEAR in which the only observed particles were an electron and a muon.[2] It was hypothesized that these events arose from production of a pair of charged heavy leptons, one of which decayed into an electron plus neutrinos while the other decayed into a muon plus neutrinoes. These observations were subsequently confirmed by several other experiments at DORIS in Germany[3] and at SPEAR[4,5], including the Lead-Glass Wall experiment.[4] These subsequent experiments also reported hadronic decay modes of the τ. All experiments have supported the hypothesis that the τ is a point-like, spin-$\frac{1}{2}$ charged lepton with its own neutrino and conserved quantum number and the usual V - A weak couplings. (A good review of the experimental data concerning the τ can be found in Reference 6.) The most accurate measurement of the mass of the τ comes from the DELCO[5] experiment at SPEAR, which places it at 1782^{+2}_{-5} MeV, about

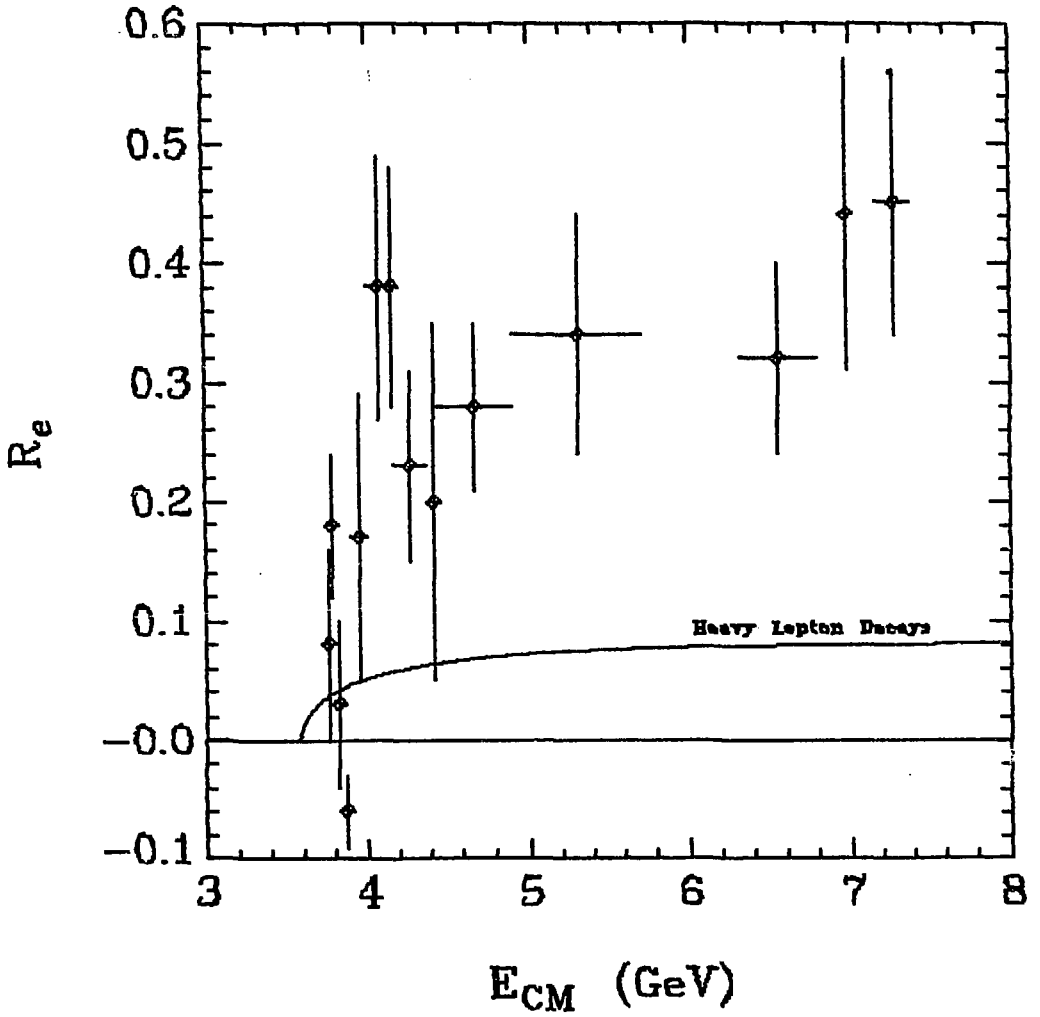

FIGURE VII.2

The ratio $R_e = \frac{\sigma(e^+e^- \to e^\pm + \text{hadrons})}{\sigma(e^+e^- \to \mu^+\mu^-)}$ from E_{cm} = 3.7 to 7.4 GeV. The curve shows the contribution from heavy lepton decays.

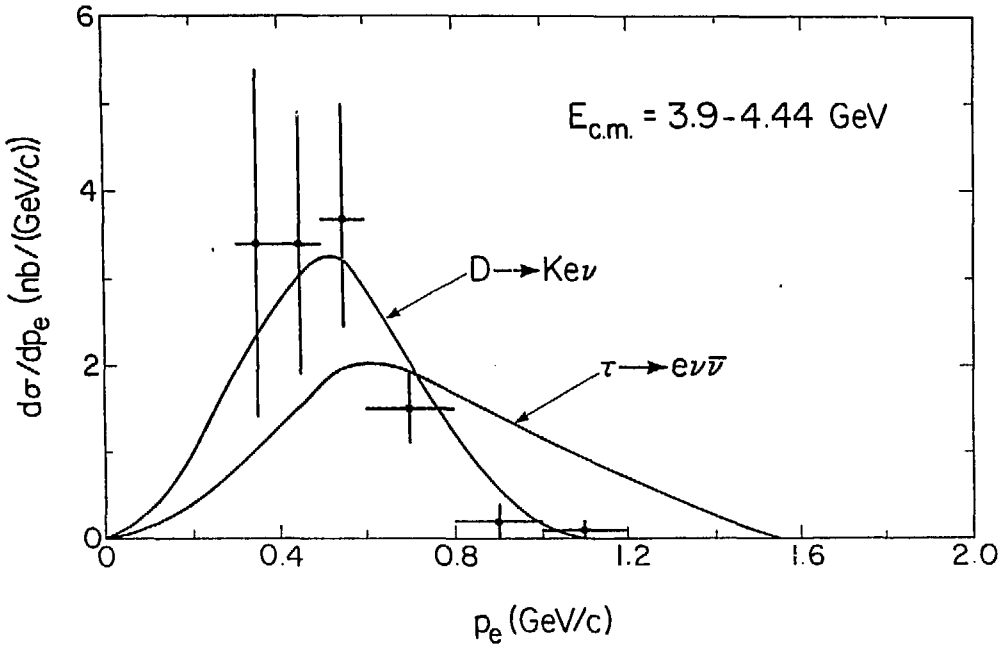

XBL 791-296

FIGURE VII.3

Electron momentum spectrum, E_{cm} = 3.9-4.44 GeV.

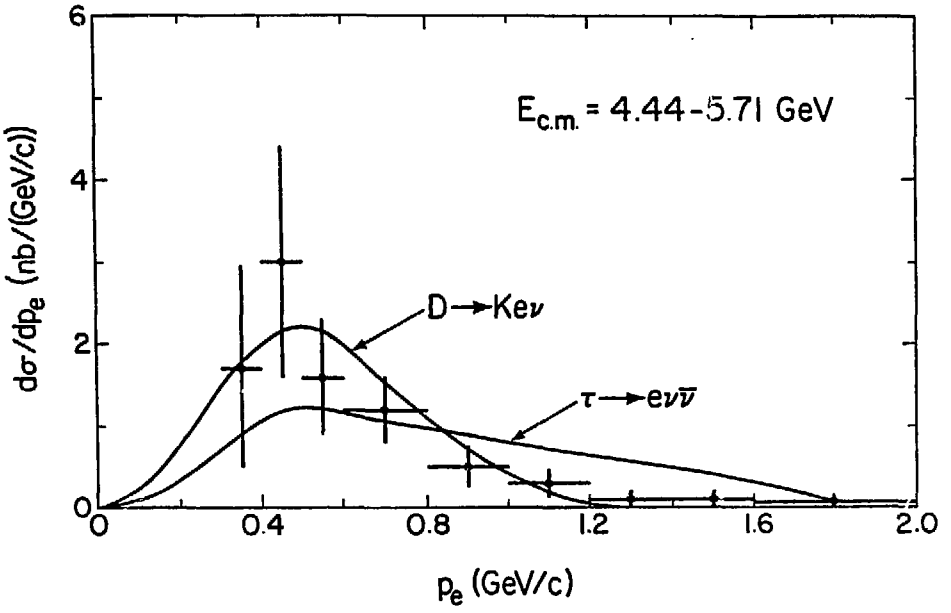

XBL 791-295

FIGURE VII.4

Electron momentum spectrum, E_{cm} = 4.44-5.71 GeV.

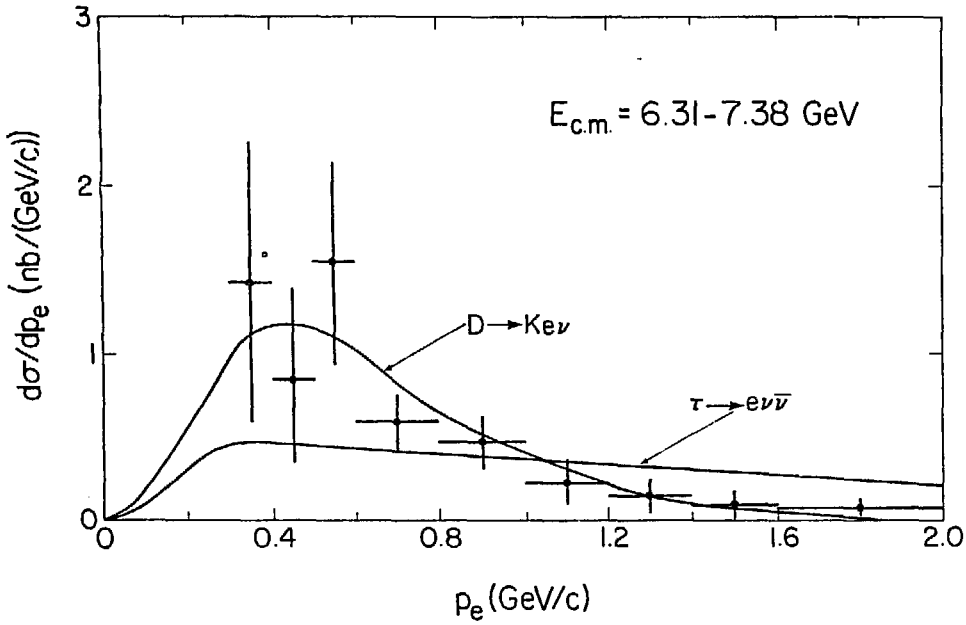

XBL 791-294

FIGURE VII.5

Electron momentum spectrum, E_{cm} = 6.31-7.38 GeV.

80 MeV below the D's.

τ decays can contribute to the cross section for producing electrons with momentum greater than 300 MeV/c in multiprong events if a pair of τ's is produced and one decays into an electron plus neutrinos while the other decays into a neutrino plus three or more charged hadrons. If we denote the branching ratio for the latter decay by $B(\tau \rightarrow \text{multiprongs})$ then the τ contribution can be written as

$$R_e(\tau) = 2\, R_\tau\, B(\tau \rightarrow e\nu\nu)\, B(\tau \rightarrow \text{multiprongs})\, F(\tau, p>300) \qquad \text{(VII.1)}$$

where R_τ is the ratio of the cross section for τ pair production to the QED muon pair cross section and $F(\tau,p>300)$ is the fraction of electrons from τ decay which have momentum greater than 300 MeV/c.

R_τ is simply the point-like cross section ratio for producing a pair of massive charged leptons:

$$R_\tau = \frac{\beta\,(3-\beta^2)}{2} \qquad \text{(VII.2)}$$

where β is the velocity of each τ divided by the speed of light.

R_τ rises from zero at τ threshold (3.592 GeV) to an asymptotic value of 1 at high energies.

The branching ratio for the τ to decay into an electron plus neutrinos has been measured in several experiments, including this one, and the world average is 17.9 $\pm$ 2.8%.[7]

The shape of the electron spectrum in τ decays may be assumed to be the same as that for muon decay. The fraction of electrons having momentum greater than 300 MeV/c is then about 0.92 and, within 2%, is independent of the center-of-mass energy in our energy range.

The contribution of the τ to R_e at high energies is therefore 0.33 times $B(\tau \rightarrow \text{multiprongs})$. Since R_e at high energies is about 0.33, this implies that the fraction of our electrons which are coming from τ decays is roughly equal to $B(\tau \rightarrow \text{multiprongs})$.

The available information on $B(\tau \rightarrow \text{multiprongs})$ is fragmentary. Measurements from DELCO[5,8] and from DORIS[3] find a branching ratio of 30% to 35%. The branching ratio for the τ to decay to three charged pions plus any number of neutral particles has been measured in our experiment, using events in which one τ decays to a muon plus neutrinos and the other decays hadronically, to be 0.18 $\pm$ 0.065.[9] For this to be consistent with the DELCO and DORIS measurements, there would have to be a significant branching ratio for the τ to decay into five or more charged pions, which is considered unlikely on theoretical grounds.

It is possible to get some information on $B(\tau \rightarrow \text{multiprongs})$ from the observed electron spectra in multiprong events in this experiment. Each of Figures VII.3 - VII.5 has two curves superimposed on it. One curve represents the electron spectrum expected from the decay of a heavy lepton with a total energy equal to half of the center-of-mass energy. The other curve represents the electron spectrum expected from the production of D mesons and their decay via

the mode $D \rightarrow Ke\nu$. (For the latter curves it was necessary to assume production modes for the D's at the three different center-of-mass energies. The modes used were phase space production of $D^*\overline{D^*}$ (3.9 - 4.44 GeV), $D^*\overline{D^*}\pi$ (4.44 - 5.71 GeV) and $D^*\overline{D^*}\pi\pi$ (6.31 -7.38 GeV). *The simplified model for the matrix element in the decay $D \rightarrow Ke\nu$ described in Chapter III* was used.) All curves are normalized to the data.

It is apparent that the D decay curves are closer to the observed spectra than the τ decay curves. We note that the D decay curves predict very few electrons with momenta greater than 1/4 of the center-of-mass energy. We can get an upper limit on the fraction of all the electrons which are coming from the τ (and therefore on $B(\tau \rightarrow \text{multiprongs})$) by assuming that all of the observed electrons with momentum greater than 1/4 of the center-of-mass energy do indeed come from τ decays. First, however, we make two cuts to eliminate events which could not come from τ decays:

1. We eliminate events which contain a charged kaon.
2. We eliminate events in which the mass of the observed charged hadrons is greater than the mass of the τ.

These two cuts together eliminate only one event with an electron with momentum greater than $E_{cm}/4$ in our entire data sample from 3.9 to 7.4 GeV, consistent with the hypothesis that most of the high-momentum electrons come from τ's.

There remain 13 multiprong events with an electron with momentum greater than $E_{cm}/4$. Assuming that all of these events come from τ decays we divide by the electron identification efficiency of the Lead-Glass Wall (0.89 for these high momenta) and the overall efficiency and then we use equation VII.1 to determine $B(\tau \rightarrow \text{multiprongs})$.

We find $B(\tau \rightarrow \text{multiprongs}) = .19 \pm .07$. This is an upper limit because we have assumed that all of the high-momentum electrons are from τ decays, but this value is probably close to the actual value of $B(\tau \rightarrow \text{multiprongs})$ because there is no other known source of electrons with momenta this high in multiprong events.

Although the error on this measurement is large, it is sufficient to show that τ decays are responsible for only a fraction of the electron signal in multiprong events.

In the calculation of the average semileptonic branching ratio of charmed particles produced between 3.9 and 7.4 GeV we need to assume a value for $B(\tau \rightarrow \text{multiprongs})$ in order to subtract the τ contribution from the electron signal. A value of 0.25 has been used, which is consistent with the measured upper limit presented above but is somewhat closer to the values measured at DORIS and in the DELCO experiment with higher statistics. The τ contribution to R_e with $B(\tau \rightarrow \text{multiprongs}) = 0.25$ is shown in Figure VII.2. We see that there is a τ contribution even at the $\psi(3772)$ but it is small compared to the statistical error on our measurements there. In the high-energy region the τ accounts for about 25% of the observed signal. A

change of 0.1 in the value used for B($\tau \rightarrow$ multiprongs) would lead to a change of about 10% in our result for the average semileptonic branching ratio of charmed particles (see Section C below).

C. Average Semileptonic Branching Ratio of Charmed Particles

We can determine an average semileptonic branching ratio for the charmed particles produced in electron-positron annihilation between 3.9 and 7.4 GeV by dividing the total cross section for electron production from charm decays by the total cross section for producing charmed particles.

As in the measurement of the D meson semileptonic branching ratio (Chapter VI) we must correct the observed electron production cross section to account for those events in which a total of only two charged particles are produced and which therefore do not enter our multiprong event sample and we must also correct for those electrons which we do not identify because their momenta are less than 300 MeV/c.

Because the precise production mechanisms and the multiplicity distributions of the decays of the various charmed particles are not known the calculation of the former correction is not as straightforward as it was for the D mesons at 3.772 GeV. Instead, we calculate the correction in a similar manner to that used to calculate the detector acceptance in Chapter III. We run a number of Monte Carlo simulations of different modes of charmed particle production and we plot the fraction of events which have only two charged particles produced versus the average multiplicity observed in the detector. We then fit a straight line to the points on the plot and use the observed average multiplicity in the data sample itself to look up on the plot the expected fraction of events which have only two prongs. The implicit assumption here is that the observed average multiplicity is negatively correlated with the fraction of two-prong events. As in the case of the acceptance calculation, this correlation is confirmed empirically by the observation that the points on the Monte Carlo plot do indeed cluster around a single curve.

We find that the fraction of events with only two charged particles produced is quite small, the correction factors being 0.94 from 3.9 to 4.44 GeV, 0.96 from 4.44 to 5.71 GeV, and 0.97 from 6.31 to 7.38 GeV, each with an estimated error of 0.04.

As pointed out in the previous chapter, the fraction of electrons from D decays which have momentum greater than our cutoff of 300 MeV/c depends on whether the dominant decay mode is $Ke\nu$ or $K^*e\nu$ but is nearly independent of the momentum of the D's. The fraction is 0.86 ± 0.01 for $Ke\nu$ and 0.79 ± 0.02 for $K^*e\nu$. We use an average value of 0.82 with an error of 0.04, sufficient to include either mode.

In order to determine the denominator in the average semileptonic branching ratio we assume that charmed particle production accounts for all of the total hadronic cross section in

excess of the 2.6 units of R from "old physics" (as determined by looking at R below charm and heavy lepton thresholds) and the contribution of the τ.

We then write

$$B(C \rightarrow eX) = \frac{R_c}{2(R - R_{old} - R_\tau)} \qquad \text{(VII.3)}$$

The factor of two in the denominator arises because charmed particles are produced in pairs.

Table VII.3 shows the total value of R, the "old" physics and τ contributions, and the resultant value of R_{charm} for each of the ten fine energy bins. The values of R are taken from this experiment.

Figure VII.6 shows the average semileptonic branching ratio of charmed particles from 3.9 to 7.38 GeV as determined by equation VII.3. The reader is reminded that this branching ratio represents a weighted average over D mesons, F mesons, and charmed baryons, weighted by their relative production cross sections at the various center-of-mass energies. We note that within errors this average is constant and equal to the semileptonic branching ratio of the D mesons measured at the $\psi(3772)$, also shown on the figure. Therefore the data contains no evidence of significant production of charmed particles which have semileptonic decay branching ratios differing substantially from that of the D.

Table VII.3

Calculation of R_{charm}

$<E_{cm}>$	R	R_{old}	R_{τ}	R_{charm}
3.954	4.43 ± .15	2.52	0.59	1.32 ± .15
4.070	5.79 ± .12	2.52	0.65	2.62 ± .12
4.162	5.45 ± .12	2.52	0.69	2.24 ± .12
4.274	4.88 ± .12	2.52	0.73	1.63 ± .12
4.416	5.66 ± .16	2.52	0.77	2.37 ± .16
4.694	5.36 ± .11	2.52	0.83	2.01 ± .11
5.312	5.53 ± .12	2.52	0.90	2.11 ± .12
6.534	5.58 ± .11	2.52	0.96	2.10 ± .11
6.970	5.95 ± .13	2.52	0.97	2.46 ± .13
7.332	5.61 ± .11	2.52	0.98	2.11 ± .11

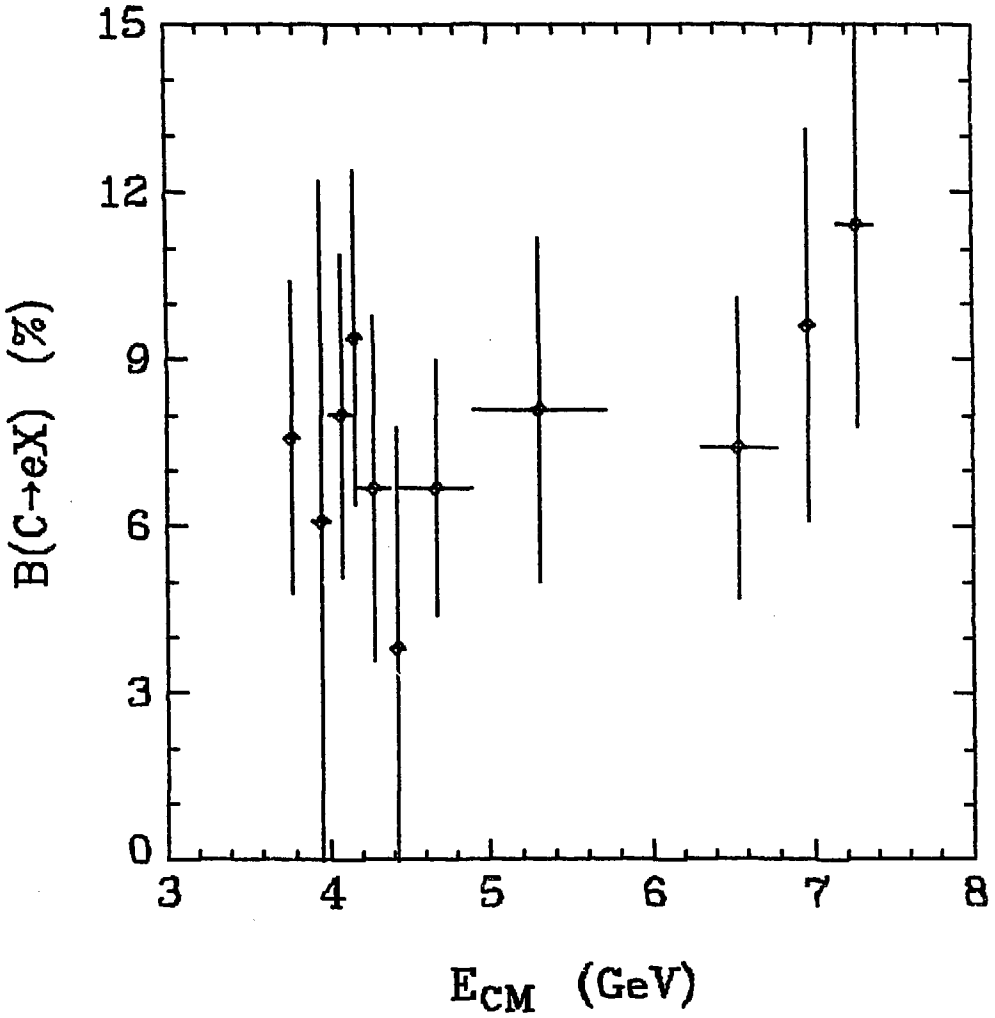

FIGURE VII.6

Average semileptonic branching ratio to electrons of charmed particles produced in e^+e^- annihilation from E_{cm} = 3.9 to 7.4 GeV. The point at 3.772 GeV is from Chapter VI.

References

Chapter VII

1. R.F. Schwitters, Proc. 1975 Int. Symp. on Lepton and Photon Interactions at High Energies, Stanford, California, 1975, p.355;
P.A. Rapidis et al., Phys. Rev. Lett. 39, 526 (1977)

2. M.L. Perl et al., Phys. Rev. Lett. 35, 1489 (1975)

3. J. Burmester et al., Phys. Lett. 68B, 297 and 301 (1977);
R. Brandelik et al., Phys. Lett. 37B, 109 (1978)

4. A. Barbaro-Galtieri et al., Phys. Rev. Lett. 39, 1058 (1977)

5. W. Bacino et al., Phys. Rev. Lett. 41, 13 (1978)

6. S. Wojcicki in Proc. of Summer Inst. on Particle Physics, SLAC Report No. 215, p.193 (1978)

7. Particle Data Group, Review of Particle Properties, Phys. Lett. 75B, 1 (1978)

8. J. Kirkby in Proc. of Summer Inst. on Particle Physics, SLAC Report No. 215, p. 309 (1978)

9. J. Jaros et al., Phys. Rev. Lett. 40, 1120 (1978)

VIII. Associated Production of Electrons and Kaons

If charmed particle production and decay is indeed the origin of the electrons observed in multiprong events then one would expect these events to have significant kaon content. Since charmed particles are produced in pairs one would expect to see an average of nearly two kaons per charm event. (Note that Cabibbo-suppressed decays can increase as well as decrease the number of kaons.)

If a charmed particle decays semileptonically and the decay includes a charged kaon then the kaon should have the opposite charge from that of the electron. If the decay of the recoiling charmed particle contains a charged kaon then that kaon should have the same charge as the electron. Thus, by measuring separately the opposite-sign and same-sign charged kaon content of the electron events we measure both the average charged kaon content of charm semileptonic decays and of all charm decays. At center-of-mass energies below about 4.1 GeV these measurements reflect only the properties of D decays. At higher center-of-mass energies F mesons and charmed baryons may also contribute and above about 5 GeV pair-production of strange particles along with charmed particles may cloud the picture.

In this chapter we also present mass spectra of opposite-sign electron-kaon pairs. These spectra are compared with those expected from the decays $D \rightarrow Ke\nu$ and $D \rightarrow K^*e\nu$. Because the mass of a system of particles is a Lorentz-invariant quantity, these spectra provide comparisons which are independent of the momentum of the D's and therefore free us from the uncertainty in specific production models.

A. Kaon Content of Electron Events

Our data sample consists of the 59 multiprong events with an electron identified in the Lead-Glass Wall at the $\psi(3772)$ resonance (see Chapter VI) and the 453 such events at higher center-of-mass energies (Chapter VII).

Charged kaons with momentum less than 1 GeV/c are counted by the time-of-flight fitting technique described in Chapter III. The corrections for decay and for inefficiency of the time-of-flight sytem are also identical to those described in Chapter III.

The solid angle correction is more complicated because we observe only those events in which three or more charged particles are seen in the detector but we want to determine the kaon content of all events which contain an electron. We define the "effective solid angle" for charged kaon detection as the number of kaons detected per event in our sample divided by the

true kaon content of all electron events. This effective solid angle is greater than the 0.73 physical solid angle of the detector because a charged kaon will itself contribute to the three charged particles necessary to qualify an event for our sample so that the events which we observe will tend to have a higher kaon content in the detector than those which we reject.

In a manner similar to that of the acceptance calculation for the electron events, a series of Monte Carlo simulations were performed with various charmed particle production modes to determine a relation between the average observed multiplicity and the effective solid angle for detecting kaons. The Monte Carlo results can be fitted with the curve

$$\frac{\Delta\Omega_{eff}}{4\pi} = 1.84 - .23 \langle n \rangle \pm .06$$

where $\langle n \rangle$ is the average detected multiplicity observed in the events which have at least three charged particles detected.

The average observed multiplicity for each of the four center-of-mass energy regions (the $\psi(3772)$ and the three coarse regions defined in Chapter VII) and the effective solid angle for charged kaons for each of these regions are presented in Table VIII.1.

Neutral kaons are identified as described in Chapter III. The determination of the acceptance is in principle somewhat simpler for neutral kaons than for charged kaons because any event in which an electron and two charged pions are detected necessarily satisfies the three-charged-particle event selection criterion. Therefore, when measuring the number of K^o's per electron event, the K^o acceptance is effectively enhanced by a factor of one over the probability that three or more charged particles will be detected in an event with an electron. This effect increases the effective acceptance for K^o's from 0.086 to 0.105, 0.110, 0.113, and 0.103 in the center-of-mass energy ranges 3.76-3.79($\psi(3772)$), 3.9-4.44, 4.44-5.71, and 6.31-7.38 GeV, respectively.

The kaon content of the background events in which a hadron is misidentified as an electron is determined by counting the number of kaons in events with a hadron in the Lead-Glass Wall.

To determine the kaon content of the genuine electron events we subtract background from both the number of kaons and the number of events:

$$\frac{N_{eK}}{N_{eX}} = \frac{N_{eK}(\text{observed}) - N_{eK}(\text{background})}{N_{eX}(\text{observed}) - N_{eX}(\text{background})}$$

$$N_{eK}(\text{background}) = \frac{N_{hK}}{N_{hX}} N_{eX}(\text{background})$$

The results are shown in Table VIII.2. For each of the four center-of-mass energy regions the average number of neutral kaons, and of charged kaons with momentum less than 1

Table VIII.1

Effective Solid Angle for Charged Kaon Detection

E_{cm}	Average Observed Multiplicity	$\frac{\Delta\Omega_{eff}}{4\pi}$
$\psi(3772)$	4.43 ± .44	.82 ± .12
3.90 - 4.44	4.17 ± .25	.88 ± .08
4.44 - 5.71	4.04 ± .27	.91 ± .09
6.31 - 7.38	4.54 ± .25	.80 ± .08

Table VIII.2

Kaon Content of Electron Events
($p \leqslant 1$ GeV/c for charged kaons)

E_{cm}	$\frac{e^+K^-}{e^+X}$ *	$\frac{e^+K^+}{e^+X}$	$\frac{e^+K^\pm}{e^+X}$	$\frac{h^+K^\pm}{h^+X}$	$\frac{e^\pm K^o}{e^\pm X}$	$\frac{h^\pm K^o}{h^\pm X}$
$\psi(3772)$	.34 ± .20	.55 ± .22	.89 ± .30	.57 ± .06	1.7 ± 1.0	.7 ± .1
3.90 - 4.44	.59 ± .14	.35 ± .13	.94 ± .19	.71 ± .12	0.4 ± 0.5	.7 ± .1
4.44 - 5.71	.42 ± .12	.36 ± .13	.78 ± .18	.61 ± .12	1.0 ± 0.5	.6 ± .1
6.31 - 7.38	.41 ± .11	.34 ± .13	.75 ± .17	.50 ± .11	0.3 ± 0.4	.8 ± .1
Average	.46 ± .07	.37 ± .07	.83 ± .10	.60 ± .06	0.7 ± 0.3	.7 ± .1

* All modes also include charge conjugate modes.

Table VIII.3

Kaon Content of "Charm" Electron Events
(τ events subtracted and charged kaons
extrapolated beyond 1 GeV/c)

E_{cm}	$\frac{e^+K^-}{e^+X}$ *	$\frac{e^+K^+}{e^+X}$	$\frac{e^+K^\pm}{e^+X}$	$\frac{e^\pm K^o}{e^\pm X}$
$\psi(3772)$	.47 ± .28	.76 ± .31	1.23 ± .42	2.2 ± 1.3
3.90 - 4.44	.82 ± .20	.49 ± .18	1.32 ± .27	0.5 ± 0.7
4.44 - 5.71	.67 ± .20	.57 ± .21	1.24 ± .29	1.4 ± 0.7
6.31 - 7.38	.83 ± .25	.69 ± .28	1.52 ± .38	0.4 ± 0.5
Average	.75 ± .12	.61 ± .13	1.36 ± .18	0.9 ± 0.4

* All modes also include charge conjugate modes.

GeV/c, per event with an electron in the LGW are shown. Separate statistics are given for charged kaons with the same charge and the opposite charge from the electron. For comparison, the average numbers of charged and neutral kaons in events with a hadron in the LGW are also shown.

The last row in Table VIII.2 contains averages over the four center-of-mass energy bins, weighted by the numbers of good electron events. We see that there is a two standard deviation enhancement of the charged kaon content in the events with an electron. We find an average of 0.83 ± .10 charged kaons per electron event as opposed to .60 ± .06 charged kaons per event with a hadron in the LGW. The errors on the neutral kaon measurements are so large that a similar enhancement is not excluded even though it is not observed.

The division between charged kaons with the same charge as the electron and the opposite charge is roughly equal, with a slight preference for opposite-charge kaons.

In order to determine the average charged kaon content of events in which charmed particle decays are the source of the electron we must make two corrections:

1. Estimate the number of charged kaons with momentum greater than 1 GeV/c and add them to the observed number below 1 GeV/c.

2. Subtract from the number of electron events (the denominator) the number which originate from heavy lepton decays. We do not subtract any τ contribution from the number of kaons (the numerator) because only about 3% of all τ decays are expected to contain kaons.

The fraction of the kaon spectrum which lies above 1 GeV/c is determined from the spectrum of the neutral kaons, for which there is no momentum cutoff. The assumption that the charged and neutral spectra are the same is confirmed by comparison of the two spectra below 1 GeV/c. The fraction of kaons which are above 1 GeV/c in momentum is found to be .07 ± .07, .05 ± .05, .14 ± .07, and .38 ± .09 in the four center-of-mass energy regions.

The number of the electron events which come from the τ heavy lepton is estimated using the same parameters used to determine the τ contribution to R_e in Chapter VII, namely, m_τ = 1.782 GeV. $B(\tau \rightarrow e\nu\nu)$ = .179, and $B(\tau \rightarrow \text{multiprongs})$ = .25. With these parameters we find that approximately 25% of the electron events come from the τ.

After these corrections , both of which increase the measured kaon content of the electron events, we obtain the charged and neutral kaon contents shown in Table VIII.3. As shown in the last row, the electron events contain an average of 0.9 ± 0.4 neutral kaons, 0.75 ± 0.12 charged kaons with the same charge as the electron, and 0.61 ± 0.13 charged kaons with the opposite charge from that of the electron for a total of 2.3 ± 0.4 kaons per event in events with electrons from charmed particle decays.

B. Electron-Kaon Mass Spectrum

In Chapter VII we presented the electron momentum spectrum measured at the $\psi(3772)$ resonance and concluded that it was consistent with the hypothesis that the electrons came from production and decay of D mesons in the decay modes $D \rightarrow Ke\nu$ and/or $D \rightarrow K^*e\nu$. The statistical accuracy of the data was not sufficient to determine which of the two was the dominant decay mode. In Chapter VII data was presented from higher center-of-mass energies with better statistical accuracy but at these energies uncertainty in the momentum spectrum of the produced charmed particles made it difficult to establish which, if either, was the dominant decay mode. However, the invariant mass of a pair of particles in a decay is a Lorentz-invariant quantity and therefore its spectrum is independent of the momentum of the parent particle.

If a charged kaon is produced in a Cabibbo-favored semileptonic decay of a D meson then that kaon will have the opposite charge from that of the electron while a charged kaon from the decay of the recoiling D will have the same charge as that of the electron. Therefore, by selecting kaons with the opposite charge from that of the electron we select kaons from the same D. (This will also be true for charmed baryons but not for F mesons which contain an $\bar{s}$ quark and can therefore decay into two kaons with opposite charges.) By plotting the mass spectrum of these kaon-electron pairs we obtain a distribution which is characteristic of the decay but independent of the parent momentum so we can combine data from all center-of-mass energies, assuming that most of the electrons at all energies come from D's. The method breaks down if there is significant F production with decays of F's containing two kaons or if the mix of produced charmed particles changes significantly with center-of-mass energy.

In order to measure this distribution it is necessary to identify individually the charged kaons. We note that the fitting procedure used to count the numbers of charged kaons did not identify individual kaons but merely arrived at an estimate of the total number of kaons in an event sample. In order to identify individual charged kaons we must introduce a cut.

We define Gaussian particle identification weights as follows:

$$W_i = \frac{\exp(-(t-t_i)^2/2\sigma^2)}{\sum_j \exp(-(t-t_j)^2/2\sigma^2)}$$

where i can be pion, kaon, or proton, W_i is the weight assigned to a particle for identification as being type i, t is the measured time-of-flight, t_i is the time-of-flight expected if that particle were of type i, and sigma is the resolution of the time-of-flight measurement (0.4 ns). For a particle to be identified as a kaon we require

$W_{kaon} > 0.75.$

This value for the cut was chosen because it yields numbers of charged kaons roughly equal to the numbers determined by the time-of-flight fitting procedure, i.e., it equalizes the loss and the background to yield the correct number of kaons.

The mass spectra of opposite-charge kaon-electron pairs with the electron identified in the LGW and the kaon identified as described above are presented for the four center-of-mass energy intervals in Figures VIII.1 and VIII.2. The dashed lines indicate the background expected from hadrons which are misidentified as electrons. We note that almost all of the events lie below the mass of the D, consistent with the hypothesis that the pairs come from D decays.

The curves superimposed on the data represent the spectra expected from the decays $D \rightarrow Ke\nu$ and $D \rightarrow K^*e\nu$. Each curve is normalized to the observed number of events. The curves were generated by a Monte Carlo simulation which produced D's according to the same production models used for comparison with the electron spectra and decayed them according to the simplified model of Hinchliffe and Llewellyn-Smith (see Chapter III and Appendix A). In the simulation the kaons were identified by the same cut on the time-of-flight weight used in the analysis of the real data. The curves would be identical for the four center-of-mass energies except for acceptance and background effects which depend on the energy. These effects lead to differences which are small compared to the difference between spectra expected from the two different decay modes.

We see that the shapes of the spectra are all consistent with some combination of the $D \rightarrow Ke\nu$ and $D \rightarrow K^*e\nu$ decays. There is some center-of-mass energy dependence of the spectra with the data from the highest and lowest energies favoring the $K^*e\nu$ decay mode while the intermediate energy data resemble more closely the $Ke\nu$ spectrum.

Each of the four mass spectra has been fitted to a combination of the $Ke\nu$ and $K^*e\nu$ decay modes using a maximum likelihood fit to determine the relative contribution from each mode. The results are:

E_{cm}	$Ke\nu$ Fraction	$K^*e\nu$ Fraction
$\psi(3772)$	0.00 ± .12	1.00 ± .12
3.90 - 4.44	0.52 ± .14	0.48 ± .14
4.44 - 5.71	0.83 ± .19	0.17 ± .19
6.31 - 7.38	0.00 ± .04	1.00 ± .04

The significance of these results and the variation with E_{cm} are discussed in the Conclusions (Chapter IX).

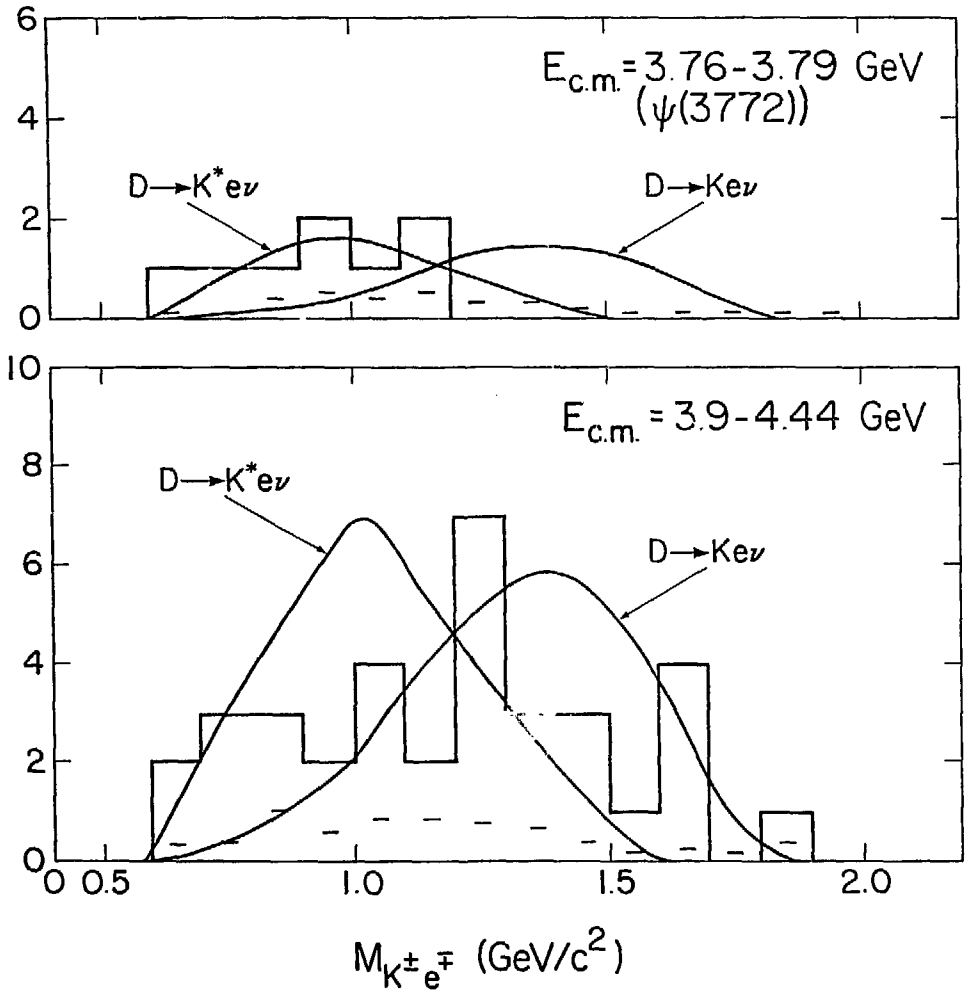

XBL 791-298

FIGURE VIII.1

$K^{\pm}e^{\mp}$ mass spectra, E_{cm} = 3.76-3.79 (ψ(3772)) and 3.9-4.44 GeV. The dashed line shows the background from hadrons misidentified as electrons.

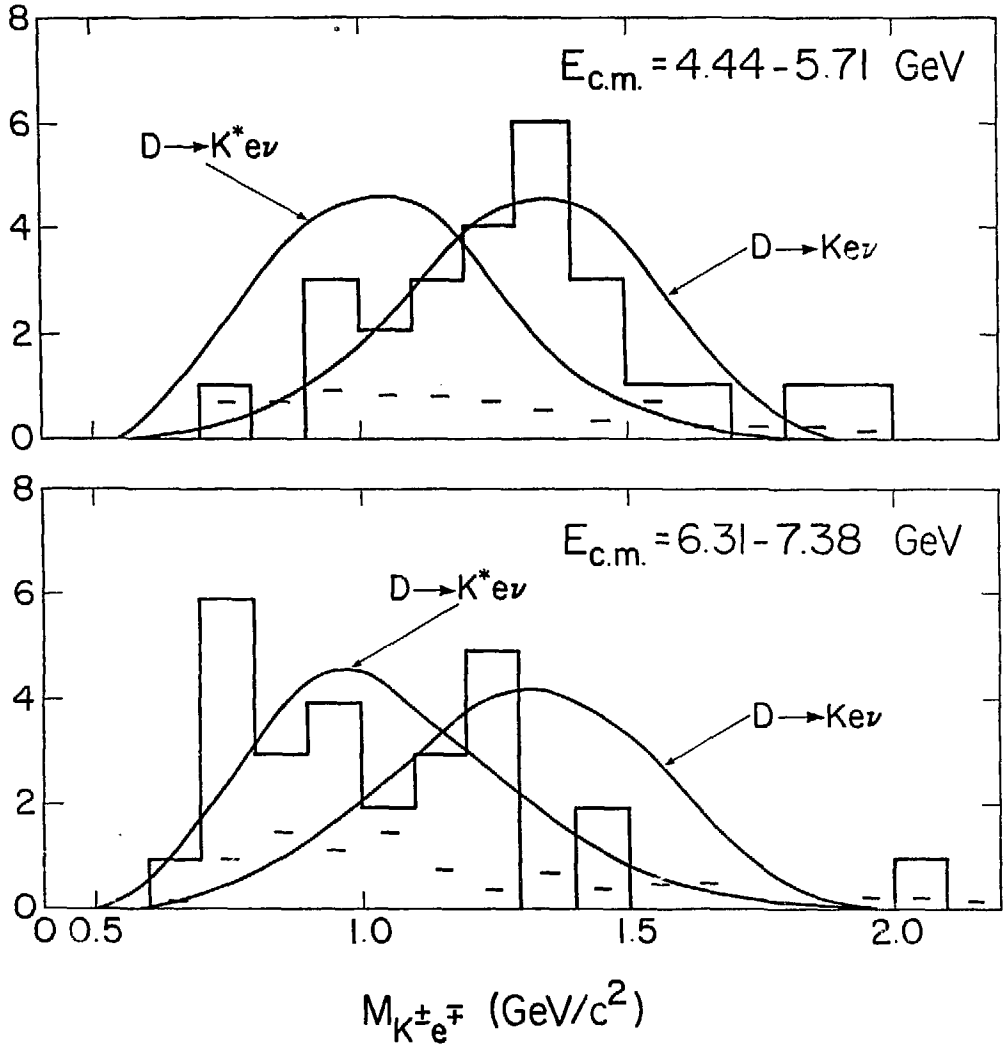

XBL 791-297

FIGURE VIII.2

$K^{\mp}e^{\pm}$ mass spectra, E_{cm} = 4.44-5.71 and 6.31-7.38 GeV. The dashed line shows the background from hadrons misidentified as electrons.

IX. Conclusions

The observation of a significant (7.6%) semileptonic branching ratio for D meson decays confirms the weak nature of charmed particle decays. The fact that the ensemble of new hadrons produced at center-of-mass energies above 3.9 GeV has an average semileptonic branching ratio equal to that of the D's (within errors) is consistent with the hypothesis that these hadrons have the same new quantum number as the D, namely charm, and that in fact D's may constitute a major part of that ensemble.

The observation of a large kaon content in D decays and in events containing electrons from decays of D's and other charmed particles tends to confirm the hypothesis of a large coupling between the charmed quark and the strange quark. The consistency of the electron momentum spectra and the kaon-electron mass spectra with the decays $D \rightarrow Ke\nu$ and $D \rightarrow K^*e\nu$ gives further evidence for this coupling.

The interpretation of all the data is not clear, however. For example, the significance of the small (10%) inclusive branching ratio for the decay $D^+ \rightarrow K^-$ plus anything and the variation of the kaon-electron mass spectrum with center-of-mass energy are not completely understood.

In the following sections each of these points is discussed more fully. The results presented in the preceding chapters are compared with results from other experiments and with theoretical predictions, an attempt is made to interpret the data in terms of models of charmed particle production and decay, and suggestions are made for future measurements which may shed light on unresolved questions.

A. Semileptonic Decays of Charmed Particles

1. Semileptonic Branching Ratios

In this experiment the semileptonic branching ratio for D meson decay into an electron plus anything has been measured at the $\psi(3772)$ resonance and found to be $(7.6 \pm 2.8)\%$. The DELCO experiment at the other interaction region at SPEAR made a similar measurement at the $\psi(3772)$ and found $B(D \rightarrow eX) = (10 \pm 2)\%$.[1] The DASP experiment at the DORIS e^+e^- storage ring has measured the average semileptonic branching ratio of charmed particles produced in the 4.03 GeV resonance region to be $(8 \pm 2)\%$.[2] This region is below the thresholds for F meson and charmed baryon production so it probably represents an average of D^0 and D^+ decays, although possibly in a different ratio than at the $\psi(3772)$.

All three of these measurements are consistent and the world average is (8.7 ± 1.1)%.

As described in the Introduction (Chapter I), a simple quark-lepton counting algorithm with no strong interaction dynamics predicts a branching ratio of 20% for the semileptonic decay of any charmed particle into an electron plus anything. The data are in disagreement with this prediction.

Experience from kaon decays, where certain nonleptonic decay amplitudes are enhanced by a factor of 20, tells us that this simple type of rule is not reliable. The enhanced amplitudes are those which belong to the octet term in the **8** X **8** product of SU(3) hadronic currents. When SU(3) is extended to SU(4) to include charm the **8**'s in the product are replaced by **15**'s (**3** X **3** = **8** + **1** → **4** X **4** = **15** + **1**). The Hamiltonian then takes the form of the product **15** X **15**. The term in this product which contains the enhanced SU(3) octet is the **20** which also contains an SU(3) **6** with charm = +1 and another **6** with charm = -1. Thus "octet enhancement" for $\Delta C = 0$ decays naturally extends to "sextet enhancement" for $\Delta C = 1$ decays, both of which can be viewed as a result of "**20** enhancement" in SU(4).[3]

If the enhancement factor for the sextet in nonleptonic decays of charmed particles were equal to the octet enhancement factor in strange particle decays then the semileptonic branching ratios of charmed particles would be less than 1%. This possibiltiy is excluded by the data.

Altarelli and Maiani[4] and Gaillard and Lee[5] have shown that final state strong interactions involving gluon exchange, which are calculable in quantum chromodynamics (QCD), can account for about a factor of 5 in amplitude (out of a total factor of 20) of the octet enhancement in strange particle decays. Ellis, Gaillard, and Nanopoulos[6] argue that the remainder of the enhancement results from longer-distance effects which would not be important in charmed particle decays because of the larger masses and momentum transfers involved. Therefore the entire enhancement in charmed particle decays should be calculable in QCD. Because the strong coupling constant in QCD is a decreasing function of the mass scale the enhancement should be smaller in charmed particle decays than in strange particle decays.

The ratio of the non-leptonic width to the semileptonic width of a charmed pseudoscalar particle (D or F) is given by[7]

$$\frac{\Gamma_{NL}}{\Gamma_{SL}} = f_-^2 + 2 f_+^2$$

where f_- is the coefficient of the term in the Hamiltonian which transforms as an SU(4) **20** (the enhanced term) and f_+ is the coefficient of the term which transforms as an SU(4) **84** (the non-enhanced term). In the absence of strong interactions $f_- = f_+ = 1$ and we get the same result as the simple quark-counting rule:

$$B(D \to eX) = \frac{\Gamma(D \to eX)}{\Gamma(D \to eX) + \Gamma(D \to \mu X) + \Gamma(D \to \text{hadrons})}$$

$$= \frac{\Gamma_{SL}}{2\Gamma_{SL} + \Gamma_{NL}} = \frac{1}{2 + f_-^2 + 2f_+^2} = 20\%$$

However the strong interaction effects modify f_+ and f_-. In QCD they are given by[7]

$$f_- = \left[1 + \frac{33 - 2F}{12\pi}\alpha_s(m_c^2)\ln\frac{m_W^2}{m_c^2}\right]^{\gamma}$$

$$f_+ = \left[1 + \frac{33 - 2F}{12\pi}\alpha_s(m_c^2)\ln\frac{m_W^2}{m_c^2}\right]^{-\frac{\gamma}{2}}$$

$$\gamma = \frac{12}{33 - 2F}$$

where F is the number of quark flavors, $\alpha_s(m_c^2)$ is the value of the strong coupling constant at the mass of the charmed quark, and m_W is the mass of the W boson.

If we take $m_c = 1.65$ GeV, $m_W = 80$ GeV, $F = 6$ (to include the b and t quarks), and $\alpha_s(m_c^2)$ in the range 0.5 - 1.0 we find $f_- = 1.9$ - 2.6 and $f_+ = 0.6$ - 0.7 and the predicted semileptonic branching ratio is

$$B(D \rightarrow eX) = \frac{1}{2 + f_-^2 + 2f_+^2} = 10 - 15\%.$$

where the higher value (15%) corresponds to the lower value of $\alpha_s(m_c^2)$ (0.5).

This prediction is closer to the experimental value (world average = (8.7 ± 1.1)%) than the more naive predictions (20% and less than 1%). In summary, hadronic enhancement is present in D decays although to a much lesser degree than in strange particle decays and most of the enhancement can be accounted for by QCD calculations.

As far as semileptonic decays of charmed particles other than D's are concerned, both this experiment and the DASP experiment[2] find the average semileptonic branching ratio for the mix of charmed particles produced at center-of-mass energies above the $\psi(3772)$ to be equal within errors to the average semileptonic branching ratio of the D's. Thus there is no evidence for large production of charmed particles with semileptonic branching ratios much different than those of the D's.

2. Specific Decay Modes

Beyond the question of the total semileptonic decay branching ratio is the matter of the specific decay channels. Both the electron momentum spectra and the kaon-electron mass spectra are consistent with combinations of the decays $D \rightarrow Ke\nu$ and $D \rightarrow K^*e\nu$. This is in agreement with the expectation that the dominant decay modes should contain strange particles.

Decay modes with extra pions are expected to be suppressed by the low available phase space

and by the fact that the matrix elements vanish in the limit that any one of the pions is soft (the "soft pion theorem").[8] For this reason $Ke\nu$ and $K^*e\nu$ are expected to be the dominant semileptonic decay modes[8-12], in agreement with the data.

In principle the electron momentum spectrum can be used to determine the relative contributions of the $Ke\nu$ and $K^*e\nu$ modes. In our experiment this has not been possible because of the limited statistical accuracy at the $\psi(3772)$ and because at energies above the $\psi(3772)$ uncertainty in the momentum spectrum of the D's leads to uncertainty in the predicted spectra for the two modes which is comparable to the difference in the two spectra.

It was hoped that the kaon-electron mass spectra (Chapter VIII), which are independent of parent momentum, would help to resolve this question. The results of that analysis were somewhat ambiguous, however, in that the spectrum was found to vary with center-of-mass energy. In the higher energy bins that variation may reflect the presence of charmed particles other than D's. The spectra could also be affected by variations in the D^+/D^o production ratio with center-of-mass energy. In the decay $D \rightarrow Ke\nu$ a D^o will yield a charged kaon while a D^+ will yield a neutral kaon. Since we only look at charged kaons in the Ke mass spectra, only D^o decays will contribute to the $Ke\nu$ component. On the other hand, in the decay $D \rightarrow K^*e\nu$ the D^o yields a charged K^* which decays 2/3 of the time into a neutral kaon while the D^+ yields a neutral K^* which decays 2/3 of the time into a charged kaon. The result of all this is that the observed Ke mass spectrum will tend to favor the $Ke\nu$ mode more in center-of-mass regions where D^o production is high and will tend to favor the $K^*e\nu$ decay more when D^+ production is high. More precisely, the observed ratio of $K^*e\nu$ to $Ke\nu$ decays in a Ke mass spectrum is given by:

$$\frac{N_{K^*}}{N_K}\,(\text{observed}) = \left(\frac{1}{3} + \frac{2}{3} R_p R_d\right) \frac{N_{K^*}}{N_K}\,(\text{produced})$$

where R_p is the ratio of D^+ to D^o production, which depends on E_{cm}, and R_d is the ratio of the D^+ semileptonic decay branching ratio to that of the D^o.

This effect may explain in part the increase in the $Ke\nu$ fraction observed between the $\psi(3772)$ and the 3.9-4.4 GeV region. At the $\psi(3772)$ D^o and D^+ are produced in almost equal quantities. In the 3.9-4.4 GeV region D^o production is dominant because most of the D's are produced indirectly by the decays of D^*'s[13] and the D mass splittings allow the decay $D^{*+} \rightarrow D^o\pi^+$ while forbidding the decay $D^{*o} \rightarrow D^+\pi^-$.[14]

In light of the above the cleanest measurement of the $Ke\nu/K^*e\nu$ ratio is at the $\psi(3772)$ where D^+ and D^o are produced nearly equally and there are no other open channels for charmed particle production. The data there favors the $K^*e\nu$ decay. This could reflect either actual dominance of the $K^*e\nu$ decay mode or a higher semileptonic branching ratio for the D^+ than for the D^o or a combination of the two.

There is some evidence from other experiments for dominance of the $K^*e\nu$ decay mode. The DELCO experiment, with higher statistics than the Lead-Glass Wall, has fitted their electron momentum spectrum with a combination of $(60 \pm 20)\%$ $D \rightarrow K^*e\nu$ and $(37 \pm 20)\%$ $D \rightarrow Ke\nu$.[1] A Columbia-Brookhaven experiment in the 15-foot bubble chamber at Fermilab has observed a mass spectrum of K^o-electron pairs produced in neutrino interactions which resembles that expected from the $K^*e\nu$ decay of the D.[15] This measurement, however, is subject to the same type of uncertainties discussed above in connection with our measurements.

Finally, we note that Ali and Yang[9] and Fakirov and Stech[10] have calculated the $D \rightarrow Ke\nu$ and $D \rightarrow K^*e\nu$ decay rates including hadronic form factors and both pairs of authors find a predicted $Ke\nu/K^*e\nu$ ratio in the neighborhood of 2. The meagre world collection of data would tend to indicate that this prediction is not correct but this is far from conclusive. Hinchliffe and Llewellyn-Smith[11] and Barger, Gottschalk, and Phillips[12] have estimated this ratio using much simpler assumptions and estimate the ratio to be in the neighborhood of 0.75, which may be closer to the actual value.

The final establishment of the branching ratios for $D \rightarrow Ke\nu$, $D \rightarrow K^*e\nu$, and any other specific semileptonic decay channels awaits a high-statistics, large solid angle experiment which can run at the $\psi(3772)$ and look at semileptonic decays of "tagged" D's in the same manner that we studied the inclusive kaon content in D decays (Chapters IV and V). Such an experiment could also easily measure the D^o/D^+ lifetime ratio by comparing semileptonic branching ratios[16]. Work of this type is currently being carried out by the Mark II detector at SPEAR and a future experiment (Mark III) is also planned.

B. Kaon Content of D Decays

In Chapter V we found a total kaon content in D^o decays of $.94 \pm .28$, in good agreement with the GIM model, and a charged/neutral kaon ratio differing by only about one standard deviation from that predicted by the statistical model of Quigg and Rosner (Table V.2).

The right-sign charged kaon content of D^+ decays, however, is unexpectedly low: $.10 \pm .07$. This could indicate either a low total kaon content or a large ratio of neutral to charged kaons. Unfortunately, the error on our measurement of the neutral kaon content is so large that we cannot distinguish these two possibilities. Clearly, a high-statistics measurement of the K^o content in D^+ decays is needed. The Mark III experiment may provide such a measurement. Meanwhile, we will speculate briefly here on possible explanations.

Because the c quark couples to an s quark (strangeness = -1), if a D^+ decay includes a charged kaon than it must be a K^- and there must then be at least two positively charged pions in order to conserve charge. This fact alone reduces the available phase space and it is reflected in the statistical model prediction of 0.33 charged K's per D^+ as opposed to 0.48 for the D^o.

The statistical model[17] predicts an average charged multiplicity in D decays of 2.7. The measured average charged multiplicity is 2.3 ± 0.3.[18] If the statistical model is revised to reproduce this average charged multiplicity then it predicts about 0.25 K^- per D^+ decay[18] which is closer to the measured value but still too large.

Because the pion system in a D^+ decay that contains a K^- is doubly charged, it must have an isospin of 2. Gaillard, Lee, and Rosner[8] have suggested that production of a system with I = 2 may be suppressed. They note that this type of suppression would be analogous with the suppression of the decay $K^+ \rightarrow \pi^+\pi^0$ in which the pions must have isospin 2, although the latter suppression is usually viewed in terms of octet enhancemant (see section A above and Chapter I). Such a suppression could conceivably explain the low charged kaon content in D^+ decays.

C. Inclusive Kaon Production

1. General

Measurements at DORIS[19] and at SPEAR[20,21] have revealed an increase in the inclusive cross section for charged kaon production in e^+e^- annihilation in the 4 GeV region which is roughly equal to the increase in the total hadronic cross section after subtraction of the heavy lepton contribution. Seemingly this would indicate an average charged kaon content of one $K^\pm$ per charmed particle pair or 0.5 $K^\pm$ per charmed particle decay. This would seem to contradict our measurements of 0.35 charged kaons per D^0 and 0.16 (0.10 right-sign and 0.06 wrong-sign) charged kaons per D^+ from the tagged events (Chapter V). The measurements of the kaon content in events which contain an electron (Chapter VIII) also seem to point towards a higher charged kaon content in charmed particle decays than the results from the tagged events would indicate. We mention three possible explanations which in combination may resolve this apparent discrepancy:

1. As mentioned above, D^* production at energies above the $\psi(3772)$ can lead to a predominance of neutral over charged D's. This would then yield an average kaon content per event which is closer to the D^0 value (.35 ± .10) than to the D^+ value (.16 ± .09). The former value is only 1.5 standard deviations away from 0.5.

2. At center-of-mass energies above F meson and charmed baryon production thresholds some of the observed charged kaons may come from decays of charmed particles with higher kaon contents than the D's.

3. The amount of kaon production from sources other than charmed particles may be increasing with E_{cm}. The inclusive cross section for kaon production at 3.6 GeV (below charm threshold) is 11 nb[19,20], more than twice the value one would expect if kaons were produced

only when the hadronic system starts with an $s\bar{s}$ pair from the virtual photon. This shows that there is significant production of $s\bar{s}$ pairs from the "sea" and this production would be expected to increase with E_{cm} as the available phase space increases.

2. Inclusive Kaon Production at the $\psi(3772)$

A useful comparison between the observed inclusive kaon production rate and that expected from decays of D's can be made at the $\psi(3772)$. Here D^o and D^+ are produced in a calculable ratio (56 ± 3% D^o ; see Chapter IV), there are no open channels for producing other types of charmed particles, and the D production cross section rises rapidly and falls again over a small range in E_{cm}. By comparing the kaon production cross sections on and off the resonance one obtains the kaon content of the resonant events. Assuming that the resonance decays nearly 100% of the time into $D\bar{D}$, one then has directly the average kaon content of D decays. We note, however, that the contributions of D^+ and D^o and of right-sign and wrong-sign kaons are not separated. The quantities measured are:

$$0.56\,B(D^o \rightarrow K^{\pm}X) + 0.44\,B(D^+ \rightarrow K^{\pm}X)$$

and

$$0.56\,B(D^o \rightarrow K^oX) + 0.44\,B(D^+ \rightarrow K^oX)$$

The resuls of this analysis are [18] 0.52 ± 0.14 for the neutral kaons and 0.42 ± 0.12 for the charged kaons. These may be compared with 0.49 ± 0.19 for neutral kaons and 0.27 ± 0.07 for charged kaons determined by taking the appropriate combination (above equation) of the inclusive branching ratios measured in the tagged events (Chapter V). The two pairs of results are consistent with each other.

References

Chapter IX

1. J. Kirkby in Proc. 6th SLAC Summer Inst. on Particle Physics, 1978, p.309

2. B.H. Wiik and G. Wolf, DESY report DESY-78/23 (1978)

3. G. Altarelli, N. Cabibbo, and L. Maiani, Nuclear Physics B88, 285 (1975)

4. G. Altarelli and L. Maiani, Phys. Lett. 52B, 351 (1974)

5. M.K. Gaillard and B.W. Lee, Phys. Rev. Lett. 33, 108 (1974)

6. J. Ellis, M.K. Gaillard, and D.V. Nanopoulos, Nuclear Physics B100, 313 (1975)

7. N. Cabibbo and L. Maiani, Physics Letters 73B, 418 (1978)

8. M.K. Gaillard, B.W. Lee, and J.L. Rosner, Rev. Mod. Phys. 42, 277 (1975)

9. Ahmed Ali and T.C. Yang, Phys. Lett. 65B, 275 (1976)

10. Dotcho Fakirov and Berthold Stech, Nuclear Physics B133, 315 (1978)

11. I. Hinchliffe and C.H. Llewellyn-Smith, Nucl. Phys. B114, 45 (1976)

12. V. Barger, T. Gottschalk, and R.J.N. Phillips, Phys. Rev. D16, 746 (1977)

13. J.E. Wiss, Ph.D. Thesis, Lawrence Berkeley Laboratory Report LBL-6725 (1977)

14. I. Peruzzi et al., Phys. Rev. Lett.39, 1301 (1977)

15. C. Baltay in Neutrinos-78, Proceedings of the Purdue Conference, 1978, p.533

16. A. Pais and S.B. Treiman, Phys. Rev. D15, 2529 (1977)

17. C. Quigg and Jonathan L. Rosner, Phys. Rev. D17, 239 (1978);
Jonathan L. Rosner in Deeper Pathways in High-Energy Physics, Proc. of Orbis Scientiae, Coral Gables, 1977, p.489

18. V. Vuillemin et al., Phys. Rev. Lett. 41, 1149 (1978)

19. R. Brandelik et al., Phys. Lett. 67B, 363 (1977)

20. V. Luth in Proc. SLAC Summer Inst. on Particle Physics, 1977, p.219

21. I. Peruzzi et al., "Inclusive D and K Meson Production in e^+e^- Annihilation", Lawrence Berkeley Laboratory Report LBL-7935, 1979 (to be published)

Appendix A

Calculation of Matrix Elements for $D \to Ke\nu$ and $D \to K^*e\nu$

<u>$D \to Ke\,\nu$</u>

$$M = \frac{G}{\sqrt{2}} \cos\theta_c \, (p_D + p_K)_\alpha \, \bar{u}_\nu \, \gamma_\lambda (1 + \gamma_5) \, v_e \quad .$$

where G is the Fermi coupling constant, θ_c is the Cabibbo angle, p_D and p_K are the D and K four-momenta, and u_ν and v_e are the neutrino and the electron spinors

$$|M|^2 = \frac{G^2}{2} \cos^2\theta_c \, (p_D + p_K)_\alpha \, (p_D + p_K)_\lambda$$

$$\cdot \; \mathrm{Tr}\,[v_e \bar{v}_e \, \gamma_\alpha \, (1 + \gamma_5) \, u_\nu \bar{u}_\nu \, \gamma_\alpha \, (1 + \gamma_5)]$$

Summing over e and ν spins:

$$|M|^2 = \frac{G^2}{2} \cos^2\theta_c \, (p_D + p_K)_\alpha \, (p_D + p_K)_\lambda$$

$$\cdot \; \mathrm{Tr}[(\not{p}_e - m_e) \, \gamma_\alpha \, (1 + \gamma_5) \, \not{p}_\nu \, \gamma_\lambda \, (1 + \gamma_5)]$$

where $\not{p} = \gamma \cdot p$

$$= \frac{G^2}{2} \cos^2\theta_c \, (p_D + p_K)_\alpha \, (p_D + p_K)_\lambda$$

$$\cdot \; \mathrm{Tr}[2 \, \not{p}_e \, \gamma_\alpha \, \not{p}_\nu \, \gamma_\lambda]$$

$$= 4 \, G^2 \cos^2\theta_c \, (p_D + p_K)_\alpha \, (p_D + p_K)_\lambda$$

$$\cdot \; [p_{e_\alpha} \, p_{\nu_\lambda} - p_e \cdot p_\nu \, \delta_{\alpha\lambda} + p_{e_\lambda} \, p_{\nu_\alpha}]$$

$$= 4 \, G^2 \cos^2\theta_c$$

$$\cdot \; [2 \, p_e \cdot (p_D + p_K) p_\nu \cdot (p_D + p_K) - p_e \cdot p_\nu (p_D + p_K)^2]$$

<u>$D \to K^* e \nu$</u>

$$M = \frac{G}{\sqrt{2}} \cos\theta_c \, \varepsilon_{K^*} \, \bar{u}_\nu \, \gamma_\lambda \, (1 + \gamma_5) \, v_e$$

where ε_{K^*} is the K^* polarization vector

Summing over K^*, e, and ν spins:

$$|M|^2 = 4G^2 \cos^2\theta_c \left(-\delta_{\alpha\lambda} + \frac{p_{K^*_\alpha} \, p_{K^*_\lambda}}{m_{K^*}^2}\right)$$

$$\cdot \left(p_{e_\alpha} \, p_{\nu_\lambda} - p_e \cdot p_\nu \, \delta_{\alpha\lambda} + p_{e_\lambda} \, p_{\nu_\alpha}\right)$$

$$= 4G^2 \cos^2\theta_c$$

$$\cdot \left(p_e \cdot p_\nu + \frac{2(p_e \cdot p_{K^*}) \, (p_\nu \cdot p_{K^*})}{m_{K^*}^2}\right)$$